Influence of Steel Fiber Addition on Workability & Mechanical Behavior of High Performance Concrete

Abdulhameed Umar Abubakar

Submitted to the
Institute of Graduate Studies and Research
in partial fulfillment of the requirements for the degree of

Doctor of Philosophy
in
Civil Engineering

Eastern Mediterranean University
July 2018
Gazimağusa, North Cyprus

Approval of the Institute of Graduate Studies and Research

Assoc. Prof. Dr. Ali Hakan Ulusoy
Acting Director

I certify that this thesis satisfies all the requirements as a thesis for the degree of Doctor of Philosophy in Civil Engineering.

Assoc. Prof. Dr. Serhan Şensoy
Chair, Department of Civil Engineering

We certify that we have read this thesis and that in our opinion it is fully adequate in scope and quality as a thesis for the degree of Doctor of Philosophy in Civil Engineering.

Assoc. Prof. Dr. Khaled Marar
Co-Supervisor

Asst. Prof. Dr. Tülin Akçaoğlu
Supervisor

Examining Committee

1. Prof. Dr. Yilmaz Akkaya
2. Prof. Dr. Özgür Eren
3. Prof. Dr. İsmail Özgür Yaman
4. Assoc. Prof. Dr. Mehmet Cemal Geneş
5. Assoc. Prof. Dr. Khaled Marar
6. Asst. Prof. Dr. Tülin Akçaoğlu
7. Asst. Prof. Dr. Eriş Uygar

ABSTRACT

In this study, the mechanism of crack propagation in concrete at discontinuity stress region under uniaxial compression was investigated and an attempt was made to determine the microcracking behavior of high-performance concrete with steel fiber addition at 7 different fiber volume (V_f) under two aspect ratios. For this purpose, fourteen different concrete mixes with steel fiber addition for 60 and 75 aspect ratio, each changing in proportions from 0.5 - 2.0 % with 0.25 % intervals were designed based on high performance concrete principles. Microcracking behavior of the produced concretes were analyzed by selecting two stress points before the linearity, the linearity end point, and one point after the end of the linearity using the tangent points (deviation from linearity) of load – time diagram.

Findings revealed that in terms of workability, with increasing V_f addition and aspect ratio, VeBe time increases exponentially; slump and compacting factor decreases linearly, and an inverse relationship exist between yield stress and slump. It is hereby suggested that in terms of workability for this kind of mixes, a combination of parameters should be considered instead of a single parameter to characterize workability. Compressive strength increases with increase in fiber addition in aspect ratio 60, while in aspect ratio 75, the increment was up to 1.0 % fiber addition level, but it was still higher than the reference specimens without fiber addition. Tensile strengths in the form of splitting and flexural tensile strength increased with fiber addition in both cases; however, the flexural strength presented results with higher strength. Area under the load – deflection diagrams increases with increase in fiber volume and aspect ratio, an indication of the improvement in toughness of the

composite. Fracture energy increases with increase in fiber volume and compressive strength, an indication of high energy required in extending cracks. Characteristic length also increases showing the increased ductility of the composite.

Residual tensile strength measured indicated that there was strain hardening behavior due to the fiber addition resulting in tensile strength gain instead of tensile strength loss in concrete with fiber addition. Results from the load – time diagram used to determine the end of the linear portion of the graph indicates that the end of ascending portion (linearity) lies within 85 – 91% of the ultimate strength, aggregate cracking was the dominant failure mode up to the end of linearity as oppose to bond cracks due to improvement in the matrix quality. Failure pattern similar to what is obtained in compressive loading is applicable here at linearity end point and post linearity with extensive damage perpendicular to the casting direction. The presence of the steel fiber improved the extensive failure pattern of cracks observed at aspect ratio 60 and 75 where it changes from macrocracks to a branched network of microcracks especially at higher fiber dosage. Critical width of the cracks measured at linearity end point was within the range of 0.01 mm – 0.07 mm.

The findings of this study will go a long way in helping our understanding of the microcracking in concretes with fiber addition which is the next frontier in structural concrete.

Keywords: High performance concrete; Steel fiber concrete; Uniaxial compression; Microcracking behavior; Critical stress; Critical crack width; Residual tensile strength

ÖZ

Bu çalışmada; çelik elyaflı yüksek performanslı beton (HPC), tek eksenli basınç yükü altındada çatlak yayılımı mekanizması, betona iki farklı boy oranı ve yedi farklı lif hacim (V_f) ilavesi durumları için incelenmiştir. Bu amaçla, yüksek performanslı beton prensiplerine dayanarak, her biri % 0,5 - % 2,0 arasında, % 0,25 aralıklarla değişen hacim oranlarında, 60 ve 75 en-boy oranı için çelik lifli, on dört farklı beton karışımı tasarlandı. Üretilen betonların mikro çatlak davranışları; betonun basınç yük-deformasyon eğrisi eğim takibinden tesbit edilmiş olan, 4 farklı gerilme noktasında (doğrusallık bitiş noktası, 2 nokta doğrusallık bitiş noktasından önce ve de 1 nokta sonra) analiz edilmiştir.

Bulgular, artan lif hacim ilavesi ve en-boy oranı ile VeBe zamanının katlanarak arttığını, çökme ve sıkıştırma faktörü değerlerinin ise doğrusal olarak azaldığını göstermiştir. Akma gerilmesi ve çökme değerleri arasında ters bir ilişki olduğu da gözlemlenmiştir. Bu tür karışımlarda, işlenebilirliği karakterize etmek için tek bir parametre yerine parametrelerin bir kombinasyonu düşünülmelidir. En-boy oranı 60'da; lif ilavesindeki artışla birlikte basınç mukavemeti artarken, en- boy oranı 75'te artış, % 1 lif ekleme seviyesine kadar devam etmiştir. Fakat yine de lif ilavesi olmayan referans numunelerden daha yüksek çıkmıştır. Her iki durumda da lif ilavesiyle yarma, eğilme ve çekme mukavemeti gibi gerilme mukavemetleri artmıştır; Bununla birlikte, sunulan eğilme mukavemeti daha yüksek mukavemet ile sonuçlanmaktadır. Yük altındaki alan diyagramları, lif hacim ve en-boy oranındaki artışla artar. Bu, kompozitin sağlamlığındaki iyileşmenin bir göstergesidir. Kırılma enerjisi, lif hacmindeki artış ve basınç dayanımı ile artar. Bu, çatlak gelişimi için

gerekli olan yüksek enerjinin bir göstergesidir. Karakteristik boy uzaması, kompozitin artan sünekliliğini de gösterir.

Lif ilavesiyle betonda gerilme mukavemeti kaybı yerine gerilme mukavemeti kazancı oluşmuştur. Yük - zaman diyagramından, grafiğin doğrusal kısmının (% 85 - % 91) basınç mukavemetine tekabül ettiği gözlemlenmiştir. Çelik lifin mevcudiyeti ile; özellikle yüksek lif dozajında, makro çatlak yerine, daha fazla sayıda dallanmış mikro çatlak oluşmuştur. Bu her iki en-boy oranında (60 ve 75) da ve de artan miktarlarda gözlemlenmiştir. Yük - zaman diyagramında, grafiğin doğrusal kısmına denk gelen basınç gerilmesi altında ölçülen çatlakların kritik genişliği, 0.01 mm - 0.07 mm aralığında ölçülmüştür.

Bu çalışmanın bulguları, lif içeren yapısal betonda mikro çatlakların oluşması, yayılması, kritik ebat ve konuma ulaşmaları konusunun daha iyi anlaşılmasına iyi bir yol gösterici olacaktır.

Anahtar Kelimeler: Yüksek dayanımlı beton; Çelik lifli beton; Eksenel basınç dayanımı; Betonda çatlak davranışı; Kritik gerilme noktası; Kritik çatlak genişliği; Çekme gerilmesi kayıbı.

DEDICATION

To my wife for her patience
To my daughter Anisa for missing her childhood without her Dad
To my parents for their sacrifices all through these years
To my siblings, family, and friends for their prayers and well wishes
To all my teachers that worked tirelessly for me to get to this point

ACKOWLEDGEMENT

I would like to give gratitude to Almighty Allah for his bounties upon me, I am grateful to my supervisor Dr. Tülin Akçaoğlu for her guidance, support and patience throughout the learning curve. I know what she has to put up with, because I can be pretty annoying when I need something. I am also grateful to my co-supervisor Dr. Khaled Marar for his input and assistance when I needed it. The laboratory engineer Mr Ogun Kilic, a friend and colleague who am indebted to for his assistance, and his technical assistant Orkan Lord without whom this work would not have seen the light of day. The foresight of my monitoring committee consisting of Dr. Mehmet Cemal Geneş and Dr. Eriş Uygar is appreciated for sacrificing their time and asking the right questions. I appreciate the entire staff of Civil Engineering Department for their kindness, and EMU for finding me worthy of a Research Assistantship Position. I owe the management of Boğaz Endüstri ve Madencilik Ltd (BEM) a debt of gratitude for supplying the cement used in this study.

May I also use this opportunity to acknowledge Prof. Kyari Mohammed, the Vice Chancellor and the Management of Modibbo Adama University of Technology, Yola, and TETFund Nigeria for awarding me a fellowship grant for this PhD studies. To my colleagues back at Civil Engineering Department MAUTECH, thank you for holding the fort while I was away. I am opportune to have friends and colleagues like Rowad Esameldin Farah, Mobarak Osman, Abiola Abiodun Ayopo, M. Hossein Masouminia, Mosab Nassar and 'Chief' Aliye Dalci, as well as others that space cannot allow me to mention.

TABLE OF CONTENTS

LIST OF TABLES

LIST OF FIGURES

Chapter 1

INTRODUCTION

1.1 Background

Concrete comes from the Latin word *concretus* meaning to grow. This is due to the ability of concrete to continue developing strength over time as a result of products of cement hydration present inside mimicking plants and living organism (Mehta and Monteiro, 2014). In 1995, core samples taken from Hoover dam were analyzed and it was found that 60 years after it was constructed, the concrete is still gaining strength and has a higher than average compressive strength (Gromicko and Shepard, 2006). Despite its many advantages, and being the most widely used construction material, as a heterogeous material, it has many disadvantages such as porosity, the variability in the position of ITZ and "bulk" paste and many more. These has resulted in many significant changes over the years to improve its performance, from normal strength concrete (NSC) to high-strength & high-performance concretes. Incorporation of fiber shifted the focus to fiber reinforced concretes (FRC), to ultra-high performance fiber reinforced cementitious composites (UHPFRCC), and the current trend is now ductile high-performance concrete (DHPC).

In practice, high-strength concretes (HSC) are concretes with a cylinder compressive strength at 28 days of 60 MPa and above depending on time and location that cannot be made with conventional aggregates CEB-FIP (1990). These concretes are highly engineered materials incorporating mineral and chemical admixtures, achieving

workable mixes with very low water contents with the addition of retarders and superplasticizers (Gettu *et al.*, 1990). The engineered material results in a very high-strength matrix that is more compact, with well-bonded aggregate-mortar interfaces (Carrasquillo *et al.*, 1981).

High-performance concrete (HPC) on the other hand is defined in terms of durability and strength as it's relates to the intended application (Mindess in Shah and Ahmad, 1994). In Neville (2005 pp. 674 - 675), HPC is defined as having a compressive strength in excess of 80 MPa with the following ingredients: good quality aggregates; cement content in the range of 450 – 550 kg/m^3; silica fume generally 5 – 15 % by mass of the total cementitious materials or sometimes fly ash or ground granulated blast furnace slag; and always a superplasticizer, the dosage which is very high resulting in a decrease in water content. He further opined that what makes a concrete HPC is the low water-cement ratio that is always below 0.35. It is also the opinion of Aitcin (1998 pp. 2) that it is not possible to make a durable HPC that does not have a high compressive strength, and he suggested 0.40 as the boundary condition for the low water/binder ratio. His argument that it is practically impossible to make a concrete with ordinary Portland cement without the use of a superplasticizer at this range. This value is closer to the theoretical value suggested by Powers (1968) for full hydration of Portland cement.

In essence for HPC mixes, durability and intended application is always the main idea behind the design because these mixes with low water-cementitious materials ratio may result in higher compressive strength (Aitcin, 1998). This is enhanced by the compactness and denser matrix impermeable to ingress of fluids or gases due to discontinuity of the capillary pores reducing the porosity and increasing its

homogeneity resulting from improvement in technology, use of supplementary cementitious materials and high range water reducer (superplasticizer) for workability and strength improvement.

Concretes that are subjected to damage or deterioration, cracks begins to manifest according to the amount of load imposed, if the width of the crack is small, it becomes the weakest link that results in future durability issues for the concrete as a result of access to the internal structure provided by these cracks where absorption, diffusion, and permeability may continuously occur. However, if the crack is large enough, the structure may fail as a result of damage to its integrity (Li *et al.*, 1998). According to van Breugel (2012) cracks in concrete are not regarded as failure of the reinforced concrete member if the crack width criterion is not exceeded since they are always designed with the provision allowing for the occurrence of tensile cracks due to concrete brittleness. However, problem arises when these cracks becomes entry points for substances such as aggressive agents that inhibits corrosion of the steel and also damaging the concrete in the process.

The need for high strength in certain construction activities which is an advantage on one hand, and the resulting increase in brittleness on the other hand has necessitated the need to incorporate fibers (steel, polymer, natural etc.) to reduce the brittleness. The addition of fiber is necessitated due to the decrement in material ductility which is a serious hindrance to the application of high strength concrete. Incorporation of the fibers reduces microcracking and crack propagation with an improvement in ductility and strength (Khaloo and Kim, 1996). The addition of steel fiber in HPC helps in increasing the post-peak properties due to pull-out resistance. This fiber addition results in the development of multiple smaller microcracking as opposed to

large cracks in conventional concrete under loading. An increase of about 30 – 40 % tensile strength is observed when steel fiber is used up to 1.5 % as crack propagation control (Panzera *et al.,* 2013). This is due to fibers suppressing the localization of microcracks into macrocracks and as a result the apparent tensile strength of the matrix increases. However, the workability properties of the concrete have to be managed properly as a result of susceptibility to balling and other tendencies in the fresh stage.

The onset of microcracking in high-strength concrete is similar to that of normal strength concrete, however, it is much delayed and occurred beyond 75 % of the ultimate strength. Akcaoglu *et al.,* (2005) reported damage to interfacial transition zone (ITZ) of HSC around 80 % of ultimate compressive strength. From this point onward, even if the stress is removed microcracking does not cease. This 'critical' point or stress point is what Newman (1968) called "*Discontinuity Stress*," and with fiber addition, multiple microcracking continue to take place as a result of the composite modification. According to Slate and Meyers (1969), when loads are greater than 70 % of the ultimate strength, creep strains are responsible for mortar cracks in normal strength concrete, and eventually failure of the specimens results under constant load. For this reason, Carino and Slate (1976) argue that the discontinuity point should serve as the failure criteria since it is similar to sustained-loading strength.

In high-strength concretes, it is known that the linear portion of the stress-strain curve extends up to 80 % of the ultimate strength, sometimes even more and according to Neville (2005) cited in Afroughsabet *et al.,* (2016), the linear portion have been found to reach up to 85 % or even more. Berra and Ferrerra (1990) and

Mehta and Monteiro (2014) attributed this to the non-existence of microcracking at initial or ascending portion of the curve responsible for the explosive failure due to very high brittleness. The significance of steel fibers manifest after matrix cracking, and when a proper material design is employed, at the onset of matrix cracking randomly distributed fibers arrest the crack, bridging proces takes place, as well as pull-out mechanism, limiting the propagation of crack (Banthia and Trottier, 1995; Kurihara *et al.*, 2000 cited in Bayramov *et al.*, 2004)

It is on this premise that a study investigating the mechanical (microcracking, fracture initiation, propagation, coalescence, and localization) behavior under uniaxial compression of a particular region where in concrete with fiber addition is further decreased to a narrow region is important. The study also take a wholistic look at the fresh, hardened and microcracking properties of HPC with steel fiber addition produced. Previous studies (Meyers *et al.*, 1969; Carrasquillo and Slate, 1983) have tried and established relationships between this point with repetitive, sustained and short-term loadings, as well as defining microcracking failure in normal and high-strength concretes.

1.2 Research Significance

Concrete is a heterogenous material made up of different phases forming a single composite, and failure is mainly from microscopic flaws that forms the weakest link. It is in light of this that the commonly held believe on the mechanism of failure in compression is that of the discontinuity point by Newman (1968); Carino and Slate (1976) defined as the point where there is a sharp increase in Poisson's ratio and volumetric strain ceased to decrease, accompanied by extensive mortar cracking.

Failure in compression at this point can either be tensile failure of cement crystals or bond in direction perpendicular to applied load (Lea, 1960).

In this study an attempt was made to evaluate the discontinuity stress region in high-performance steel fiber concrete using two aspect ratios (60 and 75) with a view of further understanding the microcracking behavior under uniaxial compression. Previous studies such as the exhaustic research by the Cornell University research group in the 60's – 80's studied different mode of loading in normal and high-strength concretes; Shah and co-workers utilized models to study crack propagations under different loading conditions, and Akcaoglu (2003) studied the interfacial transition zone (ITZ) using a single aggregate model. This study is a continuation on that line of enquiry with steel fiber addition in high-performance concrete in contrast to the rebar aggregate models which will be highlighted in Section 3.8. These models that would be highlighted have either been used in mortar, normal or medium high-strength concrete. However, in recent years, the application of steel fibered concrete in concrete construction makes it imperative to undertake this study. The application of this model to high-performance steel fiber concrete may or may not lead to a valid conclusion however, it will map out the failure mechanism especially at this critical region of stress in this type of concrete. Quantification of tensile strength by Akçaoğlu (2003) in normal, medium, and high-strength concrete has resulted in a loss of strength after pre-compression with HSC having the least damage.

However, with fiber addition, it was expected that there might be strength loss but not as much as without fiber addition, therefore, this study investigated that amount of loss if any. Microscopic examination was conducted on the loaded specimens to define the microcrack present and mechanism of propagation. It is expected that the present work will contribute to the literature on this topic and further invigorate

research in an area where interest has waned over the years, and leads towards meaningful models that can best describe this region of stress.

1.3 Objectives of the Research

The main objectives of this PhD study can be summarized as:

i. To come up with a workable mix design for high performance concrete utilizing steel fiber at different aspect ratios, and fiber volume (V_f) percentage.

ii. To study the strength properties of this concrete and establish relationships between them.

iii. To obtain concrete fracture parameters that could assist to define the microcracking behavior.

iv. To study the crack formation and propagation under different compression levels at the region of discontinuity in this type of concrete.

v. To utilize cracked specimens for microcracking behavior in this region.

1.4 Scope of the Study

This study is limited to the investigation of some mechanical properties of high performance concrete with steel fiber addition with different volume fractions in the ascending portion (around critical stress region) of load-time diagram only under uniaxial compression.

1.5 Contribution

This study is a continuation of an existing line of enquiry in microcracking and failure mechanism in concrete. Significant original contribution resulting is the utilization of compressive stress levels relative to the ultimate, from load – time diagram in HPC (in excess of 83 MPa with steel fiber addition) to follow the turning points from the graph. The point of discontinuity or critical stress was mapped out

using sufficient experimental data under uniaxial compression. Damage quantification was also done at the critical stress point taking into account the amount and type of fiber.

Extensive study on the workability aspect of HPC highlighting the impact of steel fiber on stiffening of the mix, where tests that characterize these kind of mixes were used to evaluate the concrete. Regression models were used to evaluate the experimental data, and were validated using coefficient of determination and observed versus predicted plots.

This study has significant implication in structural design due to the increased steepness of the ascending portion of the diagram. In the long term, this will go a long way in providing a reliable prediction of the structural behavior especially now that concretes in excess of 80 MPa are widely used.

1.6 Outline of the Thesis

This thesis is structured as follows: Chapter one introduces concrete as a construction material and its weakness that necessitates the need for reinforcement to make it a durable composite material, and what the thesis aim to achieve. Chapter two presents the properties of concrete in fresh and hardened state especially at macro and micro level concisely. Chapter three presents the literature studies detailing the failure mechanism of concrete. However, this literature is based on the author's point of view and as such is far from being complete, but an attempt has been made to present a very objective point of view on the topic. And since the topic is an old field, a considerable amount of effort has been placed on the old text because it forms the basis and foundation of the study. Chapter four describes the methodology involved

in the carrying out the experiments, from the material selection, to the methods chosen for each particular experiment, and the procedure used. Chapter five presents the results and discussion. Chapter six presents the conclusions and recommendations for further studies.

Chapter 2

PROPERTIES OF CONCRETE

2.1 Introduction

In this section, a critical study of the properties of concrete in the fresh and hardened state is undertaken where in the former, an in-depth look at the tests conducted on concrete with low workability is presented. While in the latter, an attempt was made to critically present the microstructure of cement, paste and concrete, and their constituents especially at the microstructure level.

2.2 Fresh Concrete Properties

In the design of high-performance concrete (HPC) mixes, durability and intended application should be on the designer's mind right from the beginning. Adequate workability results in more homogenous concrete, reduce honeycombing in normal concrete, decreased voids and pores especially in high-strength concrete (HSC). This is particularly important in harsh mixes such as high-performance concrete with steel fiber addition which is difficult to achieve. Some of the parameters used in assessing HPC have come under heavy criticism due to their inability to fully characterize the behavior of the fresh concrete. Nevertheless, they are still useful in determining workability especially for certain category of mixes i.e. harsh mixes. The tests that have so far been proposed as replacement that fully describe the rheological properties of fresh concrete are either too cumbersome, not suitable for field-based application, or require extensive technical skill and training to be conducted.

Workability is the property of fresh concrete that allows it to be worked, transported, to flow, compacted and be finished. In general, it is the property of the concrete in fresh state. A workable concrete should be able to be mixed properly in the desired proportion; be transported by any means necessary; be able to be poured in the most complicated structure or geometry without the fear of not flowing properly. It should also achieve full compaction and expulsion of air decreasing possible voids in the concrete. According to Tattersal (1991), when 5 % residual air is present, strength is reduced by as much as 30 %, and when it increases to 10 %, strength loss increases to more than half. Finally, a good finish should be obtained without deficiency resulting.

The concept of water-cement ratio is very important in workability because if the workability is very low making the concrete very difficult to work with, this can be improved by the addition of water which has the adverse effect of decreasing the strength at a certain level. However, the utilization of superplasticizers has revolutionized concrete making procedure where very low workability concrete can be produced by the addition of these substances, on the other hand, they do not come cheap. Therefore, a trade-off has to be made regarding sacrificing strength by increasing water content or increasing the cement content/superplasticizer addition, in essence cost. Knowledge of the type of workability to be utilized is very important.

An argument made by Tattersal (1991) on the basis that apart from the quantitative description of workability (i.e. slump value, compacting factor etc.), qualitative description (i.e. flowability, finishability etc.) should also be used to supplement

those values usually obtained. It is on this basis that he proposed a table fully describing those terms which is reproduced below in Table 2.1.

Table 2.1: Scheme of Nomenclature for Workability (Tattersal, 1991)

1.	Class I Qualitative	
	Workability	
	Flowability	
	Compactibility	To be used only in a general descriptive way without any attempt to quantify
	Stability	
	Finishability	
	Pumpability	
2.	Class II Quantitative empirical	
	Slump	
	Compacting factor	To be used as a simple quantitative statement of behavior in a particular set of circumstances
	VeBe time	
	Flow table spread	
3.	Class III Quantitative fundamental	
	Viscosity	
	Mobility	To be used strictly in conformity with the definitions in BS 5168: 1975 Glossary of rheological terms
	Fluidity	
	Yield Value	

Most descriptions of workability usually give a value or a certain range over which it defines the behavior is described, the addition of qualitative information will go a long way in further describing the behavior of the concrete under consideration. A best example is the Road Note 4 description of workability and compacting factor given in Neville (1995) which is reproduced here in Table 2.2.

Table 2.2: Qualitative and Quantitative Workability Description (Neville, 1995)

Description of workability	Compacting factor	Corresponding slump (mm)
Very low	0.78	0 – 25
Low	0.85	25 – 50
Medium	0.92	50 – 100
High	0.95	100 - 175

2.2.1 Slump Test

This is one of the simplest tests for measuring workability described in BS EN 12350 – 2 and ASTM C 143 using conically shaped equipment in the form of frustum. It has a bottom diameter of 200 mm, 100 mm diameter top and a height of 300 mm strategically placed on a baseplate which is non-absorbent. The cone is filled in three layers with concrete, with each layer tampered 25 times with a standard tamping rod, and lifting the cone carefully in less than five seconds. The shape of the concrete after lifting is the slump measured to the nearest 5 mm.

The limitation of this test is that for concretes with maximum size of coarse aggregates in excess of 40 mm, the test is impractical. Harsh concretes are also not suitable especially when there are few fines present; sometimes concrete having the same slump can also show different behavior when tamped (Koehler and Fowler, 2003). It does not also show the effect of plastic viscosity, despite the fact that is influenced by plastic viscosity and yield stress.

2.2.2 Compacting Factor

To be able to measure full compaction of concrete, this test was devised which is essentially a density ratio and measures the ability to achieve full compaction. This test has been standardized in BS EN 12350 – 4 and consists of a simple frame with two steel hoppers situated above a cylinder which is smaller than the two hoppers above. The upper hopper is larger than the lower hopper and concrete is placed in the former and a trap-door is opened at the bottom that releases the concrete to the latter. The trap-door in the lower hopper is also opened which deposits all the concrete into the cylinder below. Concrete that overflows is struck-off and the mass is measured on a balance, where it is compared with a fully compacted concrete using the same

cylinder either with a tamping rod or a mechanical vibrating apparatus. Compacting factor is measured as:

$$Compacting\ factor, C.F. = \frac{mass\ of\ partially\ compacted\ concrete}{mass\ of\ a\ fully\ compacted\ concrete} \quad (2.1)$$

Among the limitations of this test is that for concretes that are very cohesive, it tends to stick to the hoppers and the tamping rod has to be used to force the concrete down. The apparatus is also bulky which makes it not suitable to move around, and it also does not utilize vibration which is the most frequently used method of compaction in the field.

2.2.3 VeBe Time Consistometer

This test is standardized in BS EN 12350 – 3 and was proposed by Bahrner (1940) to be suitable for concrete to be placed by vibration consisting of a cylindrical container similar to what is obtained in Slump test mounted on a vibrating table with a frequency of 50 Hz. The cone is filled with concrete and removed, and a clear circular plate of 230 mm diameter is gently placed on top of the concrete and vibrated until when the whole surface of the clear plate is completely "coated" with concrete. At the same time taking note of the time for the whole process to have taken place with a stop watch measured in seconds. The test is attacked in many ways such as, the exact time for the concrete to coat the clear plate is not known because, the vibration does not start immediately, it takes time to build up. The apparatus is not suitable for field work. The test is only suitable for a certain range of concrete with low slump among other reasons.

2.3 Hardened Properties of Cement, Mortar, and Concrete

In most concretes and hydrated cement pastes (hcp), the hydration products formed are mostly calcium hydroxides and calcium silicates hydrates (C-S-H) and few other compounds such as ettringitte and monosulfate in smaller amounts (Mehta and

Monteiro, 2014). This section introduces these products that are formed as a result of this reaction; interfacial transition zone (ITZ), its properties and porosity is also explained.

2.3.1 Microstructure of Cement Paste

Concrete consists essentially of the macrostructure which is visible to the human eye which has a limitation of about 200 μm and the microstructure, the portion that can essentially be viewed with the aid of a microscope; it is at this level that the complex nature of concrete begins to manifest as a result of the heterogeneous composition of the constituents.

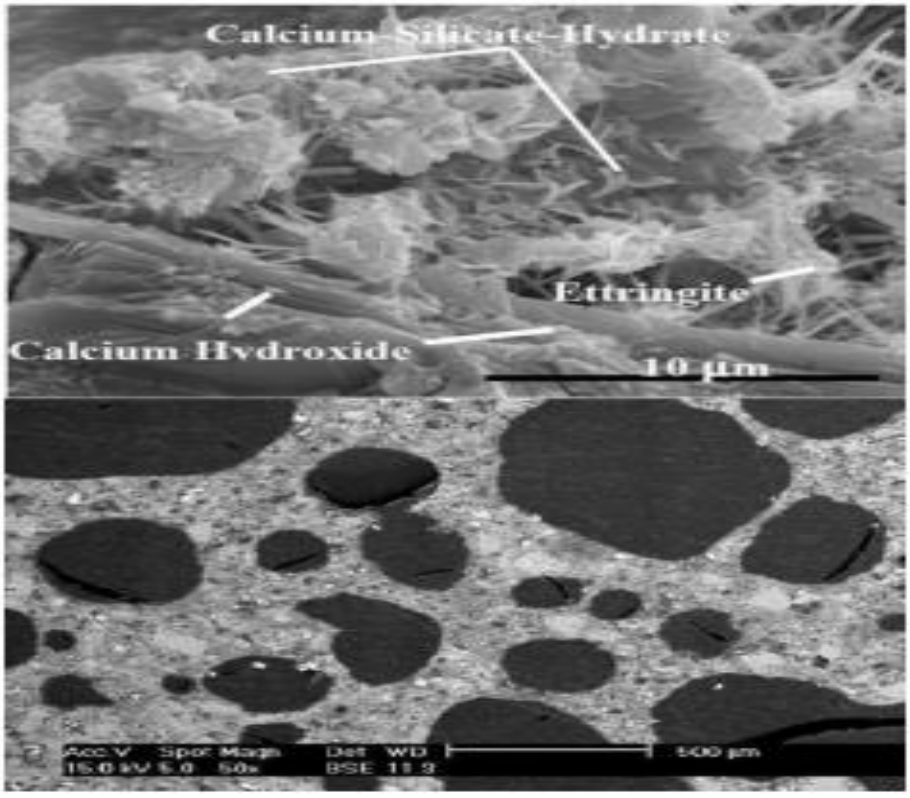

Figure 2.1: Distinction between Microstructure (above) and Macrostructure (below) of Concrete [Adapted from Emery *et al.*, (2007)]

The work of Diamond (2004) studied the microstructure of hcp and concrete utilizing Backscatter-Scanning Electron Microscope (BSEM). The investigation was only limited to ordinary Portland cement and reported that microstructure of hcp is

affected by the chemistry, cement fineness, water-cement ratio, chemical admixtures, influence of mixing procedures and changes in curing temperature at early age among other things.

In cement paste after hydration, there are always remnants of unhydrated cement particles, most especially the inner part of the cement and could remain in that condition for a long period of time.

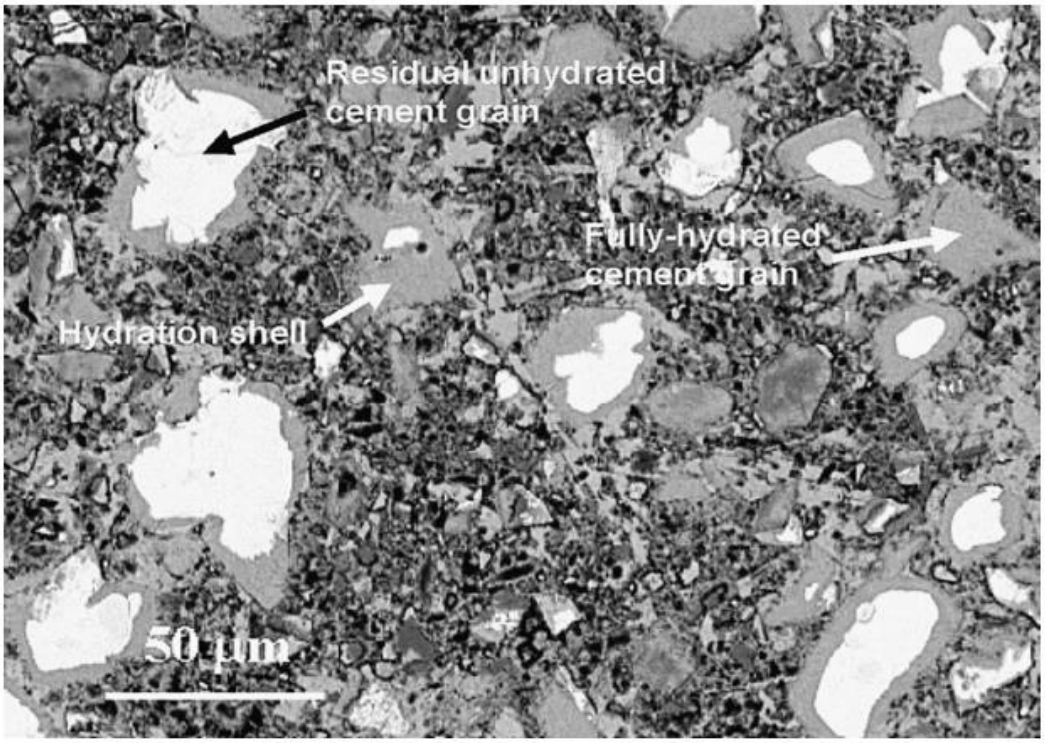

Figure 2.2: Microstructure of a 3 Month Old HCP at 0.30 W/C Ratio Cured at Room Temperature (Diamond, 2004)

It can be seen from the Figure 2.2 that the unhydrated cement grain as indicated with a black arrow is surrounded by grey-portion of fully-hydrated cement grain, and according to the author, the size of the unhydrated shell can ranges from 5 µm - 40 µm. To estimate the size of the original cement grain, it is the sum of the surrounding hydrated portion and its unhydrated component in a given image under

consideration. In view of the author, when concrete and pastes mature, the amount of unhydrated portion is usually smaller than what was presented in the Figure 2.3, however, there is always a residual component except in a situation whereby the concrete is subjected to leaching over a considerable period. Still, some unreacted C_4AF will usually remain even in concretes and cement pastes that are fully hydrated.

2.3.1.1 Calcium Silicate Hydrate (C-S-H)

This is not a well-defined compound, hence the reason it is called C-S-H. Diamond (2004) opined that it is a combination of "quasi-amorphous" masses of calcium, silica and water as a result of the hydration of C_2S and C_3S in cement with a chemical composition that keeps changing from one point to the next, so also the porosity. It makes up 50 - 60 % by volume of hcp and determines the properties of the paste. It exacts structure still remains unresolved, but a number of models have been proposed. Powers-Brunauer model viewed it as a layer structure with a high surface area. Feldman-Sereda model conceptualize it as a kinked array or irregular layers randomly arranged so as to create interlayer spaces of different sizes and shapes from 5 - 25 angstrom (Mehta and Monteiro, 2014).

As regards to its internal structure, there are still unresolved issues, in the past it was assumed to resemble the mineral tobermorite and it was sometimes referred to as tobermorite gel. Regarding its calcium to silicate content, it varies from 1.5 - 2.0 %, and the variation in water content is far more.

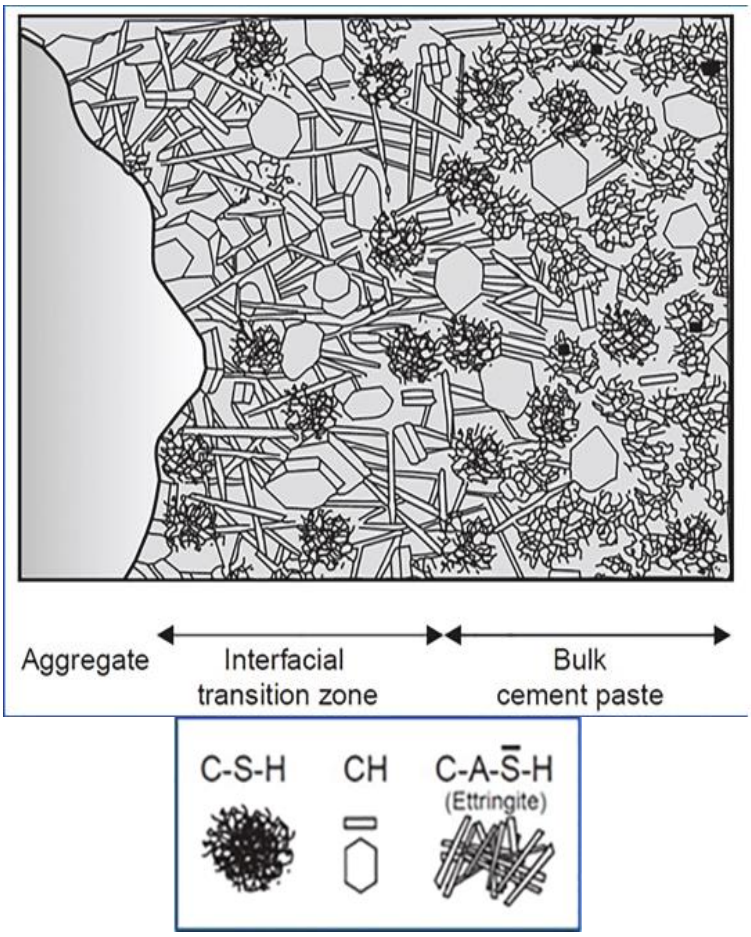

Figure 2.3: Microscopic Image of Hydration Products (Mehta and Monteiro, 2014)

2.3.1.2 Calcium Hydroxide (Portlandite)

By percentage, it is about 20 - 25 % by volume in the hydrated paste and unlike C-S-H, its definite form is $Ca(OH)_2$. Using BSEM, Diamond showed that CH could be differentiated from C-S-H gel as a result of its gray level slightly brighter than C-S-H upon close examination. It has been reported to appear as crystals, however, in cement pastes it is an irregular mass of different sizes as oppose to the euhedral crystals.

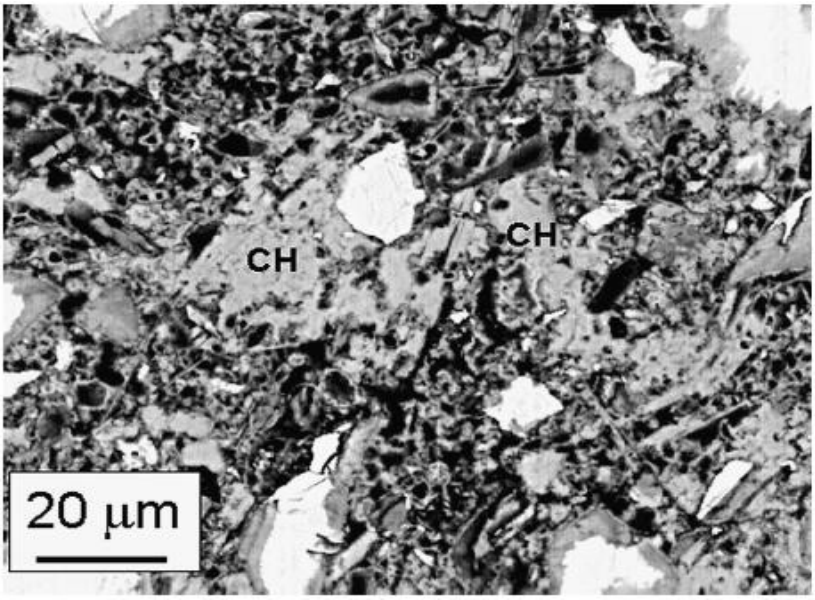

Figure 2.4: 7- Days Old Irregular CH Crystals at 0.45 W/C Paste (Diamond, 2004)

The morphology of CH is that of a hexagonal-prism crystal and varies from non-descript to stacks of large plates which may be affected by temperature of hydration, availability of space and impurities present (Mehta and Monteiro, 1993). It has a lower surface area and it is more soluble than C-S-H which is detrimental to its durability.

2.3.1.3 Calcium Sulfoaluminates

This occupies 15 – 20 % by volume of solids in hcp, as such its role is relegated to a minor one. During the initial phase of hydration, the ionic ratio of the sulfate/alumina is more disposed to the formation of trisulfate hydrate (ettringite – $C_6A\bar{S}_3H_{32}$) a needle-shaped prismatic crystals. This transforms to monosulfate hydrate $C_4A\bar{S}H_{18}$ in ordinary Portland cement paste (hexagonal-plate crystals) and is responsible for exposing the concrete to sulfate attack (Mehta and Monteiro, 1993)

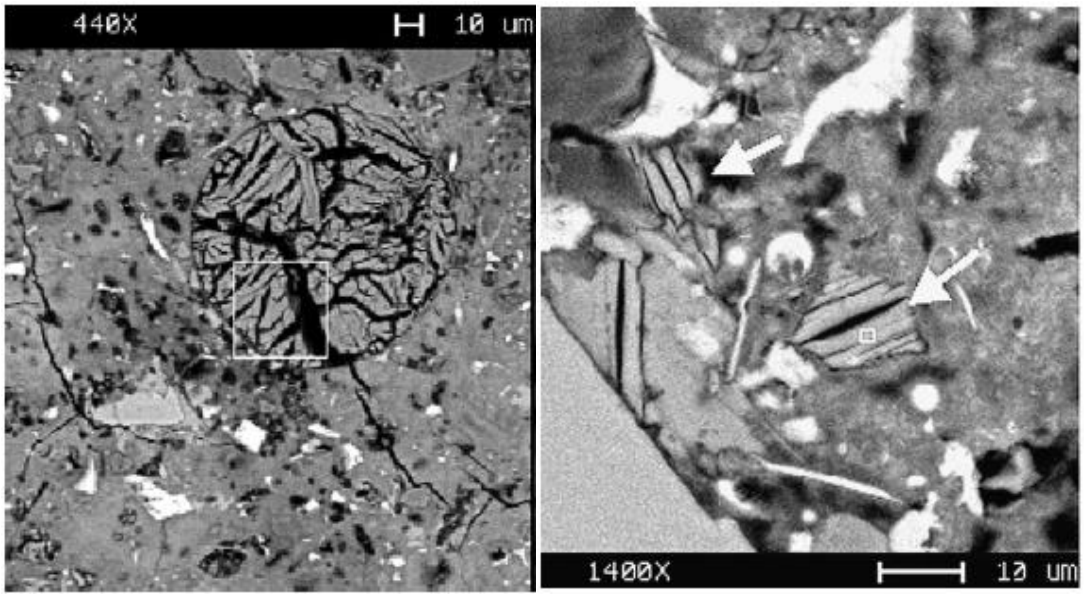

Figure 2.5: (a) Ettringite Deposit in an Air Void in Concrete with its Characteristics "Tiger Stripe" (b) Monosulfate Deposit within a Paste in a Fly Ash Concrete (Diamond, 2004)

2.3.1.4 Residual Unhydrated Cement Grains

Studies have shown that even after hydration has taken place, unhydrated clinker grains may be found in the microstructure. It is a fact that cement particle size ranges from 1 – 50 μm, and on the onset of hydration process, the smaller particles dissolve or react first followed by the larger ones. As a result of limited availability of space, at later age, hydration of particles of clinker yields the formation of a dense product of hydration resembling the original particle of clinker in morphology (Mehta and Monteiro, 2014).

2.3.2 Concrete Microstructure

The work of Diamond (2004) showed that concrete microstructure is by no means different from that of cement pastes, when he investigated a 3 – day old concrete. Specimen with a water-cement ratio of 0.45 which was hydrated at room temperature revealing that in terms of microstructure, it is much alike as in the case of cement pastes with spots of unhydrated cement pastes (A), C-S-H products (B), calcium

hydroxide (C) and an area containing porous groundmass with fully and partly hollowed grains (D & E). however, there are some features that are also present which are not found in cement pastes such as aggregates, air voids and interfacial transition zone (ITZ) which shall be explained in detail.

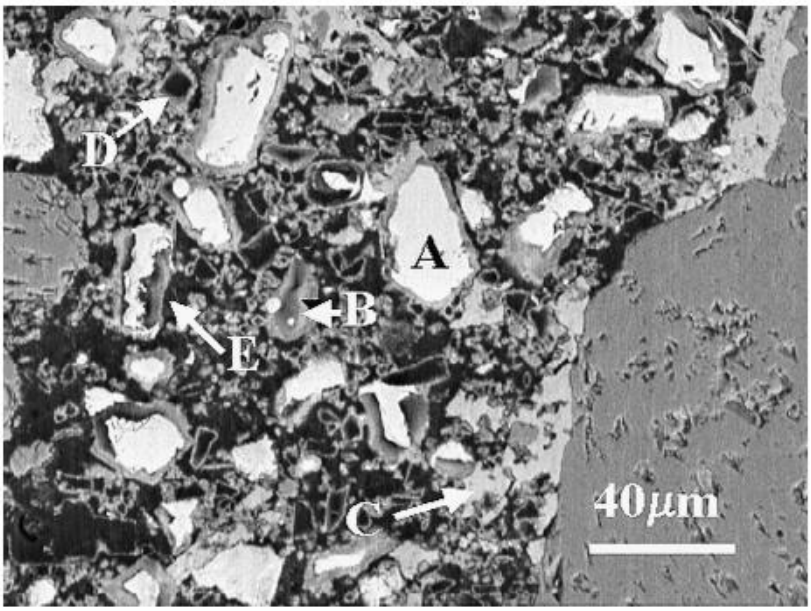

Figure 2.6: Microstructure and Composition of a 3 – Day Old Concrete (Diamond, 2004)

2.3.2.1 Aggregates

These are the components that are missing in cement pastes, and examination is mainly conducted using optical microscopy instead of SEM which major advantage is color distinction of relevant mineral properties present. On the other hand, BSEM has the advantage of chemical composition that can be assessed after the test. It can also provide information on the type of sand present either manufactured or otherwise. Additional information that can be retrieved includes shape and size of grains.

2.3.2.2 Air Voids

Most concretes are air-entrained deliberately; and contain about 15 % of non-aggregate space (Diamond, 2004) with a size between 20 μm to 1 mm making them larger than most features of hardened cement paste. On a very low magnification BSEM, air-voids from air-entrained cement paste is reproduced in Figure 2.7.

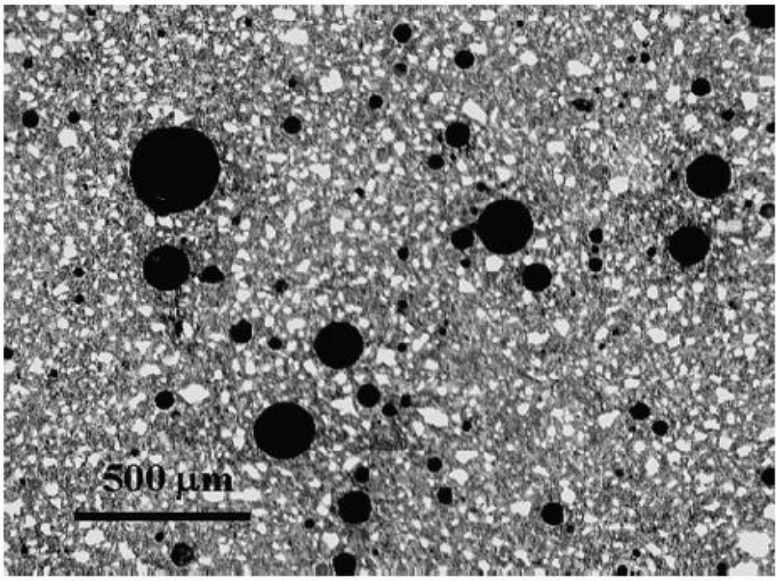

Figure 2.7: Typical Air-voids Size in an Air-entrained HCP on a Low Magnifiaction (Diamond, 2004)

From the results of the examination, it can be seen that air-entrained voids are spherical in shape and possess a “thin” lining of calcium hydroxide, however, for concretes that are subjected to exposure in alternate wetting and drying, these air-voids presents an internal deposit of ettringite or calcium hydroxide or a combination of both. Such situations rarely occur, but when they do, they might fill the air voids entirely.

2.3.2.3 Interfacial Transition Zone (ITZ)

Concrete as a composite material can be modeled as a three-phase material: matrix, aggregate and interfacial transition zone (ITZ), and the existence of the ITZ is as a

consequence of excess porosity (Ollivier *et al.*, 1995). The ITZ is the portion of the cement paste that is adjacent to sand or coarse aggregates, and this has found a special recognition in the literature. An inner part of these zones which lies within 1 – 2 μm from the aggregate has been reported to be very porous with an average porosity of 30 % (Scrivener, 1989).

2.3.2.3.1 Properties of the ITZ

Concrete as opposed to cement paste exhibit a "quasi-ductile" behavior, which has the ability to continue sustaining increasing load beyond the linear elastic limit. This shows a corresponding decline in the load carrying capacity at post peak. A plot of stress-strain behavior depicted in Figure 2.8 of cement paste and aggregate exhibit brittle-reversible elastic behavior up to a point before failure, however, concrete on the other hand that is a composite material exhibit a "quasi-ductile" behavior.

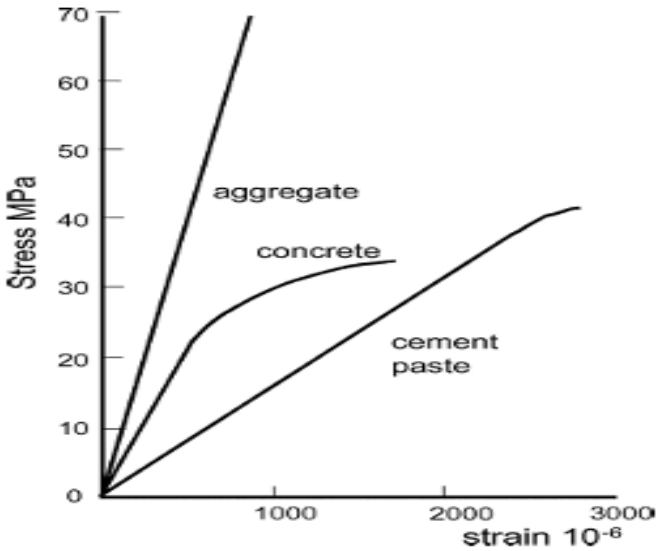

Figure 2.8: Stress-Strain Curves for Different Materials Depicting the Importance of ITZ (Scrivener *et al.*, 2004)

This is due to the multiple microcrackings that occur in the concrete which is attributed to taking place in the ITZ, and the main reason it is referred to as the

"weak link" in concrete. It is also believed that the foundation of this zone is based on what is called the "wall" effect (Figure 2.9) as a result of cement grains packing relative to flat aggregate surface. This zone is not "definite" rather a "transition" region which effective thickness varies with the microstructure under consideration during the process of hydration (Scrivener *et al.,* 2004).

Variation in the properties of hcp or "bulk" cement paste and the ITZ has been reported to be due to a reduction of anhydrous cement in the ITZ with near absence on the surface of the aggregate, and due to the distribution of anhydrous, porosity is increased in the ITZ (Nemati and Gardoni, 2005). Studies by Scrivener and co-workers suggested that packing of the cement grains that affect the thickness of ITZ is about equivalent to the biggest particle of cement (up to 100 μm, since the range of cement particle size is 1 – 100 μm). Regions closer to the aggregate mainly contain small grains and higher porosity as compared to the large grains that are far away from the zone.

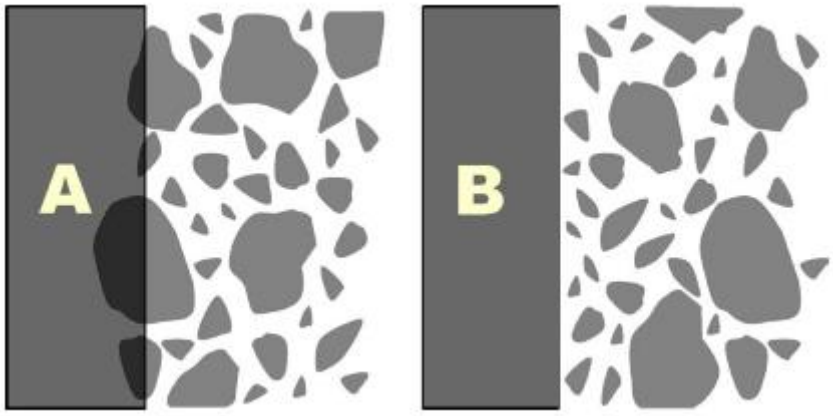

Figure 2.9: A Description of the "Wall" Effect where Packing of Grains is Disrupted to Produce a Zone of Higher Porosity and Smaller Grains in the Zone Close to the Aggregate (Scrivener *et al.,* 2004)

It is also important to note that each separate region of ITZ will have different microstructure since packing process takes place randomly. However, the distance at which there is a substantial rise in porosity is around 35 – 45 μm (Crumbie, 1994). It is at the same time expected that there would be a lower permeability as a result of combination of the cement paste and aggregate as oppose to the cement paste alone because most aggregate do have low permeability.

In the opinion of Diamond (2004), the higher content of pore is limited to an area adjacent to the aggregate surface, which he attributed to the fact that aggregate surface is covered by a layer of calcium hydroxide with limited or near zero porosity. An observation he made on aggregate to cover about one-third of its surface from the plane of observation.

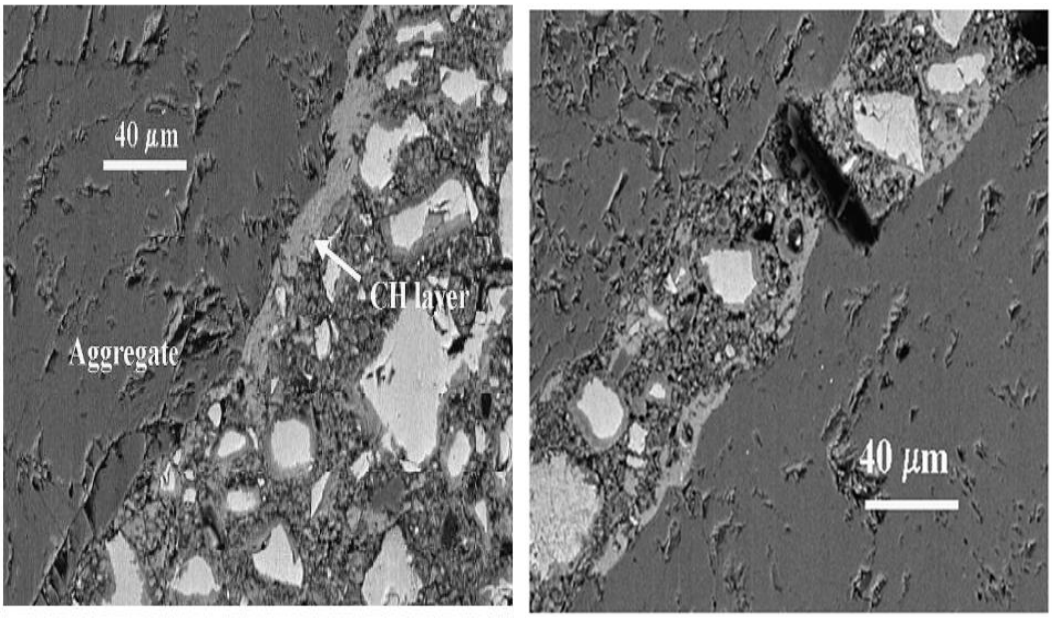

Figure 2.10: (a) View of a Portion of Zone of Contact between Aggregate and Paste with CH Covering much of the Interface (b) Area of HCP between Two Closely Spaced Grains in a Concrete of 0.5 W/C Ratio (Diamond, 2004)

2.3.2.3.2 Porosity in the ITZ

The porosity and w/c ratio of the fresh concrete is increased to the surface from the bulk paste due to rearrangement around the aggregate particles that becomes loose. In addition, during the vibration, water accumulates beneath the aggregate particles due to “micro bleeding.” Two techniques that have been used to quantify the porosity of ITZ are:

i. Back-scattered imaging using SEM of polished flat surface
ii. Mercury intrusion porosimetry.

With the first method, porosity is measured as a function of distance to the surface of the aggregate, a technique developed to analyze ITZ by Scrivener and Pratt (1986). Porosity was observed to increase near the surface of the aggregate particle in younger OPC mixture, and the porosity variation reduces with age because of the presence of hydrates development. When there is a modification to the paste (use of silica fume) porosity remains fairly constant as a result of decrease in packing ability of the cement grains in the zone.

To establish the micro bleeding theory under the aggregate particles, Hashino (1988) used dye penetrant to observe variation on cut surfaces of a modeled aggregate in a cement paste. He reported that there is no uniformity in the dye from the cut surface, which leads him to believe that there is an increase in water-cement ratio before hardening under the aggregate. However, Scrivener and Pratt (1986) had a contrary opinion in that they observe small difference above and beneath the aggregate at a water-cement ratio of 0.4. In conclusion, porosity is generally twice as much in the ITZ than in the bulk cement paste, and also the pre-existence of coarse pores which

might be due to improper order or arrangement around the aggregate particles by the cement grains (Ollivier *et al.,* 1995).

In regards to mobility of ions in the ITZ, it follows the Le Chatelier mechanism that the ions, which are more mobile after anhydrous compounds dissolution, travel under the influence of gradients from the bulk to the interface. This is all because of availability of spaces in the aggregate surroundings that can be filled with water. In the case of OPC, the ions that diffuse faster are $Ca^{2+,}$ Na^{+}, K^{+}, Al $(OH)_{4}$-, and SO_4^{2-} (Maso, 1980).

Regarding the influence of mineral additions, their effects are mainly to improve the packing of the particles by densifying the microstructure when the mineral addition is finer than cement particles; it modifies the process of hydration. A study conducted by Hanna (1987) which was reported by Ollivier *et al.,* (1995) showed that the addition of microfiller has a filling effect both in the ITZ and the bulk, and the process is more effective when superplasticizer is utilized. Goldman and Bentur (1992) reported also on the use of silica fume and fine grains of carbon black.

When fly ash or slag additions is used to modify the ITZ microstructure in the first few days, effects of these materials is mostly slow or poor because the fineness of these material is equal or close to that of cement grains and packing in the vicinity of the aggregate particle is not much influenced due to the stated reasons. However, C-A-H is easily formed in the presence of a high water-cement ratio in the transition zone as against ettringite and also there is an improvement in the calcareous filters which leads to the formation of calcium carbonate.

Chapter 3

FAILURE MECHANISM IN CONCRETE

3.1 Foundation of Fracture Mechanics

Fracture mechanics seeks to identify and eliminate potential failures of engineering materials that might erstwhile be catastrophic resulting in loss of lives and damage to properties worth millions. According to Roylance (2001), this is a vital specialization that is a branch of solid mechanics where the existence of a crack is assumed, thereby finding quantitative relations for crack length, material resistance to crack extension, and stress where propagation of crack cause catastrophic failure.

In atomic structure, properties are described by the interatomic energy that holds them together, where at infinite separation; the interaction between two atoms is small but increases as they move towards each other. This interaction is dependent on the shape, bonding energy as well as potential energy curve. The process of fracture starts with nucleation of crack at stress concentration points followed by crack growth and coalescence of voids which results in failure of the material. Fracture is a response to imposed stress that is static (constant or slowly changing) at a temperature that are low relative to the melting temperature of the material. It can either be ductile or brittle fracture. The former is characterized by substantial plastic deformation in the surrounding of the advancing crack and proceeds at a relatively slow phase as the crack propagate with high-energy absorption. The latter on the other hand proceeds with little or no plastic deformation with low energy absorption

and rapidly sometimes with catastrophic failure. It is noteworthy that crack propagation once initiated will proceed even without an increase in the applied stress. According to Broek (1986), fracture mechanics should answer the following questions: what is the residual strength as a function of crack size? What size of crack can be tolerated at the service load? How long does it take a crack to grow from a specific initial size to the critical size for failure? What size of pre-existing flaw can be permitted at the moment the structure starts its service life? How often should the structure be inspected for cracks?

Prior to the adoption of "safe life" design criteria that requires a longer initialization time for crack, the basic criteria used were:

i. Tensile strength in brittle fracture
ii. Tresca or Von Mises criteria when it comes to yielding and
iii. In the case of fatigue, impact and cyclic loading, toughness or energy absorption was used (Erdogan, 2000).

In the 70s, a new design criterion was developed based on the ability to monitor cracks initiation and propagation resulting from cyclic loading, corrosion and other causes. This ensures that there is an extended growth life for a crack, which is larger than the pre-determined service loads accrued.

The general assumption when it comes to fracture mechanics is that all materials contain flaws inherent in them that become the nuclei. This was the basis of Griffith paper of 1920 where he postulated the existence of flaws in a glass where stress is concentrated at the crack tip, breaking the atomic bonds, which ultimately results in splitting the body in two.

Earlier on in 1913, Inglis has presented his approach based on perfectly elastic material to determine the stress intensity at the edge of the crack using stress concentration factor. As this factor approach an infinite stress in a very sharp crack, stresses induced internally approaches infinity at the sharp crack-tip which was the paradox of his theory because it is not realistic, as no material is capable of sustaining an infinite stress.

On the other hand, Griffith proposal based on the global energy balance and modeled based on the second law of thermodynamics that "cracks would initiate, propagate, or continue when the energy decreases." At the tip of the advancing crack, a non-linear zone exist which concentrate stress creating new surfaces that increases the surface energy but reducing the elastic energy. It is important to note that Griffith experiment utilize glass sheet which does not account for plastic deformation ahead of the advancing crack tip which causes a wide variation when the same experiment is conducted on a steel specimen. This variation is due to the plastic zone, a small portion ahead of the crack that yielding takes place. For a small-scale yielding condition, the size of the plastic zone is much smaller than the length of the crack or the body. Under this condition, much of the deformation is elastic, and the crack can attain a steady-state crack. This elastic zone varies from material to material which may range from few nanometers in silica to few millimeters in steel. The discovery of fracture mechanics techniques or methods and subsequent validation lead to two important specializations:

i. Materials engineering
ii. Structural analysis

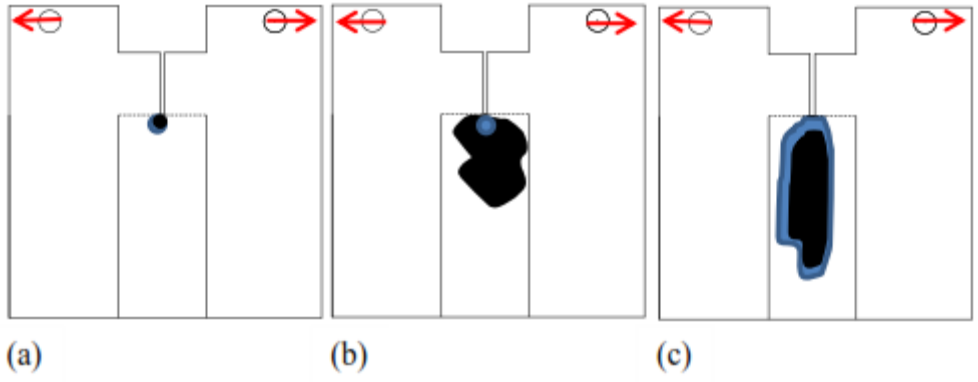

Figure 3.1: Plastic Zone Size in Brittle, Elastic-plastic and Quasi-brittle Materials (Karihaloo, 1995)

3.2 Application of Fracture Mechanics to Cementitious Composites

Application of fracture mechanics is necessitated due to failure of structures resulting from cracking out of which some might occur with disastrous consequences. However, the ultimate goal of fracture analysis is better understanding of crack widths and dimensions; deformations as a result of service loads; to be able to provide safety factors for ultimate loads as well as to have a better understanding of response of post-failure during collapse. There are three failure modes that normally occurs as a result of fracture, however, it is worthy of mention that most crack mode in concrete is mode I fracture.

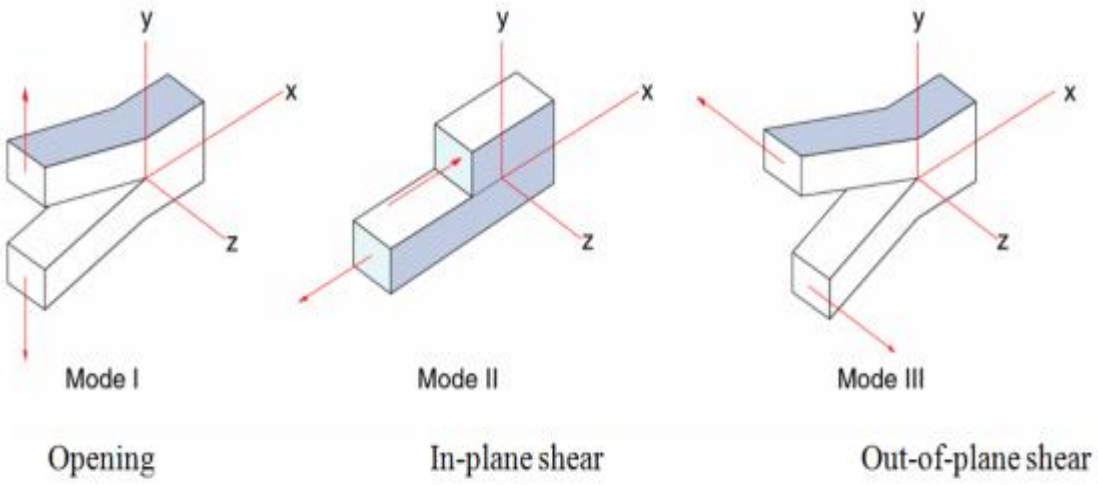

Figure 3.2: Crack Failure Modes (Asmaro, 2013)

In a sharp crack or notch, the stress along the crack plane is of the form:

$$\sigma = \frac{K_I}{\sqrt{2\Pi x}} + C_1 + C_2\sqrt{x} + C_3 x + \cdots \quad (3.1)$$

Where C_1, C_2, C_3, … is dependent on loading and geometry, ~~as X~~ →0 near the crack tip. K_I describes the intensity of the stress in the vicinity of the crack called the stress intensity factor, which depends on the applied stress, and is a function of the geometry of the structure and crack length:

$$K_I = \sigma F\sqrt{\Pi a} \quad (3.2)$$

'σ' is the applied stress, 'a' the crack length, and 'F' depends on geometry

The subscript attached to the K represents the mode of crack, where there are three basic modes represented in Figure 3.2. There are situations where two or more modes occur simultaneously (mixed-mode fracture), and a useful relationship for this mode is the one relating load and structural dimension:

$$K_I = \frac{P}{b\sqrt{d}}\, f(\propto) \quad (3.3)$$

Where P is the applied load, b panel thickness, and d panel width. f (α) is given based on the span to depth ratio for a geometry of 4:

$$f(\alpha) = 6\sqrt{\propto}\left\{\frac{1.99 - \propto(1-\propto)(2.15 - 3.93\propto + 2.7\propto^2)}{(1+2\propto)(1-\propto)^{3/2}}\right\} \quad (3.4)$$

where α is a/d the relative crack length. From the theory of LEFM, K_{IC} otherwise known as fracture toughness can be determined using three point bend test as:

$$K_{IC} = \sqrt{E'G_c} \quad (3.5)$$

Where *E'* is the elastic modulus, and G_c the critical energy release rate. However, the application of LEFM is only limited to materials such as glass, ceramics etc. where there is small plastic deformation.

3.3 Fracture Mechanics of Concrete

Concrete structural sections may be under the influence of tension, compression, flexure or bending, or sometimes a combination of flexure and compression which might lead to failure of the member ultimately. It is known that concrete is weak in tension which is about 10 – 15 % of its compressive strength; in high-strength concretes, the brittleness increases with an increase in compressive strength. Cracks, flaws and voids present in the concrete coalesce under tension and eventually leads to failure perpendicular to the axis of the specimen. In essence, cracks extends perpendicular to the applied load, on the other hand, under compressive loading, crack extends in the same plane as the applied load. Shah *et al.*, (1995) have attributed the lower value of tensile strength to strain localization compared to tension.

The mechanism of crack propagation can be explained in terms of damage mechanics or fracture mechanics based on the above. The former characterize the linear portion of the stress – displacement diagram up to the point where distributed cracks forms, while the latter explains the portion where strain localization begins to manifest with macrocracks growth due to coalesces of those multiple

microcrackings. This coalesce of cracks eventually leads to the failure of the member by weakening or making it unsafe for use. It was on this basis that fracture mechanics was developed which aid in materials selection and design so as to minimize damage or fracture. Prior to that, stress-based failure criteria was utilized which had the demerits of not accounting for larger cracks or flaws present in the member.

The applicability of fracture mechanics involves thorough inspection to ascertain the presence of cracks and their geometry so as to provide remedy or repair before its causes catastrophic failure. It is known from the concept of fracture mechanics that linear elastic fracture mechanics (LEFM) allows infinitely large stress at crack tip, and since at a point plastic deformation has to develop ahead of the crack. As a result of the existence of small scale yielding, the region ahead of the crack can be characterized by stress intensity factor, hence the load carrying capacity can be found by the fracture toughness (K_{IC}) and crack size of the material and maximum applied stress becomes less than tensile strength, f_t.

RILEM TC 50-FMC outlined the following points as some of the reasons why the principles guiding the application of fracture mechanics may not be completely suited for concrete without modifications:

i. The fracture process zone (FPZ) in concrete may be as much as 100 mm when at maximum load, while in the conventional approach it is assumed small relative to the structural size.
ii. In the fracture zone of concrete, stresses decrease with an increase in the load, which is not the case in the original theory, stresses increases or remain constant with load increase.

iii. The fracture mechanics principles consider an already existing crack, however in concrete, there is strong interest in how the crack is formed and subsequently what happens afterwards.

These points enumerated makes it imperative to develop models that can analyze those problems highlighted; Van Mier (2010), echoed that there is no precise agreement as to the size of the FPZ, but in some cases, the size might be bigger than characteristic length, l_{ch} of the structure. In rocks and ice, it thus becomes a global parameter instead of local effect. The consequence is that if FPZ size equals or is larger than l, then size-effects and boundary conditions effects will play a dominant role.

In general, FPZ consumes a lot of energy supplied by the applied load, and as such, crack can propagate steadily even before the peak load is reached. Therefore, it results in a stable crack growth before the peak load. This will result in the avoidance of catastrophic failure; the stress start reducing gradually when the peak load has been attained producing a tension softening stress-strain relationship.

3.4 Crack-tip Plasticity and Crack Bridging Mechanism

The existence of an infinite stress in real life materials is nearly impossible, because no material can sustain infinite stress without failure, however, a sharp crack could be sustained, thus converting the infinite stress to a finite value of stress.

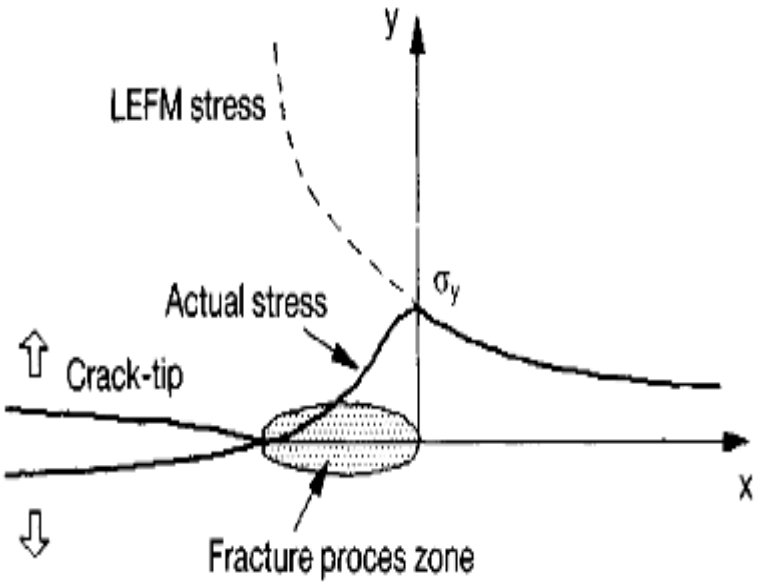

Figure 3.3: Stress Distribution ahead of the Crack (Shah and Ahmad, 1994)

It is note worthy that in the vicinity of the crack-tip, a plastic zone exist where large plastic deformation can take place. This is prevalent in metals (ductile materials) where the sharp tip of the crack is blunted to small non-zero radius to convert the infinite value to finite. In polymers, however, this phenomenon is called “crazing” where a craze zone exist characterized by an elongated fibrous bridging structure. This same phenomenon in brittle materials such as ceramics is depicted by the existence of multiple microcrackings ahead of the cracks redistributing the high stresses that elsewhile exist near the crack-tip sending these stresses farther away making it possible to have a finite value (Dowling, 2013).

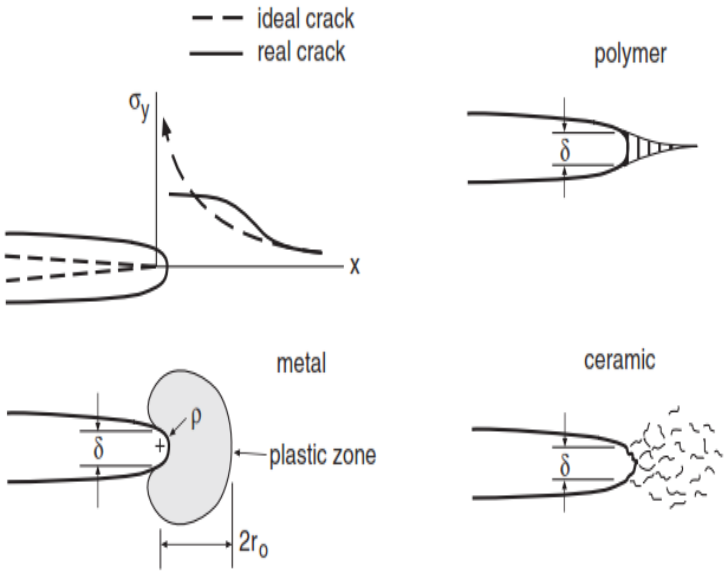

Figure 3.4: Crack-tip Plasticity in Different Materials (Dowling, 2013)

In concrete, due to its heterogeneity, the inelastic zone ahead of the crack is what is called fracture process zone (FPZ) characterized by a series of complicated processes taking place. According to Mindess and Diamond (1982) this region is very tortous and complicated, and results in complex crack process. It has been reported (Shah *et al.*, 1995) that some toughening mechanism are responsible for the fracture processes in concrete resulting from the inherent flaws in the concrete created from shrinkage cracks, air voids, and pores. Cracks in concrete when they initiate will continue to propagate in a random fashion along the crack path and decrease in density with an increase in length (Krstulovic-Opara, 1993). In essence, cracks follow path of least resistance, and might be blunted when a void is encountered, deflected when it comes in contact with an aggregate or even split and branch in the process.

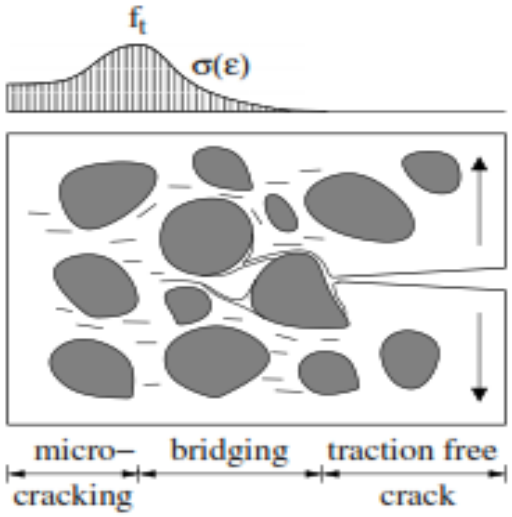

Figure 3.5: Microcracking, Crack Propagation, Deflection, Tortousity of Crack Path (Karihaloo, 1995)

Regarding deflection, when the aggregate particle is more stronger and presented an obstacle in front of the crack, going round the aggregate shows that the matrix is weaker. In crack branching, more energy is dissipated in order to form new branches. These processes are some of the limitations that restrict the use of LEFM in concrete, hence the FPZ, its size and processes that occur must be determined (Shah *et al.*, 1995).

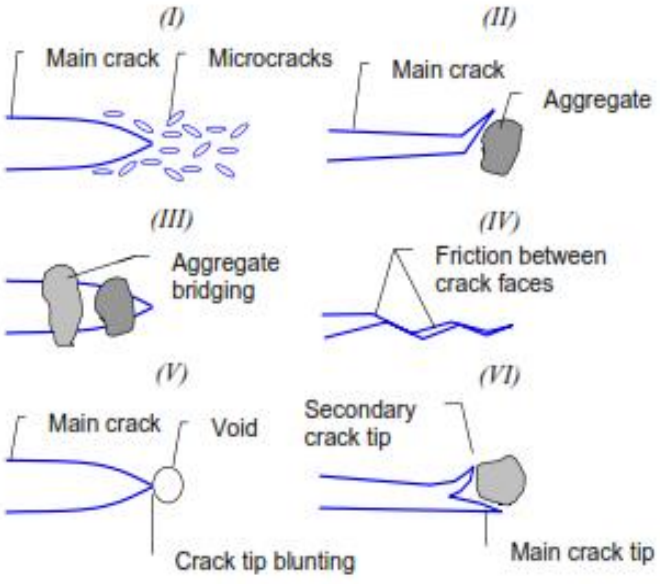

Figure 3.6: Toughening Mechanisms (Shah *et al.*, 1995)

In crack bridging, crack propagate and pass the aggregate particle inducing stresses up to the point of rupture dissipating high energy due to friction between the aggregate particle in the process. The crack continue to propagate between the matrix-aggregate interface, and when the concrete reaches peak stress, strain localization begins leading to bridging and branching of the crack. Concretes with fiber addition have similar processes, however, the ability of the crack to close properly depends on the width of the crack (with smaller cracks bridging quickly as a consequence), and the fiber bridging capacity (Babafemi, 2015).

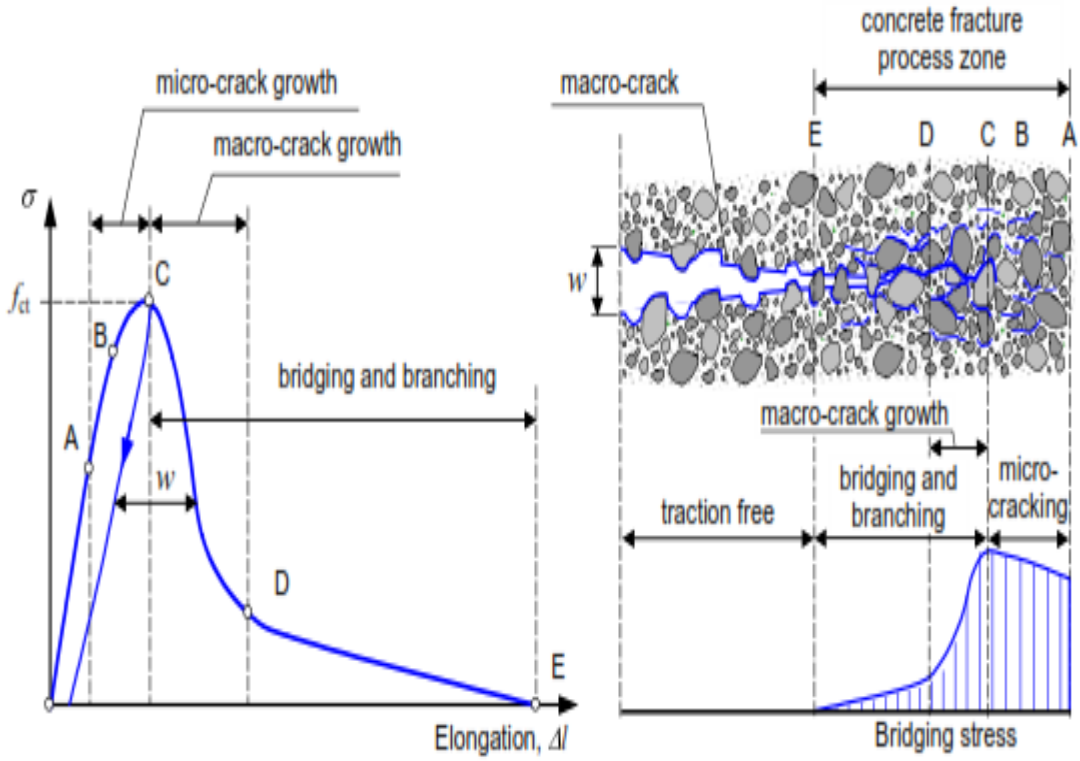

Figure 3.7: Fracture Processes in Uniaxial Tension (Löfgren, 2005)

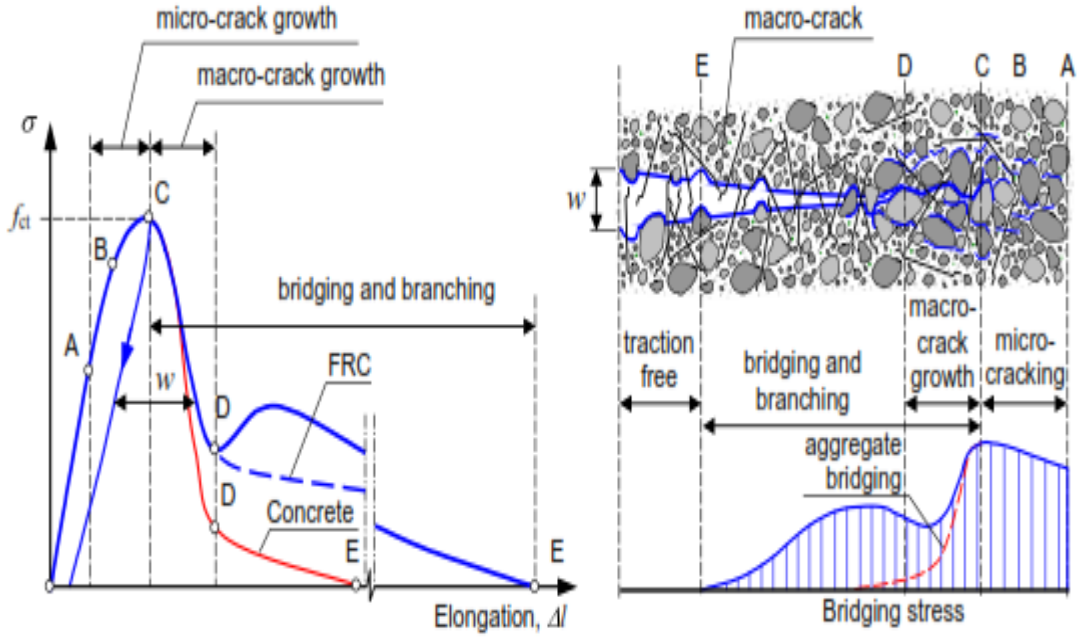

Figure 3.8: Effect of Fibers on Fracture Processes in Uniaxial Tension (Löfgren, 2005)

The action of the fiber leads to a reduction in crack-tip stress intensity factor (Singh *et al.*, 2004). Fiber bridging capacity is influenced by factors such as orientation of the fiber, fiber volume, aspect ratio, geometry, the interface strength and compaction of the matrix (Babafemi, 2015).

3.5 Concrete Fracture Parameters

Fracture of quasi-brittle materials is a complex process and many basic phenomena is still unclear (Shah *et al.*, 1995). The presence of FPZ in concrete also creates a conundrum, and that means the concept of fracture mechanics cannot be directly applied in other to fully describe the failure mechanism in concrete. Other factors include the tortuosity of the crack path, as well as the crack bridging and other processes in the direction of the path.

In the fictitious crack model, the most important material parameters are the tensile strength, f_t, fracture energy, G_F, and crack separation, σ (ω – separation

displacement). The fracture energy is the energy absorbed per unit area of crack, and is regarded as a material fracture parameter. Higher fracture energy means increased resistance of material to crack formation and opening. It is calculated as the total energy consumption divided by the cross-sectional area of the ligament over the notch. However, G_F has come under severe criticism on using it as a sole parameter to measure fracture toughness of a material because of the inclusion of the ligament area which consists of the FPZ and elsewhere. On the other hand, if energy absorption outside the FPZ is assumed to be purely elastic and considering energy absorption to take place only in the FPZ, then it will be considered that stresses are low in substantial part of the beam. In most cases, a deep notch is applied to keep the bending moment low, resulting in a low value of peak load.

It is known that the tensile strength of concrete is less than one-tenth of its compressive strength, and an increase in the former, results in an increase in the brittleness of concrete, and in the cohesive crack model resistance to crack is evaluated by tensile strength, f_t. This lead to the concept of characteristic length l_{ch} defined by Hillerborg (1985) as proportional to the length of the FPZ at crack growth, and is entirely dependent on the compressive strength of concrete. This parameter is a material property:

$$l_{ch} = \frac{EG_F}{f_t^2} \tag{3.6}$$

Where E is the elastic modulus of the concrete

Typical values of l_{ch} ranges from 5 – 15 mm in hardened cement paste, 100 – 200 mm in mortar, 55 – 200 mm in normal concrete, and 2 – 20 m in steel fiber concrete (Hillerborg, 1983). The heterogeneity of concrete increases the values of l_{ch}, an indication that the concrete becomes less brittle due to tortuosity of the crack path.

The maximum size of the aggregate and roughness of the fracture surfaces are some of the factors that influence l_{ch} (Van Mier, 1997; Beygi *et al.,* 2014).

3.5.1 Influence of Aggregate Size on Fracture Energy, G_F

The variation in values of G_F is due to coarse aggregate present in the mix, which increases the tortuous path of the crack. It is known that crack prefers path of least resistance when it propagates such as ITZ and other deficiencies that may exist in the concrete. An increase in the size of the aggregate results in high energy absorption to create a unit crack, hence the reason for the increase in G_F. Concretes with smaller size aggregates are subjected to less stress compared to their counterparts with larger size due to a considerably higher specific surface, and thus would have lower G_F and less tortuous path (Rao and Prasad, 2002). There is a diminished likelihood of bond stresses at the interface making bond failure less likely to occur. And in most concrete with silica fume addition, the interface is very strong behaving similar to a composite. This leads to an improvement in the ITZ and porosity of the concrete in comparison with the larger sized aggregates. Transgranular type of fracture in coarse aggregate has been reported to be the dominant effect in concrete with silica fume addition with the interface becoming stronger (Tasdemir *et al.,* 1996). It has been opined by Hillerborg (1985) that an increase in maximum size of the aggregate from 8 – 20 mm results in an increase in G_F, and this has been backed by Bazant and Oh (1983). Also, Zhou *et al.,* (1995) stated that the increase is accompanied by increased stiffness. This increase in G_F with respect to D_{max} is with concrete strength (Giaccio *et al.,* 1993). In the opinion of Rao (2001), this increase in G_F with strength in HSC, the total energy dissipated is utilized in either to overcome the surface force, or the cohesive forces due toughening mechanisms mentioned earlier in the FPZ.

In general, G_F, increases with maximum size of the coarse aggregates, concrete strength, and deceases with an increase in f_t.

3.5.2 Influence of Aggregate Size on Characteristic Length, l_{ch}

In the past, characterization of concrete resistance to crack propagation was done using a single parameter which was not enough, since the brittleness of concrete increases with compressive strength. Concrete brittleness which is the measure of the concrete ductility is evaluated using characteristic length which is proportional to the length of the FPZ. The higher the value of l_{ch}, correspond to a higher ductility in the concrete and higher resistance to cracking. With increased concrete strength, l_{ch} have been shown to decrease drastically, and HSC have presented values twice lower than NSC (Giaccio *et al.,* 1993). This decrease has been attributed to strengthening mechanism of the interfacial bond by the cement paste-aggregate (Rao and Prasad, 2002). In concrete with silica fume addition, l_{ch} has been shown to decrease resulting from the increased brittleness of the concrete, and cracks traverse the aggregates as opposed meandering round the aggregate particle due to tortuosity (Tasdemir *et al.,* 1996). Zhou *et al.,* (1995) also reported a decrease in the value of l_{ch} resulting from an increase in f_c attributed to low w/b ratio.

The effect of aggregate size on the other hand results in an increase in the value of l_{ch} with increase in the size of the aggregate due to weakening of the ITZ and meandering of the crack path when large aggregate particles are encountered. Petersson (1980) reported that l_{ch} increases with maximum size of the aggregate. The work of Giaccio *et al.,* (1993) also agrees well with their findings. Tasdemir *et al.,* (1996) reported that G_F and l_{ch} depends strongly on the size of the aggregate increasing with an increase in D_{max}. It has also been linked to the roughness of fracture surfaces resulting from large aggregate particles (Beygi *et al.,* 2014).

However, in HSC, this roughness is virtually non-existence and is smooth especially in concrete with silica fume addition (Sabir *et al.,* 1997).

3.5.3 Influence of Steel Fiber on Fracture Energy, G_F

Steel fiber-reinforced concrete has found a wide range of utilization especially in structures subjected to impact where they serve to improve the toughness resistance of these structures. It is also known that crack resistance increases with compressive strength, however, in the event of fiber addition, resistance of concrete to crack increases considerably (Gettu and Shah, 1994). This is because fibers bridge the gap between adjacent microcracks which serves to delay the initiation of cracks and limit the propagation, producing a small crack opening displacement. They control the opening as well as the propagation of the cracks resulting in very high fracture energy. It has been shown that the fracture energy increases with increasing tensile strength of the fiber (Sahin and Koksal, 2011). According to Van Mier (1997), the fracture energy of concrete increases due to one of the following: when mixture becomes heterogeneous, due to fiber addition in the mixture, and when concrete strength increases. The role played by fiber in concrete is to increase the energy needed for fracture from crack arresting mechanism, fiber pull-out, and debonding during the fracture process by forming a bridge that results in tortuous crack path (Bayramov *et al.,* 2004). However, the behavior of the fibers during the aforementioned mechanisms depends on the volume fraction, aspect ratio of the fiber, orientation and distribution. It is the opinion of Kazemi *et al.,* (2017) that V_f has a direct influence on the fracture energy, the higher the V_f, the more the number of fibers will intersect the fracture plane requiring more crack energy. Also, Koksal *et al.,* (2013) concur, and added that the tensile strength of the fibers and matrix strength are the two most significant factors which should be considered in the mix

design. Values in excess of 22,027 N/m have been reported by Koksal *et al.,* (2013); Van Mier *et al.,* (1996) reported that in reactive powder concretes with 3 mm long fiber, fracture energy up to 20 – 40 kN/m have been obtained; Ono and Ohgishi (1989) which was reported in Van Mier (1997), that at 3 % steel fiber addition, fracture energy as much as 48,670 N/m have been obtained from four-point bending test.

3.5.4 Influence of Steel Fiber on Characteristic Length, l_{ch}

It has been highlighted that l_{ch} becomes higher in concretes that are more heterogeneous decreasing the brittleness resulting in an increase in the ductility and fracture energy, transforming the concrete from quasi-brittle to ductile. The addition of fibers in concrete results in large values of l_{ch} especially at higher V_f (Bayramov *et al.,* 2004; Aydin, 2013; Kazemi *et al.,* 2017). Fibers with high tensile strength have also been found to produce high values of l_{ch} compared with their counterparts with low tensile strength (Sahin and Koksal, 2011).

3.5.5 Fracture Toughness, K_{IC}

From the theory of fracture mechanics, the stress intensity factor K_I depends on the magnitude of the applied load, on the other hand, fracture toughness K_{IC} is a material parameter that when it is unstable rapid crack propagation occurs. In other to prevent brittle failure, K_{IC} is used in design (Shah, 1988). When $K_I < K_{IC}$, the material is stable. In concrete however, aggregate particles are stronger than the ITZ, and crack propagation proceeds in the ITZ or within the paste. When the matrix strength is stronger than that of the aggregate, then the crack will propagate in a transgranular fashion into the aggregate. This happens only when $K_I > K_{IC}$. The implication is that resistance to crack growth increases with increase in compressive strength, and in concrete with fiber addition, this increase is significant (Gettu and Shah, 1994). K_{IC}

increases with an increase in compressive strength (Zhou *et al.*, 1995) which is consistent with what has been reported by Shah (1988). However, the disadvantage is that the concrete becomes more brittle, which can be overcome by fiber addition.

3.6 Microcracking and Crack Propagation Mechanism

Concrete is known to be a brittle material with very little plastic deformation, and failure results from microscopic flaws in the concrete according to postulation by Griffiths (1920) where the weakest flaw will be the source of the failure. These defects and flaws only propagate and coalesce to form large cracks when there is stress concentration in front of the advancing cracks that results in the FPZ. This is what is obtained in a typical normal concrete, but in HSC where the microstructure is dense and multiple individual microcracking exists, the cracking is not as extensive as in the former. A number of reasons are responsible such as the matrix strength, the presence of an obstruction such as aggregate which discontinues the process, steel fiber that arrest the mechanism or even hcp (Gettu and Shah, 1994). If the load is increased further, the crack meander ahead of the obstruction where the possibility of branching is increased [Van Mier (1991); Mindess and Diamond (1982); Diamond and Bentur, (1985)].

In a nutshell, the process zone in concrete is caused by microcracking, crack bridging and separation due to frictional effects (Gettu and Shah, 1994). However, there have been a lot of contradictory evidence on the existence of the process zone, but holographic interferometry by some researchers (Miller *et al.*, 1988; Castro-Montero *et al.*, 1990) concluded that strains behind the tip of the crack gradually decreases to zero, and the energy dissipation near the crack faces is most significant. They went on to define this zone as “the region where the experimentally determined strain-field

deviates considerably from linear elastic fracture mechanics (LEFM)". Also, in the view of Gettu and Shah (1994), all shielding mechanisms can be lumped into a conceptual FPZ that lies ahead of the traction-free zone of the crack or in the wake of the 'actual' crack front. This zone can also include the toughening effects of other inelastic mechanism such as the crack-deflection and crack-bowing.

Cracks in concrete follows path of least resistance, and subsequently, are considerably tortuous with rough crack-faces. In mortar, the crack follows the interfaces between the sand grains and the hardened cement paste, and when cement paste consists of silica fume, the roughness on the crack – face is less (Mindess and Diamond, 1982). Since the weakest phase in normal concrete is the aggregate-mortar interface, cracks tends to avoid the aggregates and propagate through the interfaces (Hsu *et al.,* 1963). In silica fume concrete, the interfaces and the mortar are much stronger, and therefore cracks are less tortuous and sometimes pass through the gravel (Carrasquillo *et al.,* 1981; Bentur and Mindess, 1986; Van Mier, 1990). Also, cracks propagate through coarse aggregates that are weaker than the mortar, as in lightweight concrete (Faber and Evans, 1983; Bentur and Mindess, 1986). The tortuosity of the crack gives rise to a higher R (crack extension) value due a larger surface area.

The existence of microcrack or very fine cracks in concrete is known even prior to loading, and this can be attributed to the mismatch between the properties of the aggregate and cement paste, as well as shrinkage and thermal movement. In terms of size that defines microcracks, there is no agreed upon size range for the definition of microcrack. The most widely accepted one is that of the upper limit for microcrack proposed by Slate and co-workers from Cornell University. Also, Jornet *et al.,*

(1993) proposed an upper limit of 0.1 mm, which is the smallest size that can be visible to the human eye. When load is increased up to 30 % of the ultimate, these cracks begins to multiply in number, length and width. This increment is dependent on the water-cement ratio (Neville, 1995). Beyond 60 % and between 70 % and 90 %, mortar cracks manifest and subsequently continuous cracks forms. There is a slight variation in the stress level at which this last stage occurs in HSC compared with normal concrete, where it is relatively delayed. The beginning of continuous rapid crack propagation corresponds to discontinuity stress point. It should be noted that the aggregate-cement paste boundary which is the weakest link in concrete and the place where these microcracks or flaws are concentrated, at the same time, coarse aggregate serves as crack arrestors.

In a notched flexural specimen, when the depth of the notch is small, there is the possibility that the advancing crack may likely meet a considerable amount of coarse aggregates responsible for the tortuous region during crack propagation. With silica fume addition, the porosity of the concrete is greatly reduced, improving the ITZ and homogeneity of the concrete. On the other hand, in normal concrete, crack path follows a direction round the coarse aggregate while in the former; it passes through the aggregate by breaking them due to improvement in the matrix strength (Sabir *et al.*, 1997).

According to Hsu (1963), the amount of internal tensile stresses that build up depends on the spacing of the aggregate, and when this distance (aggregate – aggregate radius) is less than 0.20, there is a build up at the aggregate-matrix interface of tensile stresses. However, in most concrete, this value is between 0.05 – 0.20. this has been confirmed by photoelasticity, it is either the shortest distance

between the adjoining aggregate otherwise referred to as tensile hoop stress or by hydrostatic tension resulting from the midpoint of the widest clear distance between aggregates [McCreath, (1968); Theocaris and Koufopoulos (1969)]. It has also been shown that as the size of the maximum size of the aggregate decreases, the bond strength increases, and a point would be reached where the paste and the bond strengths would be equal (Alexander and Wardlaw, 1960).

The features of the crack initiation have been shown to follow the order (i) aggregate cracks having an inclination angle to the applied stress of 45° (ii) large aggregates with sides bond cracks (iii) the existence of air voids (iv) the exhibition of local segregation by large aggregates (Moavenzadeh and Bremer, 1969).

Jones and Kaplan (1957) cited in Neville (1995, pp. 292) argued that there are valid reasons to suggest that the mechanism responsible for initial cracks in uniaxial compression and flexure are the same. This is because cubes that were pre-cracked and tested in compression produced what they termed “local” breakdown of adhesion between coarse aggregates and cement, the pre-cracking process was observed not to be the immediate source of fracture. On one hand, flexural specimens pre-cracking was the immediate cause of the fracture, leading them to conclude that the mechanisms are the same.

3.7 Discontinuity Stress Region in Concrete

A comprehensive study into the gradual failure mechanism in concrete began with Richart *et al.*, (1928; 1929) when they noticed progressive increase in concrete volume during uniaxial compression test around 75 - 85 % of the ultimate load, and they called this point the “critical load.” In other to develop a failure theory, they

made the assumption that this point signifies the onset of gradual disintegration internally of smaller sections inside the concrete (Hsu, 1984). The work of Jones (1952) reported "crackling noises" at about 25 – 30 % during a fracture study by sonic means at the ultimate load, this same occurrence was heard by L'Hermite (1954) at 50 – 75 %. Five years later, Rusch (1959) and Sell (1959) observed that same noises at 50 % but it became more pronounced at 75 %. What all these researchers agreed upon is that modifications to the concrete takes place up to 75 % of the ultimate load (Hsu, 1984). Years later, at Cornell University, a study by Hsu *et al.*, (1963) on a sliced cylindrical specimen loaded to specified strains revealed that:

i. Shrinkage cracks from carbonation, hydration, and drying, exist in the concrete that forms into bond cracks prior to loading.

ii. With increasing strains, these bond cracks increases in size, length and width are insignificant at about 30 % of the load ultimate which translate to the linear portion of the graph. However, as they begin the multiply and coalesce above 30 % to around 70 % increasing the bond cracks probably explain the observed curvature in the stress-strain diagram.

iii. At 70 – 90 % of the ultimate load, mortar crack patterns multiply and the shape of the stress-strain diagram distinctly changes and approaches parallel to the x-axis. This sudden change explain three things observed that was highlighted above:

    a. This loading level corresponds with the critical load that was reported by Richart *et al.,* accompanied by the volume expansion of concrete.

    b. It also concurs with the sustained strength and lastly;

    c. The elevation of noises noticed by Rusch, Sell, and Jones.

In summary, Hsu (1984) outlined this process with a single definition incorporating what happened as climax of 'quasi-elastic' behavior, long and sustained strength, point of continuous increase in Poisson's ratio, and continuous propagation of mortar cracks, calling it *Discontinuity Stress* a term coined by Newman (1968) which characteristics was described. However, what has been extremely difficult is the measurement of this stress. Attempts have been made by Robinson (1967) and Vile (1968) using acoustic measurement. Shah and Chandra (1968) found that microcracking increases with increase in the loading as well as the duration of cyclic loading. A series of experiments using Biaxial loading was conducted at Cornell to measure the discontinuity stress and the ultimate strength by Buyukozturk *et al.,* (1971); Liu *et al.,* (1972); Carino and Slate (1976); Tasuji *et al.,* (1978) and it was established that the discontinuity stress was 76 % of the ultimate load. In zones of a combination of compression - tension or biaxial tension, the discontinuity point was taken as where stress versus maximum tensile strain turn, showing a significant departure from the straight line which was 63 %.

The work of Hsu (1984) conducted a fatigue strength test using the Wohler curve (so-called *f*-N curve) in other to give a measurable definition to discontinuity stress, and he found that mortar cracks forms continuous network at low - cycle, and the fatigue strength is above the discontinuity stress. On the other hand, microcracks develop into bond cracks in a slow gradual process in high-fatigue cycle where the strength is below the discontinuity stress, and on this basis a definition of discontinuity was derived based on fatigue cycles by what he called a measurable "kink". This "kink" region is an intersection point of two planes which above and below represents discontinuity stress in high (bond cracks) and low (mortar cracks) cycle of fatigue stress.

3.8 Models that Characterize Crack Propagation Mechanism

Compressive failure in concrete is largely due to crack propagation that might have been caused by factors such as thermal and shrinkage cracking, segregation of the mix constituents as well as inherent flaws existing in the concrete at the interface (Shah *et al.*, 95). It is well known that the strength of concrete in compression is much better than that in tension, and in concrete prior to loading, flaws (interfacial cracks and matrix voids) exists within, and upon sustained loading, interfacial cracks give rise to a major crack. Mehta and Monteiro (2014) have attributed this phenomenon to (i) the size of interfacial crack being much larger than matrix voids; (ii) the weak nature of ITZ which results in weak fracture resistance. Shah *et al.*, (1995) summarized the failure process in uniaxial compression of concrete as:

i. Initially, there is an increasing linear relationship between stress and strain, and at approximately 30 % of peak stress, microflaws begin to open;
ii. This is closely followed by a point which corresponds to about 50 % of the peak stress were interfacial flaws manifest characterized by propagation of bond cracks in different directions as a result of aggregate shape;
iii. At about 80 % of the peak stress, those bond cracks propagate, and coalesce into the matrix as a single crack or multiple major cracks in the direction of the applied compressive load (strain localization);
iv. Those multiple major cracks developed earlier, might reach a critical length as a result of strain localization and the failure of the specimen is accelerated. At that point, the specimen might have reached its peak compressive stress, and beyond this point, these major cracks continue to propagate even at decreased load, and a strain softening type of branch is observed from this point. Shah and Chandra (1968) opined that a loaded specimen continue to

contract up to a point before strain localization, and beyond that point the volume of the concrete increase. However, in HSC, as a result of interfacial bond improvement, the interfacial bond might not be the source of crack initiation (Shah *et al.*, 1995).

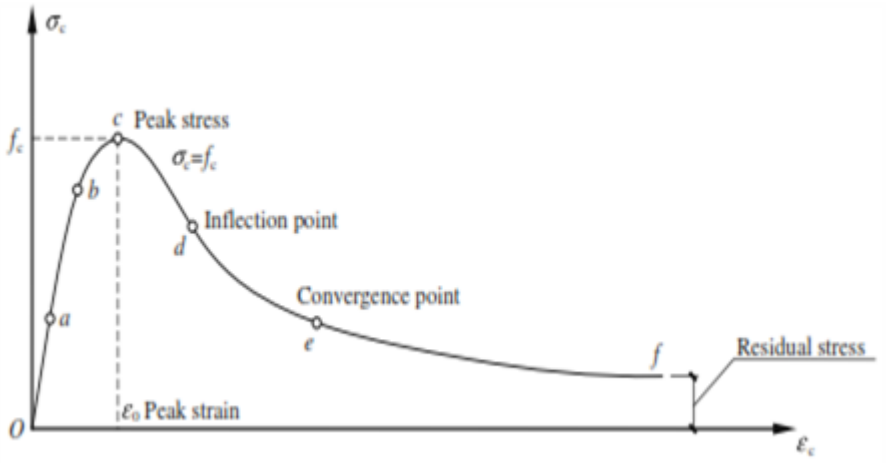

Figure 3.9: Stress-Strain of a Prismatic Concrete under Uniaxial Compression (Ghou *et al.*, 2016)

Figure 3.9 is similar to what was described by Shah et al., (1995) were the ascending portion OC can be analyzed using Damage Mechanics, while the descending portion CF can only be analyzed using Fracture Mechanics due to nonlinear processes taking place. Shah and Sankar (1987) monitored concrete cylinders in uniaxial compression and presented a stress-axial displacement relationship. They reported that there is a uniform lateral displacement with specimen height up to 80 % of the peak load, however the deformation was observed to be faster, an indication of strain localization. They also used petrographic techniques to observe longitudinal and transverse crack patterns at each deformation level that the specimen was loaded. Observations were that up to 83 % of the peak load cracking was basically bond type between coase aggregate and mortar matrix and were uniformly distributed in both

directions. These bond cracks coalesces when the applied stress was increased. At postpeak, these cracks were extensive and uniform in both transverse and longitudinal directions. The work of Shah and Chandra (1968) reported a substantial increase in volume of the specimen beyond 80 % of the peak load.

A number of models have been proposed for the study of stress-strain microfracture such as Shah and Winter (1966) on a single cylindrical circular aggregate model simulating structural response of concrete under uniaxial compression. The basic assumption was that aggregate and matrix were linear elastic materials, while interfacial bond was assumed to have an elastic-plastic stress-strain relationship. They reported that the bond between the matrix and aggregate was linear from the beginning as a result of lower strength offered by the bond layer, until the yield stress is reached at a certain load generating a yield zone (bond crack that propagates with an increase in loading). Beyond the yield, the stress-strain relationship becomes linear. It is widely accepted that non-linearity of the stress-strain curve is as a result of bond cracking. Shah and Winter's model was capable of predicting the stress level at which bond cracking will start and the onset of matrix cracking. Buyukozturk *et al.,* (1971) improved on the Shah and Winter's model incorporating nine cylindrical aggregates placed in three rows, and finite element analysis conducted on the different phases; results were used in the study of coalescence of isolated bond cracks that initiates at aggregate interfaces after strain localization. Finite element analysis reveals the initiation of cracks occur at a weak bond layer in the vicinity of the various aggregates at 70 % of peak load, and these cracks propagate into the matrix. Upon further increase in loading, the major cracks multiplied and eventually the system fails at peak stress, and predicted crack patterns correlated well with experimental observations as they reported.

A study by van Mier (1986) on the effect of specimen height on the stress-strain relationship indicated that for the three specimens used (L = 20 cm, 10 cm & 5 cm respectively), the relation was almost the same until the peak stress where shorter specimens showed a longer strain-softening curve compared to the long ones. Shah *et al.*, (1995) opined that there is the possibility that some bond cracks extending into the matrix at the onset of strain localization, and that at the aggregate interface, some isolated bond cracks might coalesces into one or few major cracks. The validity of the model is up to about 80 % of the peak stress, the onset of strain localization since matrix cracking plays an important role after strain localization.

It has been reported by Ozturan and Cecen (1997), that in concrete with low w/c ratio and a compressive strength in excess of 40 MPa, the interfacial bond is comparable to that of coarse aggregate strength, and its full potential can be exploited thereby improving the strength of the concrete. They reported a higher tensile and flexural strengths in NSC incorporating limestone aggregate which was attributed to iterfacial bonding due to surface characteristics of the coarse aggregates, improvement in ITZ quality, and mortar strength. In their opinion, appropriate amount of silica fume and a reduced w/c ratio will have a significant influence on concrete tensile strength. A 30 % increase in splitting and flexural strengths were obtained when a cement of higher strength category was utilized in their mix design at the same time keeping other factors constant, leading to the conclusion that tensile strength is influenced by mortar strength in HSC as opposed to compressive strength that is influenced by coarse aggregate surface characteristics and strength.

Wu *et al.*, (2001) investigated the effect of coarse aggregate type on properties of high-performance concrete which was centered on compressive strength, splitting

strength, fracture energy, characteristic length and elastic modulus. It is known that the quality of concrete relies heavily on the properties of the mortar (quality), but with the advent of high-performance concretes, attention has now been focused on the contribution of the aggregate (de Larrard and Belloc, 1997). This can be attributed to the limited amount of water in high strengths and high-performance concretes which improves the quality of the mortar. This makes bond strength similar to strength of the aggregate particles, on the other hand, increasing the brittleness of the concrete. Results of fracture energy of concretes indicates an increase with an increasing fracture energy of the aggregates. As highlighted above, low w/c ratio results in matrix quality in high-strength concretes as well as better monolithic concrete behavior, as such fracture in this case propagates through the coarse aggregate particles in contrast to how it occurs in normal-strength concrete. Thus, highlighting the effect of how influencial the fracture energy of aggregates on fracture energy of concrete. With regards to the characteristic length, l_{ch}, the same effect was observed as that of the fracture energy with an increasing brittleness of the concrete with increasing strength.

Akçaoğlu *et al.,* (2004) investigated the effect of a single coarse aggregate model on the matrix quality of ITZ under uniaxial compression on mortars at two different water-cement ratios. They utilized single spherical steel aggregates of different sizes, and it was observed that the effect of aggregate smooth surface, and large variations between aggregate and matrix moduli had a significant effect on the properties of the ITZ. With increase aggregate size and improved matrix quality, ITZ becomes more critical. Similarly, Akçaoğlu *et al.*, (2005) reported similar findings on microcracking behavior through SEM analysis.

3.9 Influence of Loading History on Residual Tensile Strength

Tensile strength and resistance to fracture can be decreased substantially under the influence of transverse compression, this is because when compressive load is applied distributed cracks run parallel to the direction of the loads (Gettu *et al.,* 1992). The direction of the cracks propagation is important because it determines the fate of the process. According to Van Mier (1985) orientation is significant in concrete under multi-axial loading. In Shah and Sankar (1987), microcracks tends to have a bias towards compression, and are oriented at about 10° with the direction of loading prior to peak.

These cracks that form as a result of the application of pre-compression results in the decrease in tensile strength until a critical stage is these cracks localize resulting in rapid propagation. This damage that results have been quantified and significant losses have been reported depending on the type of concrete.

Tinic and Bruhwiler (1985) reported a 10 – 15 % loss in tensile strength from the application of compressive stress in normal strength concrete. Liniers (1987) observed that transverse loading is more damaging to tensile strength with losses of up to 40 % for NSC increasing with the amgnitude and duration of applied pre-compression. In HSC, Gettu *et al.,* (1992) reported this loss to be around 25 %; Oliveira (1992) tested 100 mm cubes and cylinders with pre-compression from 0.25 f_c – 0.85f_c and found that tensile strength reduces significantly with pre-compression up to 25 %. Lower losses were recorded in HSC due to less flaws inherent in the material. In Akcaoglu (2003), it is reported that microcracking is accompanied by an appreciable loss of tensile resistance in the direction normal to the microcracks.

Extend of damage was highest in low strength concrete and lowest in HSC at all compressive stress levels applied.

This study is predicated on the desire to apply this technique in concrete with steel fiber addition, and understanding the mechanism of microcrack growth subject to loading history in HPC . This will serve to enable accurate prediction of failure behavior of concrete, and enhancing structural performance by combining steel fiber of different aspect ratio in concrete to monitor damage process.

Chapter 4

METHODOLOGY

4.1 Materials

In this section, explanation is presented on the type of materials that were utilized, the methods employed, and an attempt has been made to explanation reasons why those materials and methods were used.

4.1.1 Cement and Silica Fume

Blast-furnace Slag Cement CEM II/B-S 42.5 N that conforms with ASTM C 595 having a specific gravity of 3.15 and silica fume with 82 % SiO_2 content was utilized at 10 % of the cement content.

Literature has shown that HPC class I (50 MPa), II (75 MPa) and III (100 MPa) can all be produced with Portland cement, slag, fly ash and silica fume combination. However, for class IV (125 MPa) and V (150 MPa), until now it has been shown that silica fume is a must (Aitcin, 1998). The use of silica fume comes at a considerable cost because it is 5 – 10 times that of Portland cement; therefore, it has to be really justified before its application especially from an economics point of view.

The dosage of silica fume in other to correct all future lime liberated hydration of C_3S and C_2S shall be within 25 – 30 % which is in turn might require a high dosage of superplasticizer. However, in HPC 3 – 10 % has been successfully applied. It has been found that in class I HPC, dosage between 5 – 10 % give a significant strength

gain, but beyond that dosage strength increase is minimal. Aitcin suggested a range of 8 – 10 % by mass of cement in HPC.

Table 4.1: Chemical Analysis

Property	Cement (%)	Silica Fume (%)
SiO_2	18.72	82.20
Al_2O_3	4.04	0.50
Fe_2O_3	2.56	0.42
CaO	60.44	1.55
MgO	2.00	0.00
SO_3	2.24	3.03
*Loss on ignition	10.88	5.66
**Insoluble residue	0.10	-
Fineness (m^2/kg)	4,007	29,000
Specific gravity (g/cm^3)	3.15	2.2
45 μm residue	5.24	-
Consistency	0.26	-
Initial setting time (minutes)	163	-
Final setting time (minutes)	294	-
28 days f_c (MPa)	41	-

*This shows the extent of carbonation and hydration of free lime and free magnesia due to exposure to atmosphere. BS 12:1991 & ASTM C150-94 allow 3 % while 4 % is allowed for cements in the tropics.

**This is a measure of adulteration of cement arising from impurities from gypsum. BS 12:1991 limits to 1.5 % while ENV 197-1:1992 that allows 5 % content of filler limits to 5 % of the mass of cement exclusive of the filler.

4.1.2 Water and Superplasticizer

High range water reducer GLENIUM 27 was utilized conforming to ASTM C 494 ether brown in color with a density of 1,023 – 1,063 kg/lt, color content < 0.1 % and alkali content < 3 %. Tap water was utilized which conform to BS EN 1008-02 specification.

4.1.3 Aggregates

4.1.3.1 Fine Aggregates

The use of coarse sand with a fineness modulus of 2.7 – 3.0 has been recommended based on:

i. High-strength mixtures are rich in fine particles because of their high cement or cementitious content, so it is not necessary to use fine sand from the workability and segregation point of view.
ii. It also results in a slight decrease in the amount of mixing water necessary for a given workability, which is advantageous from a strength and economic point of view.
iii. The use of coarse sand results in an easier shearing of cement paste during mixing.

However, the general rule is that it should be clean and free from clay and silt, in this study fineness modulus of 3.22 was used.

4.1.3.2 Crushed Stone or Gravel

The significance of this section becomes paramount as the compressive strength of HPC increases; selection process to ensure that the aggregates are strong and can withstand premature failure when used in high-strength concrete.

4.1.3.3 Choice of Maximum Size of Aggregates

This is necessitated by the fact that when it increases, the ITZ becomes more heterogeneous and larger, and smaller aggregates are mostly stronger than larger ones as in most rocks with the elimination of internal defects. In most cases, size ranges from 10 – 12 mm is the best and safe choice for maximum size of aggregates (Aitcin, 1998). In general, aggregates used were crushed limestone rock conforming to the specification of ASTM C 33. Sieve analysis was conducted in accordance with

ASTM C 136, and the result presented Table 4.2 for coarse and fine aggregates, which was depicted graphically with the specified grading limits based on ASTM C 33 in Figure 4.1.

Table 4.2: Particle Size Distribution of Fine and Coarse Aggregates

Sieve Sizes (mm)	Percentage Passing Coarse Aggregate	Percentage Passing Fine Aggregate
12.5	100	-
9.5	100	-
4.75	9.4	100
2.36	0.2	82
1.18	0.2	48
0.6	-	29
0.3	-	17
0.15	-	7
0.075	-	3

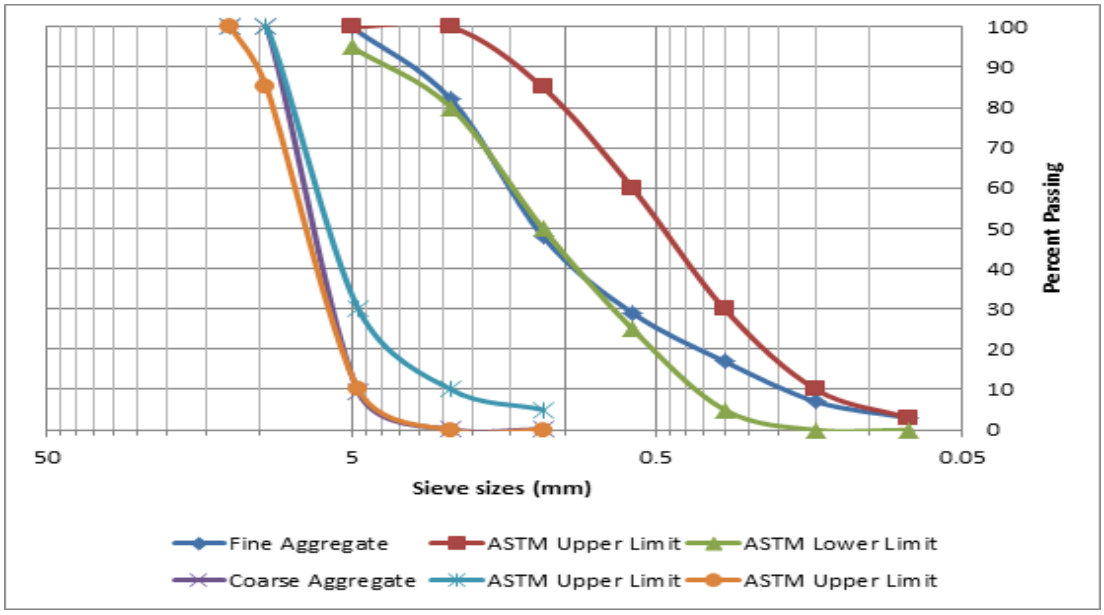

Figure 4.1: Particle Size Distribution of Aggregates

In Table 4.3, physical properties of aggregates are presented for the crushed limestone rock used. Strength property was measured by evaluating the aggregate crushing value (ACV) where the result is less than 35 %. If it has been greater, it would have been an indication of a weak aggregate. Toughness was measured with aggregate impact value (AIV) which is less than 30 %, when it is greater, it is an indication of weakness of the aggregate.

Table 4.3: Physical Properties of Aggregates

Test	Standard	Fine Aggregates	Coarse Aggregates
Relative Density (SSD)	ASTM C 127 & 128	2.68	2.65
Absorption (%)	“	3.0	0.7
Bulk Density (kg/m^3)	ASTM C 29	2083	1203
Void Content (%)	“	25	50
Dust - 75µm (%)	ASTM C 117	3	-
Crushing Value (%)	BS EN 1097	-	22
Impact Value (%)	“	-	7.9

4.1.4 Steel Fiber

Hooked-end steel fibers based on the specification of ASTM A820 with two aspect ratios (60 and 75) were used with a length of 30 mm and 60 mm; diameter of 0.50 mm and 0.80 mm; tensile strength of 1,250 MPa and 1,100 MPa for aspect ratio 60 and 75 respectively. Quantity of steel fiber based on the percentage addition is presented in Table 4.4.

Table 4.4: Volume and Amount of Steel Fibers

S/No	Fiber Volume (%)	Quantity (kg/m^3)
1	0.50	39.25
2	0.75	58.88
3	1.00	78.50
4	1.25	98.13
5	1.50	117.75
6	1.75	137.38
7	2.00	157.01

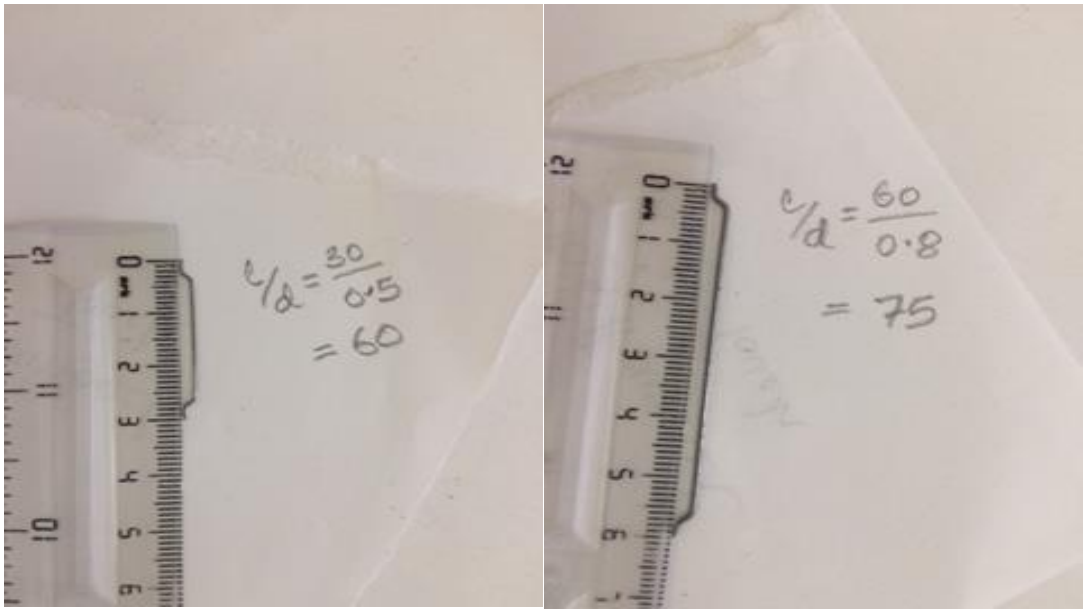

Figure 4.2: Steel Fiber Aspect Ratio Utilized

4.2 Proportioning, Mixing Operation and Casting

In this study, the materials selected were proportioned as seen in Table 4.5, and mixing was done using a pan mixer with a capacity of 150 liters as prescribed for steel fiber in ACI 544.1R with fiber additions at 0, 0.50, 0.75, 1.00, 1.25, 1.50, 1.75, and 2.00 % by volume. The fibers stacked in a fibrillated bundle of water soluble

glue placed last by distribution in small amount to avoid balling. Immediately upon contact with moisture they were dispersed but the mixing time was relatively longer for high volume percentages. To ensure good fiber dispersion, visual inspection was consistently maintained during this stage to ensure adequate dispersing fibers. Fresh concrete mixes were casted in plastic molds and compacted with a 50 Hz frequency (3,000 rpm) vibrating table. They were subsequently covered and placed in the curing room based on the specifications of ASTM C192 and were stripped and placed in the curing tank 24 hours later until testing age.

Table 4.5: Mix Design Utilized

Material	Cement 42.5 N(Slag)	Water	Coarse (D_{max} 10mm)	Fine (D_{max} 5mm)	Silica Fume	HRWR
Quantity (kg/m^3)	470	165	1050	700	47	14

4.3 Methods

4.3.1 Fresh Concrete Properties

VeBe time test was conducted in accordance with BS EN 12350 – 3 and Compacting factor to BS EN 12350 – 4. Slump determination and unit weight of concrete were done to ASTM C143 and ASTM C 138 respectively. These tests were selected because they best describe the behavior of the produced concrete at the fresh state as V_f begins to increase. This is because initial tests (flow and flow table) selected have failed in that regards.

4.3.2 Hardened Concrete Properties

4.3.2.1 Strength Determination Tests

Concrete compressive strength was tested at age of 28 days in accordance with ASTM C39 using 150 x 300 mm cylinders at a loading rate of 0.5 MPa/s at the

beginning, as well as splitting tensile strength using the same dimension based on ASTM C496. However, during the splitting test with cylindrical specimens it was observed that at lower V_f in both aspect ratios, the results were less than 2 MPa in concrete with fiber addition. In comparison to the prismatic specimens when tested based on BS EN 12390 – 3 with 150 mm cubic prisms with a loading rate of 0.5 MPa/s on a 3,000 kN capacity machine for compressive strength and splitting tensile strength of concrete to BS EN 12390 – 6 with same dimension with a loading rate of 0.4 kN/s. In light of the above, a conscious decision was made to switch from ASTM cylindrical specimens to BS EN test based on prismatic specimens. This will have a significant effect in the outcome of the results because in cylindrical specimens' steel fibers align themselves during casting in vertical direction, while in prismatic specimens' fibers align themselves horizontally during vibration.

Flexural strength was determined from notched beams of constant depth of 50 mm, span of the beam was 500 mm, height and width of 100 mm; loading rate used was 0.07 mm/min with a closed loop servo-controlled device 200 kN capacity flexural testing machine. The following formula was used to evaluate the flexural strength:

$$Flexural\ Strength\ f_{\mathrm{r(notched)}} = \frac{3\mathrm{Pmax\ S}}{2\mathrm{b(h-a)^2}} \qquad (4.1)$$

Where P_{max} is the ultimate load, *S*, *b*, *h* and *a* are the span, thickness, height, and notch depth respectively. Strength effectiveness for the compressive, splitting tensile and flexural strengths were determined based on the following formula:

$$Strength\ Effectiveness, fe = \frac{HPC\ with\ Fiber\ Sample - Reference\ Sample}{Reference\ Sample}\ X\ 100\% \quad (4.2)$$

4.3.2.2 Elastic Modulus Test

The modulus of elasticity was determined based on the specification of ASTM C469 Chord Modulus method using 150 mm x 300 mm cylinders after 28 days of moist

curing. The specimens were loaded up to 40 % of the ultimate load at 0.3 MPa/s, and the modulus calculated from:

$$E_c = \frac{\sigma_2 - \sigma_1}{\varepsilon_2 - 0.000050} \quad (4.3)$$

Where:

E_c = Chord modulus of elasticity (MPa)

σ_2 = Stress (MPa) corresponding to 40 % of ultimate load

σ_1 = Stress (MPa) corresponding to a longitudinal strain of 0.00005

ε_1 = Longitudinal strain produced by stress σ_2

4.3.2.3 Load-Deflection Relationship

The load – deflection relationship was determined from three-point bending test on a series of notched beams specimens using two linear variable differential transducers (LVDT) attached to a yoke to measure the average vertical displacement of the beam at the point of fracture. A closed loop servo-controlled device 200 kN capacity flexural testing machine with a loading rate of 0.07 mm/min was used; beam dimension is as given in Section 4.3.2.1. A 50 mm notch depth was kept constant throughout the test to keep the maximum bending moment low for the test based on RILEM TC 50 – FMC recommendation. The size of the beam depends on the maximum size of aggregate (10 mm) and sawing of the notch was done under wet condition a day before the test.

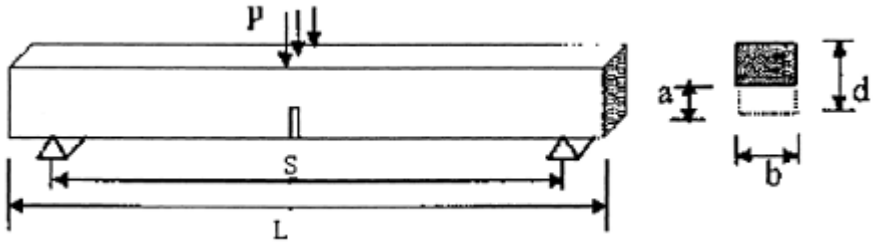

Figure 4.3: Notched Three-Point Bend Test Specimen (Wu *et al.,* 2001)

4.3.2.4 Concrete Fracture Parameters Determination

Fracture parameters were determined using Eqn. 4.4 – 4.8 from Figure 4.3 where the area under the curve (W_o) for the load – deformation diagram was determined using trapezoidal rule in excel spread sheet:

$$AUC\ (W_o) = \Sigma[\frac{(Y0+Y1)}{2} * (X1 - X0) + \frac{(Y1+Y2)}{2} * (X2 - X1) + \cdots] \quad (4.4)$$

The process is continued till the last data point where the summation is taken, and the fracture energy determined from:

$$G_f = \frac{W_o + mg\delta_o}{A_{lig}} \quad (4.5)$$

Where:

W_o = area under load vs deflection curve (N/m)

mg = selfweight between supports of specimen(mass in kg and g = 9.8 m/s^2)

δ_o = maximum displacement (m), in this case 1.5 mm (0.0015 m)

A_{lig} = fracture area [d(b-a)] (m^2)

b & d = height and width of the beam.

It is assumed that energy absorption takes place only in the fracture zone, this implies that all deformations outside this zone are pure elastic and might be true if stresses are low in the major part of the beam. The basic assumption of RILEM TC-50 is that all the energy expanded to create a crack of unit area goes to crack intiation and propagation; and specific fracture energy is found to vary with specimen dimension.

The characteristic length which is an indication of the brittleness of the concrete defined as:

$$l_{ch}\ (m) = \frac{EG_F}{f_t^2} \quad (4.6)$$

Where f_t is the tensile strength (MPa),

Critical stress intensity factor K_{IC}:

$$K_{IC} = \frac{3PS\sqrt{(\pi a_o)}\,F(\propto)}{2bd^2}\ MPa\sqrt{m} \quad (4.7)$$

$$F(\propto) = \frac{1.99 - \propto(1-\propto)(2.15-3.93\propto+2.7\propto^2)}{\sqrt{\pi}\,(1+2\propto)(1-\propto)^{3/2}}\ for\ \frac{S}{d} = 3 \quad (4.8)$$

Where $\alpha = a_o / d$

4.3.2.5 Residual Tensile Strength and Tensile Strength Loss (TSL) Measurement

Initially, the determination of ultimate compressive strength, stress-strain diagram (under deformation control), and splitting tensile strength were all using cylindrical specimens mentioned in Section 4.3.2.1. However, the following problems arose:

i. During the stress-strain test under deformation control, the universal testing machine could not fully plot the diagram because of the duration of the test. The hydraulically operated machine became hot and automatically shut down midway into the test, making the specimen unusable in the process. This persisted from a loading rate of 0.03 mm/min – 0.08 mm/min, and it became apparent that the stiffness of the machine is not enough to conduct the test under deformation control. This necessitated switching to load control which has the possibility of explosive failure and the softening branch could not be obtained.

ii. Secondly, during splitting tensile test with cylindrical specimens, at lower V_f the test results were mostly below 2 MPa until at percentage of 1.5 % when the results will pick up. However, when prismatic specimens were tested, the results were a bit better.

iii. Third, explosive failure of the specimens despite the presence of fibers under load control test. In other to minimize damage to the machine and LVDT's

utilized, we switched to load – time diagram, and we made used of the load to determine the stresses.

These reasons resulted in changing the testing procedure and specimen dimension, and as such, concrete compressive strength was determined at 28 days for an average of four cubes, and Load - Time diagram plotted to determine the linearity end-point. The results were used to estimate the corresponding compressive strength at the point where linearity deviated, two points before that and another point post linearity for each of the V_f levels from 0.50 % - 2.00 %. These corresponding values of compressive strength were used to load the specimens in each case as presented in Table 4.6 were at least four specimens were loaded to these points at the same loading rate used previously.

Table 4.6: Four Stress Levels Chosen as Percentage of Ultimate Compressive Strength

	Per cent of Compressive Strength Aspect Ratio 60				
Fiber Volume (%)	1st Stress Level	2nd Stress Level	3rd Stress Level	4th Stress Level	Tensile Strength (MPa)
0.00	40	60	70	75	4.98
0.50	75	85	89	95	5.74
0.75	70	80	86	95	5.82
1.00	70	80	90	96	6.19
1.25	70	80	89	95	6.78
1.50	70	80	87	95	7.94
1.75	70	80	91	95	8.77
2.00	70	75	85	95	8.93
	Per cent of Compressive Strength Aspect Ratio 75				
Fiber Volume (%)	1st Stress Level	2nd Stress Level	3rd Stress Level	4th Stress Level	Tensile Strength (MPa)
0.00	40	60	70	75	4.98
0.50	70	80	88	95	3.30
0.75	70	80	85	93	4.30
1.00	70	80	88	95	4.80
1.25	70	80	90	95	5.30
1.50	70	80	85	93	7.00
1.75	70	80	90	95	10.10
2.00	70	80	87	95	11.80

Loading was applied perpendicular to the casting direction, and subsequently, splitting tensile strength was conducted on each of the four specimens loaded earlier at different compressive strength levels until failure of the specimens and the results recorded. Both tests were conducted using a 3,000 kN capacity closed loop servo-controlled universal testing machine. A total of 64 number cubic specimens were casted for determining the loading levels for the two aspect ratios (60 and 75), while

390 cubic specimens were casted for the determination of residual tensile strength. Tensile strength loss (TSL) was determined using the following formula:

$$TSL\ (\%) = \left(\frac{f_t - f_{tr}}{f_t}\right) * 100 \quad (4.9)$$

Where f_t is tensile strength (MPa) from splitting test, and f_{tr} the tensile strength after compressive loading (MPa).

4.3.2.6 Microscopic Examination and Crack Definition

Immediately after loading the specimens and splitting tensile test conducted on the specimens. Microscopic examination was thereafter conducted on the split specimens, and in the case of concrete with fiber addition, the loaded specimens were split open using a 3 mm thick power saw under wet condition. A 150x (40.97 pixel/micrometer) magnification optical stereomicroscope with a maximum field of view of 23 mm attached with a 10 megapixel USB digital camera was used for this purpose. Most critical section was then selected (Figure 4.5) for critical crack width measurement at linearity-end point.

Figure 4.4: Optical Stereomicroscope used in this Study

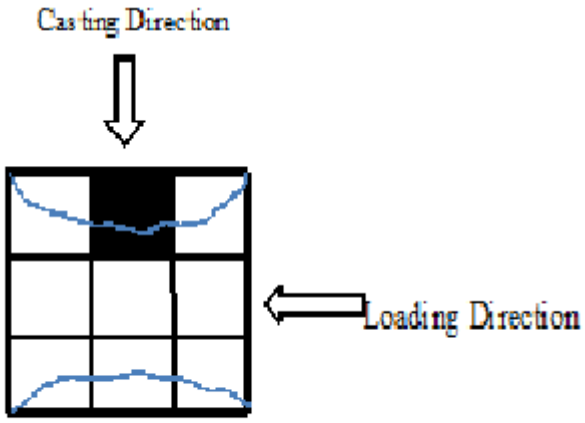

Figure 4.5: Depiction of the Casting and Loading Direction and Pattern on the Specimen

Chapter 5

RESULTS AND DISCUSSION

5.1 Introduction

In the following sections, results and discussion pertaining to workability, strength, load – deformation relationship, fracture and microcracking mechanism in high-performance concrete with steel fiber addition is presented.

5.2 Effect of Proportion and Aspect Ratio of Fibers on Fresh Concrete Properties

5.2.1 VeBe Time

This test intended for concrete that cannot be properly evaluated using the slump test, and it is known to be sensitive to change in consistency, compactability, and mobility. It was conducted for the two aspect ratios under consideration, and the result presented in Table 5.1. It can be seen that the addition of steel fiber in the mix resulted in an increase in the VeBe time for all mixes. Aspect ratios 60 seem to have a higher workability than 75. The minimum values for VeBe time with fiber addition were 6.58 and 7.50 seconds, while the maximum values were 39.62 and 44.64 seconds respectively. In Figure 5.1 VeBe time values were plotted against V_f and it was apparent that VeBe time increases exponentially with fiber length due to interparticle friction.

Table 5.1: Workability Test Results

Aspect Ratio	Fiber Volume (%)	FRI	VeBe Time, (s)	Slump, (mm)	Compacting Factor	Density, (kg/m^3)
	0.00	-	4.70	150	0.90	2406
	0.50	30	6.58	130	0.89	2508
60	0.75	45	9.71	110	0.85	2514
	1.00	60	12.18	100	0.88	2511
	1.25	75	14.07	80	0.84	2504
	1.50	90	19.54	70	0.81	2550
	1.75	105	33.45	60	0.75	2534
	2.00	120	39.62	40	0.71	2581
	0.50	37.5	7.50	95	0.88	2539
75	0.75	56.25	9.85	90	0.89	2546
	1.00	75	11.45	85	0.87	2569
	1.25	93.75	16.43	60	0.78	2582
	1.50	112.5	25.85	40	0.77	2573
	1.75	131.3	32.73	20	0.69	2599
	2.00	150	44.64	15	0.70	2565

FRI = fiber reinforcement index ($L/d * V_f$)

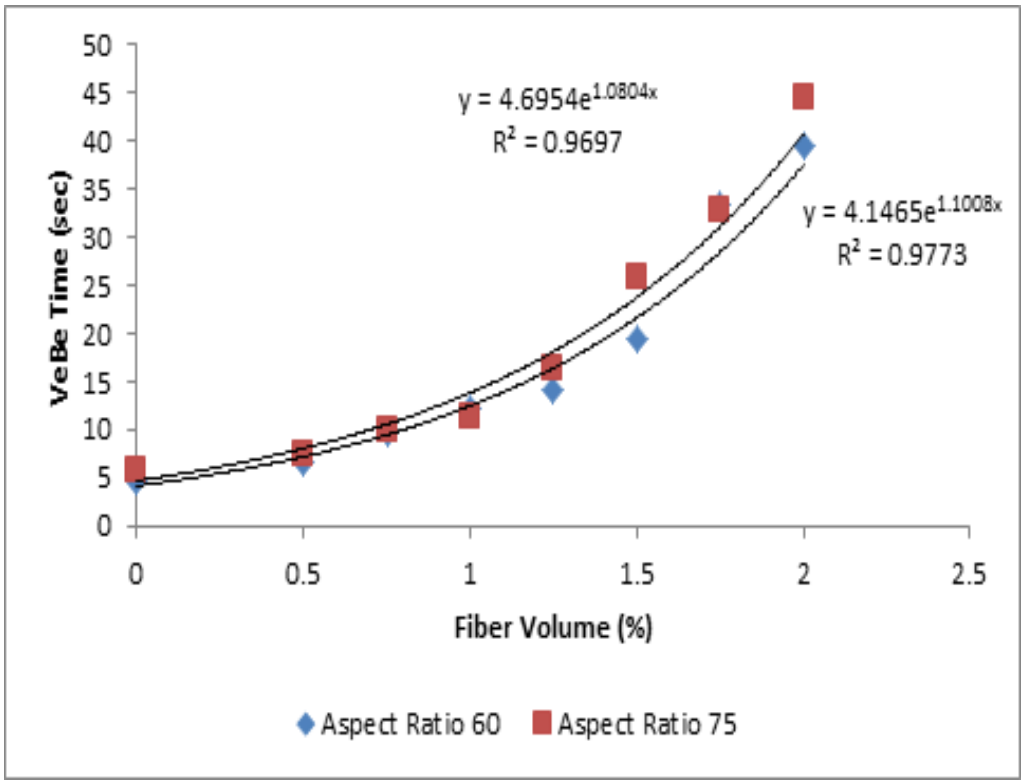

Figure 5.1: Relationships between Fiber Volume and VeBe Time

5.2.2 Slump

This widely applicable test was conducted and results presented in Table 5.1. In normal range concrete mixes, values of compacting factor are between 0.80 – 0.92, and BS 1881: Part 103 view this test unsuitable for values less than 0.70 and above 0.98. It is evident from the results that slump decreases with an increase in V_f and aspect ratio. This decrement is due to the shape of the hooked-end fiber and its surface area. In this study, except in aspect ratio 75 volume fraction of 1.75 % that was 0.69, the test proved to be efficient or useful. A plot of slump versus V_f depicted in Figure 5.2 indicates a reduction in the flow as the V_f increases. This is due to a decrease in the flowability as V_f increase resulting in a stiffer mix. In Figure 5.3 – 5.4, correlation between yield stress, VeBe time and slump is presented showing an inverse relationship between yield stress and slump as well as VeBe time with slump.

Yield stress which is the magnitude or limit before the onset of the flow defined in Eqn. 5.1 developed by [Hu et al., (1996)] has been used to estimate the values.

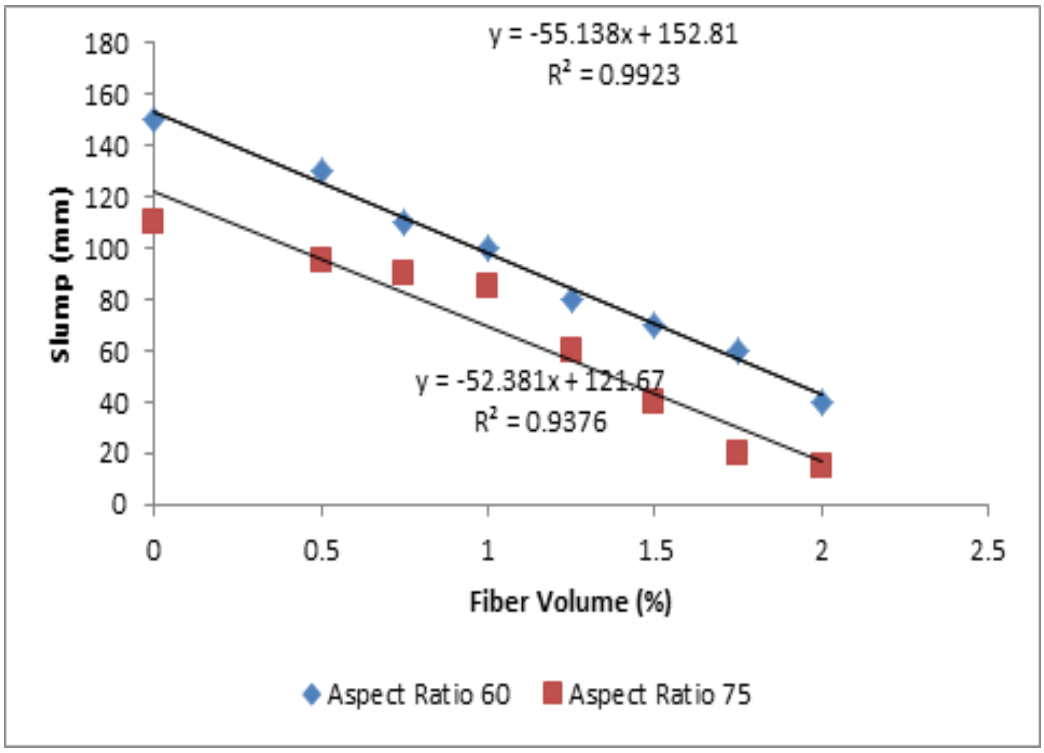

Figure 5.2: Relationships between Fiber Volume and Slump

$$\tau_0 = \frac{\rho}{270}(300 - s) \qquad (5.1)$$

Where:

τ_0= yield stress in Pa; s = slump in mm; ρ = density in kg/m^3

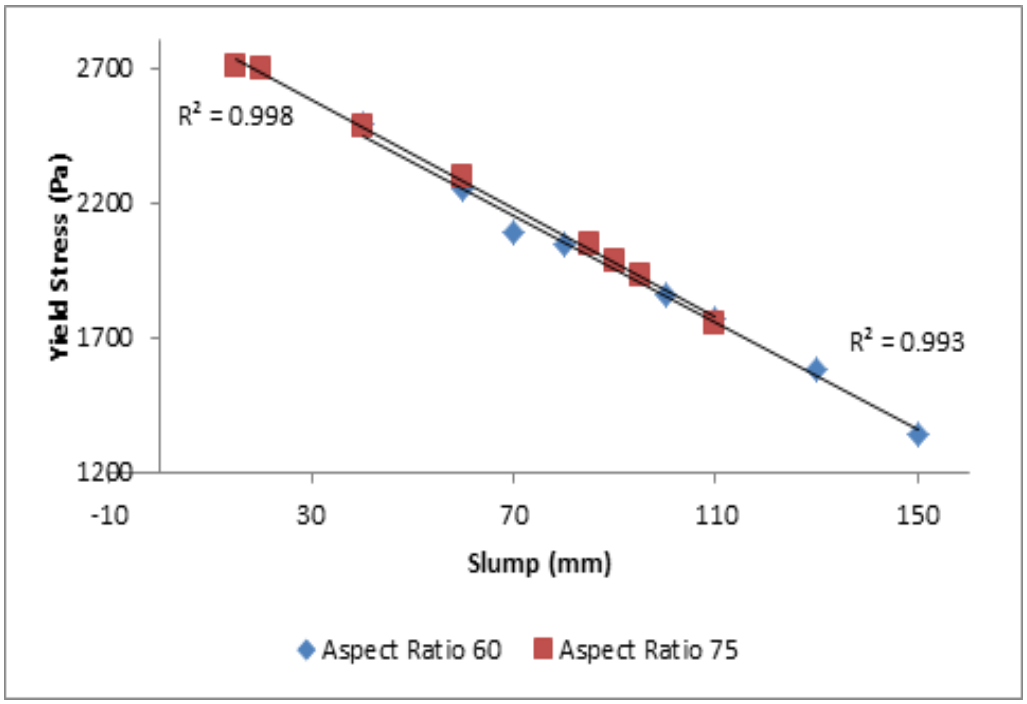

Figure 5.3: Relationships between Yield Stress versus Slump

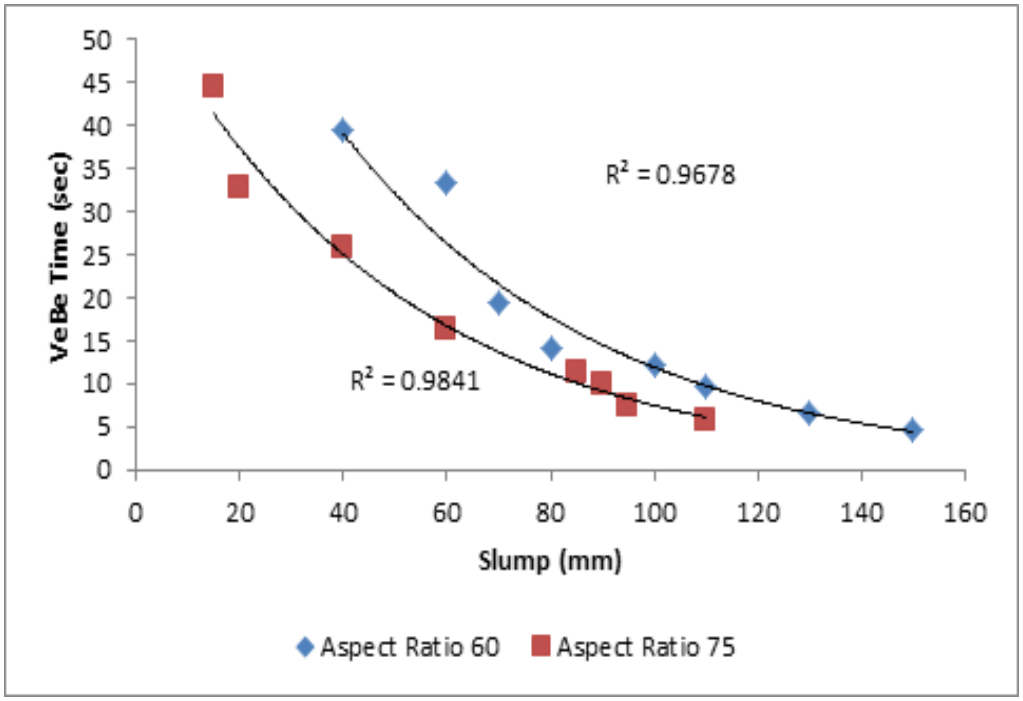

Figure 5.4: Relationships between VeBe Time and Slump

5.2.3 Compacting Factor

This is essentially a density ratio between a partially compacted to fully compacted concrete measuring the degree of compactibility of concrete. It is affected by

entrapped air, shape and surface texture of the aggregates. In this study, compacting factor test was conducted and results shown in Table 5.1, Figure 5.5. The maximum compacting factor value was 0.90 and the minimum was 0.69. Here, the value of the compacting factor decreases with aspect ratio and V_f, due to reduced interparticle friction, and mobility of the concrete as was found in slump test results. Results showed that development of cohesive forces increases shear stresses changing the concrete mix condition from a flowable to stiff. According to Ritchie (1962), a good measure of workability correlation can be obtained by combining VeBe test and compacting factor. This type of correlation is presented in Figure 5.6 – 5.7, showing a good correlation for the combination. However, it can also be seen that the influence of fiber length is clearly visible (aspect ratio 75) where despite the higher coefficient of determination; the lower value of the compacting factor is still evident, moving towards very low workability mixture of less than 0.7.

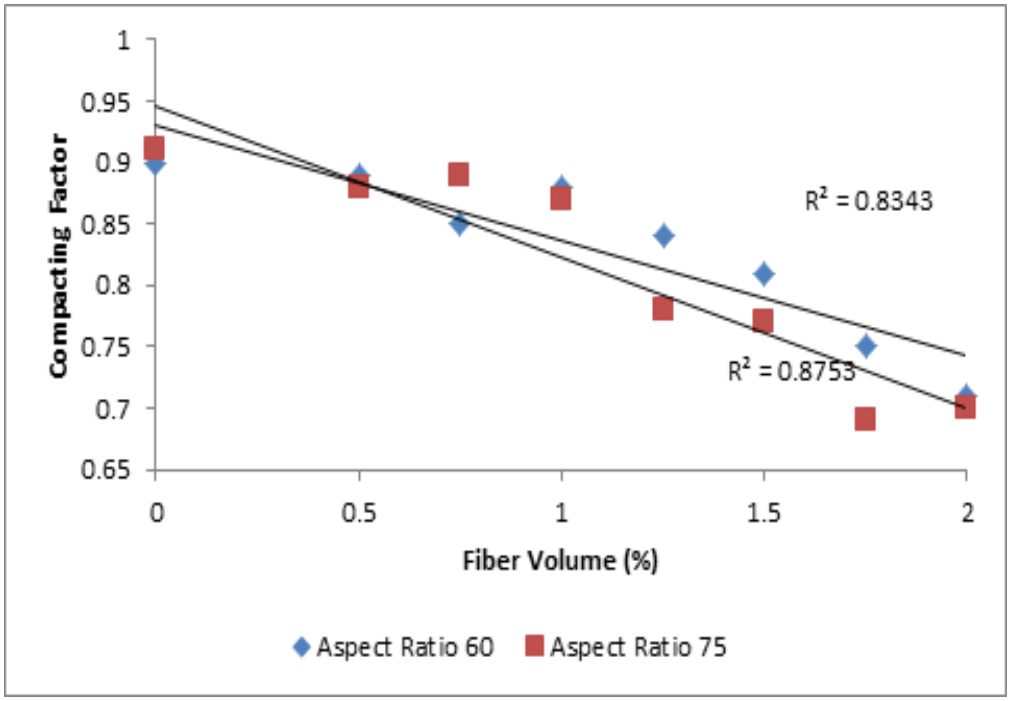

Figure 5.5: Correlations between Compacting Factor and Fiber Volume

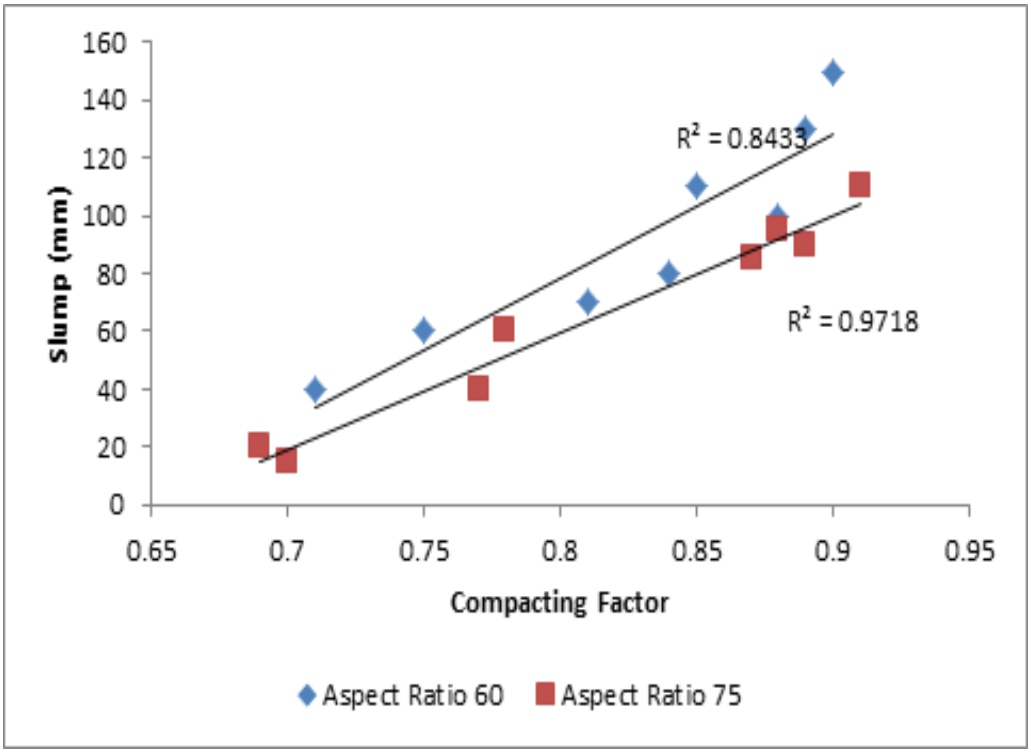

Figure 5.6: Correlation Factor between Slump and Compacting Factor

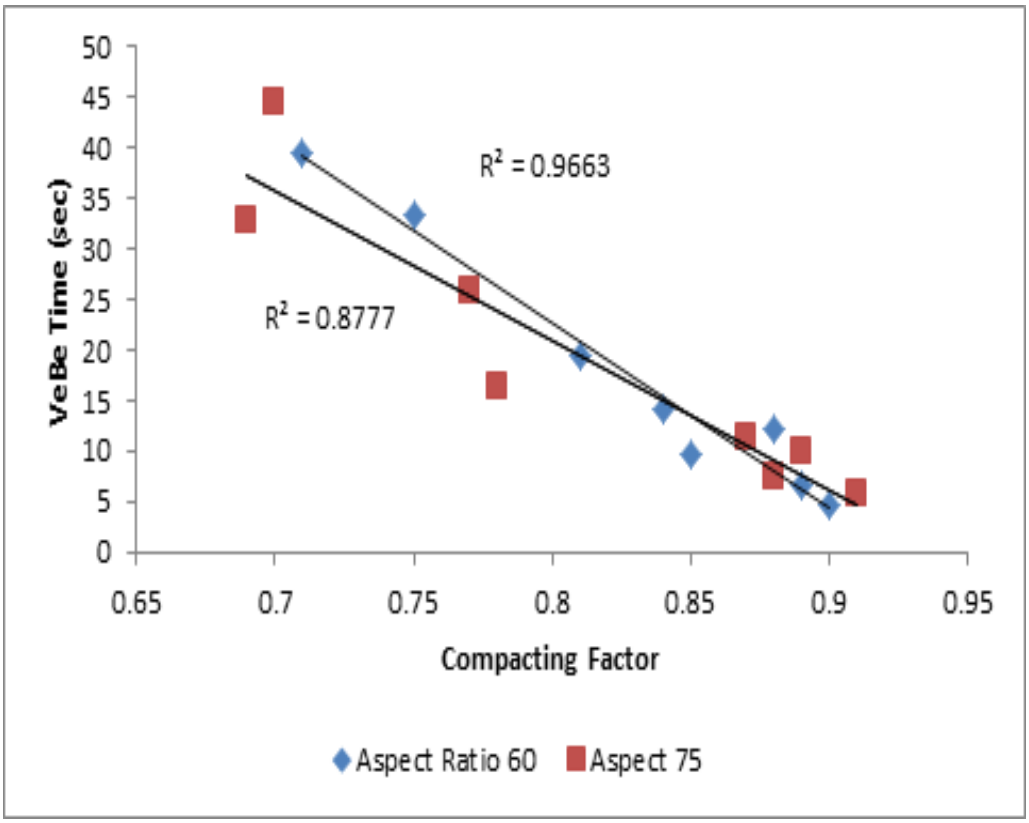

Figure 5.7: VeBe Time versus Compacting Factor

5.2.4 Unit Weight

In high-performance concretes, it is expected that the unit weight would be higher than that of normal concrete due to very low water-cement ratio and higher cement content. The unit weight difference between normal and high-performance concretes could be as much as 100 kg/m^3 as was observed by (Aitcin 1998). This is an indication of the important role proportioning plays and the increased amount of fine aggregate content. Unit weight test results of this study shown in Figure 5.8 indicated that trend, and values are in the range of 2505 kg/m^3 – 2599 kg/m^3 for concretes with fiber addition, while the reference sample was 2406 kg/m^3.

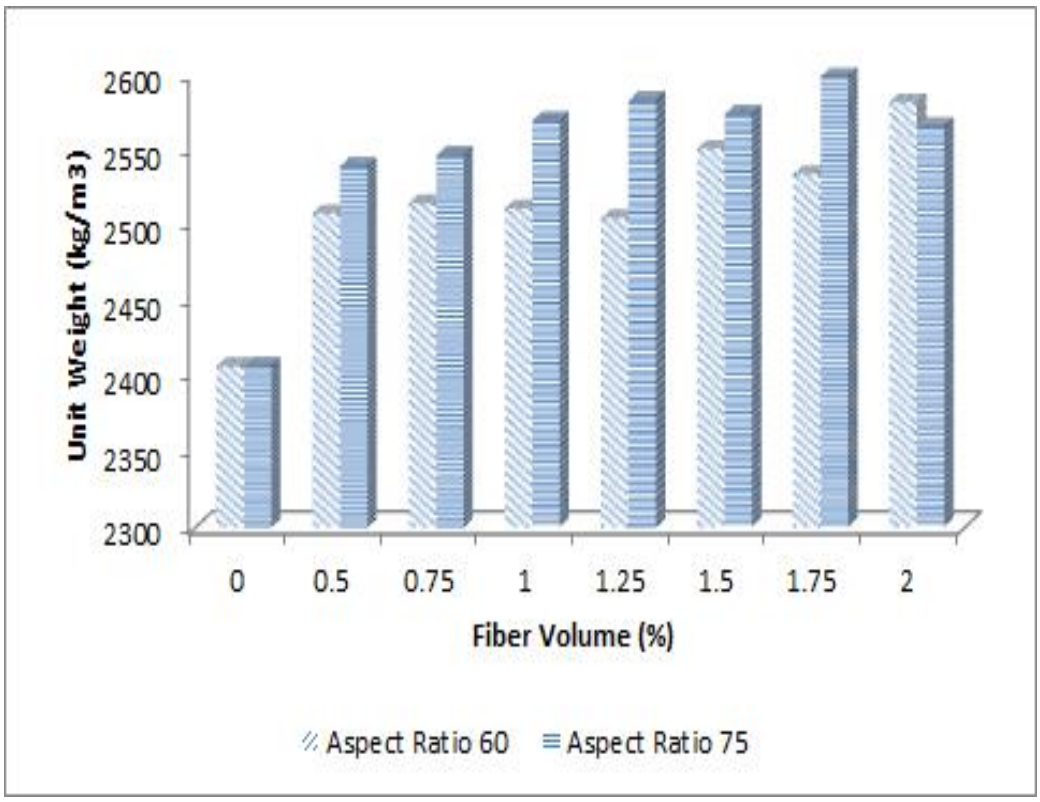

Figure 5.8: Effect of Unit Weight on Fiber Volume

5.2.5 Regression Analysis

The most widely used regression models are of the form in Eqns. 5.2 – 5.4,

$$y = a + bx \qquad (5.2)$$

$$y = a + bx + cx^2 \quad (5.3)$$

$$y = a + bx + cx^2 + dx^3 \quad (5.4)$$

Where a, b, c, and d represents regression coefficients and x is an explanatory item or the independent variable. This study holds FRI as the independent variable, and VeBe Time, Slump, Compacting Factor and Unit Weight, as the dependent variables. For every FRI (independent variable) increment presented in Table 5.2, there is a corresponding change in the dependent variables. It became apparent that an increase in FRI resulted in an increase in the VeBe time, however, a decrease in both Slump and Compacting Factor values was also observed. This could be possible due to the harshness of the mixture resulting from fiber addition which makes it difficult for interaction among the mixture's constituents.

Table 5.2: Modelling of each Response

Responses	Aspect Ratio L/d	Coefficients				R^2	Standard error of estimate
		a	b	c	d		
VeBe Time	60	6.85	-0.0206	0.00062	0.000016	97.6	2.74
	75	11.34	-0.2007	0.002813	-	99.6	1.09
Slump	60	185.70	-2.3700	0.01958	-0.000082	99.4	3.45
	75	30.00	3.129	-0.04368	0.000147	99.4	3.54
Compacting Factor	60	0.8807	0.000225	-0.000004	-0.000000	95.4	0.02
	75	0.98	-0.0020	-	-	90.4	0.03
Unit Weight	60	2328.00	10.6200	-0.183800	0.000945	78.4	25.59
	75	2551.00	-1.1950	0.027930	-0.000128	83.0	11.90

Table 5.3: Fitted Model Equation for VeBe Time

Aspect Ratio	Fiber Volume, (%)	FRI	VeBe Time, s (E)	VeBe Time, s (P)	VeBe Time, s (P/E)
	0.00	0	4.70	0.00	0.00
60	0.50	30	6.58	7.23	1.10
	0.75	45	9.71	8.64	0.89
	1.00	60	12.18	11.31	0.93
	1.25	75	14.07	15.55	1.11
	1.50	90	19.54	21.69	1.11
	1.75	105	33.45	30.05	0.90
	2.00	120	39.62	40.96	1.04
75	0.50	37.5	7.50	7.77	1.04
	0.75	56.25	9.85	8.96	0.91
	1.00	75	11.45	12.12	1.06
	1.25	93.75	16.43	17.25	1.05
	1.50	112.5	25.85	24.37	0.95
	1.75	131.25	32.73	33.46	1.03
	2.00	150	44.64	44.53	1.00

E = Experimental Results (Laboratory); P = Predicted Results from Table 5.2

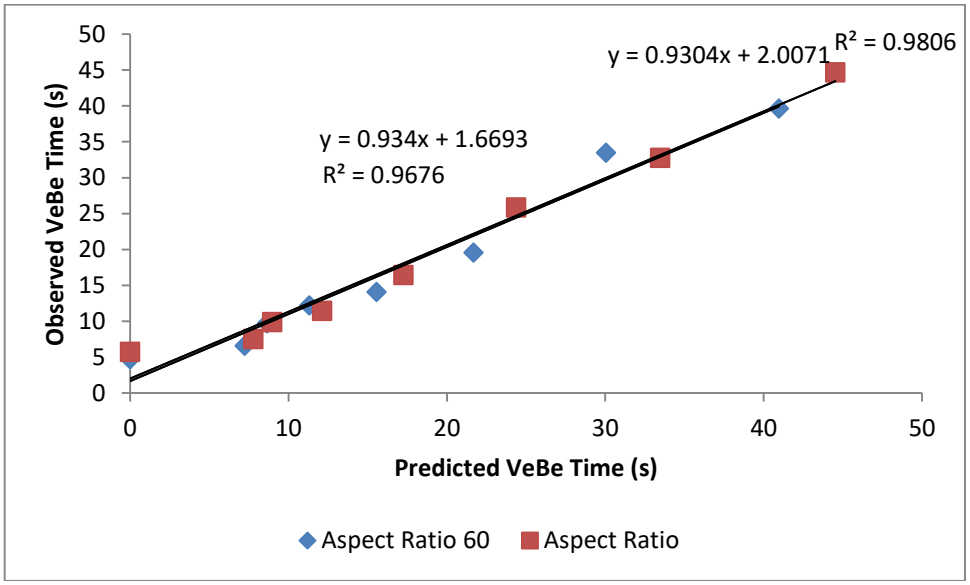

Figure 5.9: Observed versus Predicted Values for VeBe Time

Table 5.4: Fitted Model Equation for Slump

Aspect Ratio	Fiber Volume, %	FRI	Slump, mm	Slump, mm (P)	Slump, mm (P/E)
	0.00	0	150	0	0
60	0.50	30	130	130	1.01
	0.75	45	110	111	1.02
	1.00	60	100	96	0.97
	1.25	75	80	84	1.05
	1.50	90	70	71	1.02
	1.75	105	60	58	0.97
	2.00	120	40	42	1.04
75	0.50	37.5	95	94	0.99
	0.75	56.25	90	94	1.05
	1.00	75	85	81	0.96
	1.25	93.75	60	61	1.01
	1.50	112.5	40	39	0.97
	1.75	131.25	20	21	1.03
	2.00	150	15	13	0.85

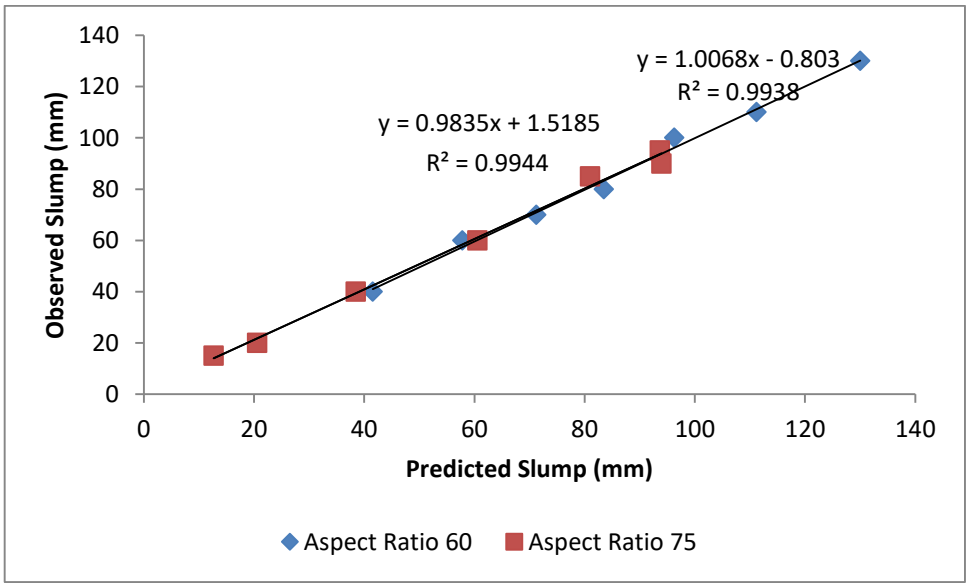

Figure 5.10: Observed versus Predicted Values for Slump

Table 5.5: Fitted Model Equation for Compacting Factor

Aspect Ratio	Fiber Volume, (%)	FRI	Compacting Factor (E)	Compacting Factor (P)	Compacting Factor (P/E)
	0.00	0	0.90	0.00	0.00
60	0.50	30	0.89	0.89	1.00
	0.75	45	0.85	0.89	1.04
	1.00	60	0.88	0.88	1.00
	1.25	75	0.84	0.88	1.05
	1.50	90	0.81	0.87	1.08
	1.75	105	0.75	0.87	1.15
	2.00	120	0.71	0.86	1.20
75	0.50	37.5	0.88	0.91	1.04
	0.75	56.25	0.89	0.88	0.98
	1.00	75	0.87	0.84	0.96
	1.25	93.75	0.78	0.8	1.03
	1.50	112.5	0.77	0.77	0.99
	1.75	131.25	0.69	0.73	1.05
	2.00	150	0.70	0.69	0.98

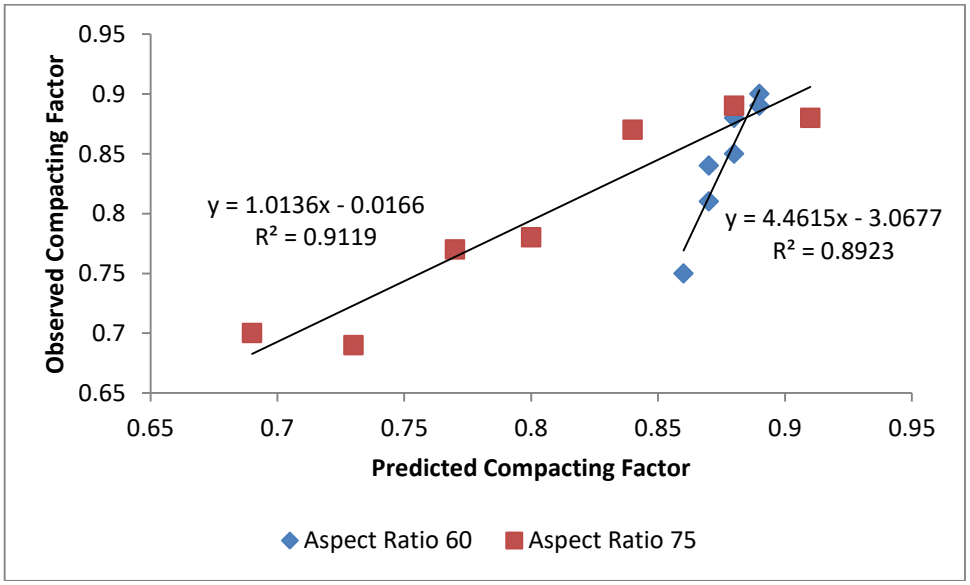

Figure 5.11: Observed versus Predicted Values for Compacting Factor

Table 5.6: Fitted Model Equation for Unit Weight

Aspect Ratio	Fiber Volume, (%)	FRI	Density, kg/m^3 (E)	Density, kg/m^3 (P)	Density, kg/m^3 (P/E)
	0.00	0	2406	0.00	0.00
60	0.50	30	2508	2506	1.00
	0.75	45	2514	2519	1.01
	1.00	60	2511	2507	1.00
	1.25	75	2504	2489	1.00
	1.50	90	2450	2483	1.02
	1.75	105	2534	2510	1.00
	2.00	120	2581	2588	1.01
75	0.50	37.5	2539	2538	1.00
	0.75	56.25	2546	2549	1.01
	1.00	75	2569	2564	1.00
	1.25	93.75	2582	2578	1.00
	1.50	112.5	2573	2587	1.01
	1.75	131.25	2599	2585	1.00
	2.00	150	2565	2568	1.01

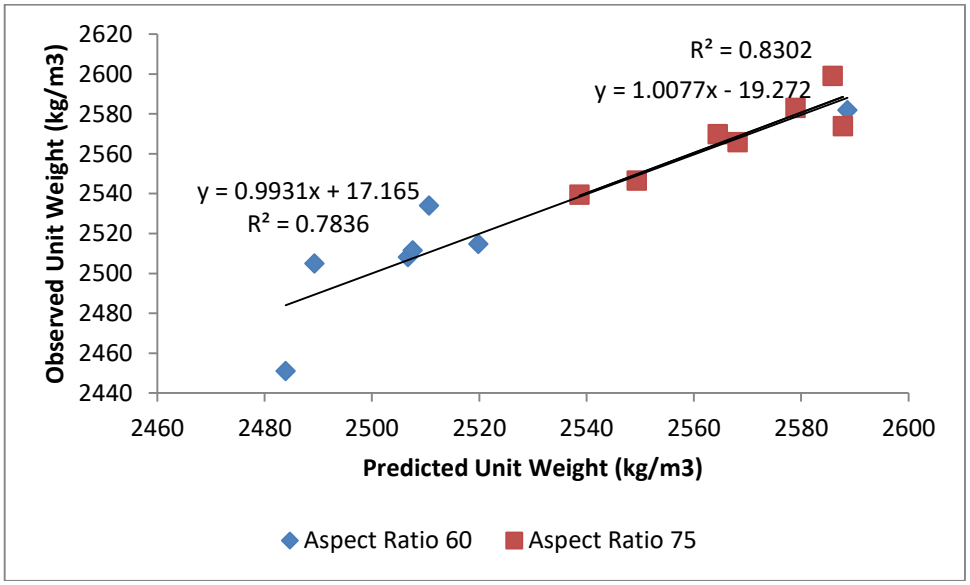

Figure 5.12: Observed versus Predicted Values for Unit Weight

5.3 Effect of Proportion and Aspect Ratio of Fibers on Mechanical Properties

5.3.1 Compressive Strength, f_c

The ultimate strength of concrete depends on the behavior of the concrete at the region that is very close to the failure load. This is where there is rapid propagation of multiple cracks from micro to macro by coalescing together, and these cracks moves parallel to the direction of the loading. At this point, the fibers that are in the direction of these cracks intercept the cracks, which results in the high carrying capacity of the composite. However, if the fibers are aligned in the direction of the cracks, the crack will progress parallel to the fiber, and little resistance to the crack growth will be offered.

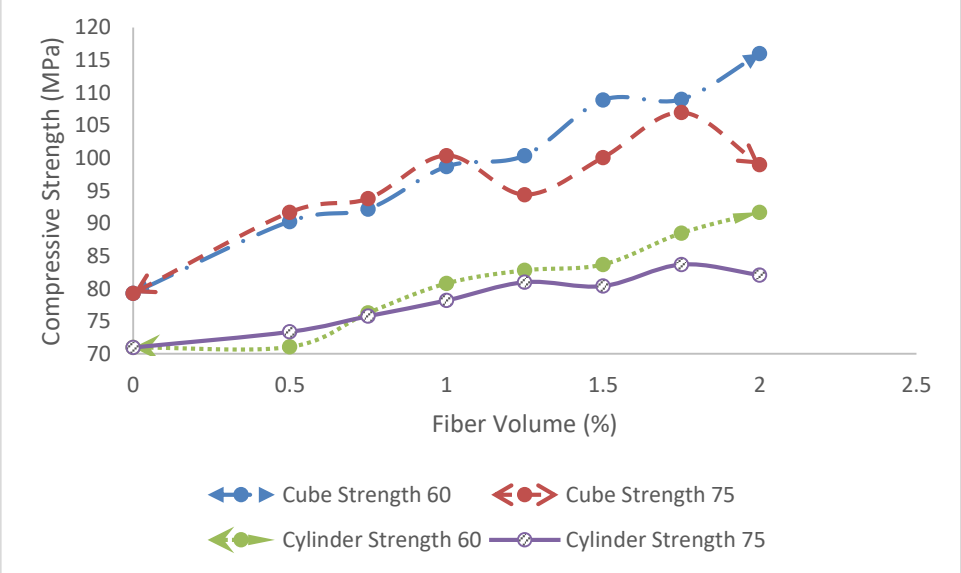

Figure 5.13: Effect of Fiber Volume and Aspect Ratio on Compressive Strength

In Figure 5.13 and Table 5.7 – 5.8, the strength results in compression for the specimens incorporated with fibers at aspect ratio 60 and 75 respectively for cubic and cylindrical specimens are presented. Results indicates that the strength in aspect ratio 60 increases with V_f compared with the plain concrete from 14.4 % – 46.3 % (cubic specimens) when strength effectiveness was considered. However, in aspect ratio 75, compressive strength increment with V_f was observed up to 1 %, and beyond this point it decreased in a fluctuating manner. Strength effectiveness on the other hand varies from 15.6 % - 34.9 % (cubic) consistent with the observation made in f_c. Results obtained in aspect ratio 75 were still better than the reference sample despite the decline in the values, but the aspect ratio 60 results fared better. In both cubic and cylindrical specimens, it can be seen that the same kind of trend exist; it is reported in ACI 544. 1R that there is an increase in compressive strength with V_f up to 1.5 %, the same observation was made by Song and Hwang (2004). Generally, in concrete with steel fiber addition there can either be an increase, decrease or none at all [Traina & Mansour (1991); Barros & Figueiras (1999); Eren *et al.,* (1999)]. This decrease in the value of compressive strength has been attributed to difficulties in achieving compaction of the concrete (Eren *et al.,* 1999).

There is also the issue of flaws and deficiencies in the concrete some of whom are inherent, while others are induced such as those resulting from the use of plastic moulds which was used in this study. It has been reported that there is as much as a 10 % decrease in compressive strength when 150 mm plastic cube moulds is used, compared with 7 % in 100 mm cubes (Imam *et al.,* 1995). This can be attributed to the surface roughness of the plastic moulds, and the inability of the moulds to transmit mechanical vibration immediately compared with steel moulds.

The increase in f_c can be attributed to the improvement of ITZ which becomes compatible with the aggregate in terms of mechanical properties. The increase in f_c in high strength concretes is due to delayed microcrack formation within the concrete under uniaxial compression. At the onset of the microcracks, the discrete randomly distributed fibers serves as crack arresting mechanism through crack bridging limiting the length and width of the cracks through stress transfer. This process of resistance offered by the steel fiber to crack growth and propagation reduces the brittleness of the concrete and therefore increases its ductility by continuing to sustain load even after matrix cracking by producing multiple microcracks. This process will continue until the specimen reached critical stress, where even if the load is removed, the crack propagation does not cease. At higher V_f, this effect of fiber bridging is more pronounced especially at lower aspect ratio.

There is also the effect of a strong bond between the fiber and matrix interface especially at higher V_f thereby decreasing the distance between fiber to fiber hence improving the strength of the composite. Also, a combination of silica fume addition and the use of D_{max} 10 mm could be attributed to the improvement in the concrete microstructure leading to the decrease in the porosity and ITZ. This is because at the interface, bond stress is less when smaller size aggregates are used.

Table 5.7: Compressive Strength Results for Cubes

Aspect Ratio 60 Cubic Specimens						
Fiber Volume (%)	Sample 1	Sample 2	Sample 3	Average	Standard Deviation	Variance
0.00	79.30	77.40	81.20	79.30	1.90	3.61
0.50	89.40	92.20	90.40	90.70	1.42	2.01
0.75	92.20	93.00	91.40	92.20	0.80	0.64
1.00	100.50	98.00	97.60	98.70	1.57	2.47
1.25	102.60	99.70	98.90	100.40	1.95	3.79
1.50	110.40	108.00	108.30	108.90	1.31	1.71
1.75	107.10	109.20	109.60	108.90	1.34	1.80
2.00	115.60	117.20	115.00	116.00	1.14	1.29
Aspect Ratio 75 Cubic Specimens						
Fiber Volume (%)	Sample 1	Sample 2	Sample 3	Average	Standard Deviation	Variance
0.50	90.90	92.40	91.80	91.70	0.75	0.57
0.75	92.90	95.00	93.40	93.80	1.10	1.20
1.00	98.30	100.90	102.30	100.50	2.03	4.12
1.25	94.30	94.60	94.20	94.40	0.21	0.04
1.50	98.00	102.00	100.30	100.10	2.00	4.03
1.75	108.30	107.00	105.70	107.00	1.30	1.69
2.00	99.80	98.00	99.20	99.00	0.92	0.84

Table 5.8: Compressive Strength Results for Cylinders

Aspect Ratio 60 Cylindrical Specimens						
Fiber Volume (%)	Sample 1	Sample 2	Sample 3	Average	Standard Deviation	Variance
0.00	70.90	71.10	71.00	71.00	0.10	0.01
0.50	72.00	70.30	71.00	71.10	0.85	0.73
0.75	77.50	76.10	75.30	76.30	1.11	1.24
1.00	80.00	82.00	80.40	80.80	1.06	1.12
1.25	81.90	82.90	83.60	82.80	0.85	0.73
1.50	83.20	83.00	84.90	83.70	1.04	1.09
1.75	87.80	88.80	88.90	88.50	0.61	0.37
2.00	92.00	91.80	91.30	91.70	0.36	0.13
Aspect Ratio 75 Cylindrical Specimens						
Fiber Volume (%)	Sample 1	Sample 2	Sample 3	Average	Standard Deviation	Variance
0.50	73.50	73.90	72.80	73.40	0.56	0.31
0.75	76.00	75.20	76.20	75.80	0.53	0.28
1.00	77.90	78.40	78.30	78.20	0.26	0.07
1.25	81.00	82.00	80.00	81.00	1.00	1.00
1.50	79.70	80.60	80.90	80.40	0.62	0.39
1.75	83.10	83.70	84.30	83.70	0.60	0.36
2.00	81.70	82.70	81.90	82.10	0.53	0.28

5.3.2 Splitting Tensile Strength, f_{st}

Tensile strength which was measured using the Brazilian test and the result presented in Figure 5.14. It can be seen that f_{st} showed a slight increment up to 1 % $V_{f,}$ however beyond that level (from 1 – 2 %), higher rate of increment relative to the reference sample has been observed. Strength effectiveness changed from 15.3 - 79.3 %. In

aspect ratio 75 on the other hand, from 0.5 - 1 % V_f values obtained for f_{st} were all lower than the reference sample. This could be attributed to the random orientation of the fibers and their distribution, as well as high amount of coarse aggregate at a lower volume fraction that serve to reduces the efficiency of the fibers in deflecting and bridging the splitting crack. There is also the issue of unknown stress distribution after first matrix cracking according ACI 544.2R where it is difficult to determine the first crack. However, from 1.5 % and above, there is an astronomical increase where the strength effectiveness was up to 136.9 % at 2.0 % fiber addition.

Table 5.9: Splitting Tensile Strength Results

Aspect Ratio 60 f_{st} (MPa)						
Fiber Volume (%)	Sample 1	Sample 2	Sample 3	Average	Standard Deviation	Variance
0.00	4.72	4.95	5.27	4.98	0.28	0.08
0.50	5.75	5.82	5.65	5.74	0.09	0.01
0.75	5.73	5.94	5.79	5.82	0.11	0.01
1.00	6.12	6.35	6.10	6.19	0.14	0.02
1.25	6.50	6.85	6.99	6.78	0.25	0.06
1.50	6.99	7.48	9.35	7.94	1.25	1.55
1.75	8.90	8.72	8.69	8.77	0.11	0.01
2.00	9.08	9.21	8.50	8.93	0.38	0.14
Aspect Ratio 75 f_{st} (MPa)						
Fiber Volume (%)	Sample 1	Sample 2	Sample 3	Average	Standard Deviation	Variance
0.50	3.17	3.09	3.67	3.30	0.31	0.10
0.75	3.95	4.33	4.62	4.30	0.34	0.11
1.00	4.99	4.70	4.71	4.80	0.16	0.03
1.25	5.48	5.31	5.11	5.30	0.19	0.03
1.50	7.14	6.98	6.88	7.00	0.13	0.02
1.75	10.12	10.10	10.08	10.10	0.02	0.00
2.00	11.64	12.65	11.65	11.80	0.58	0.34

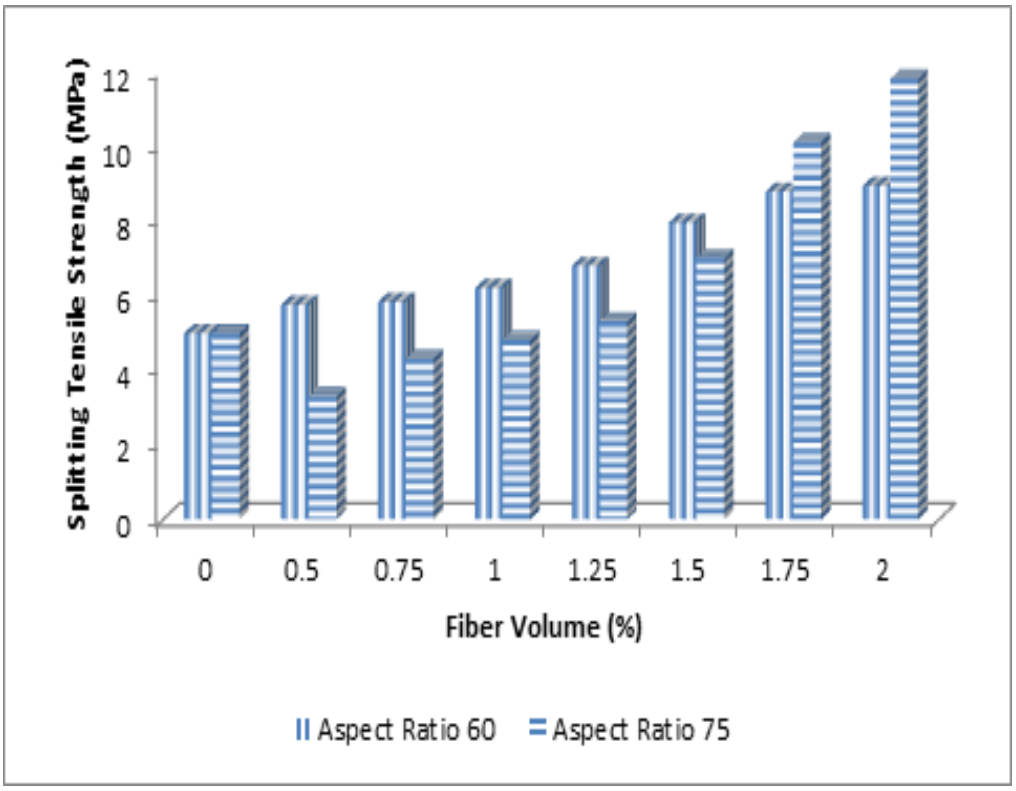

Figure 5.14: Effect of Fiber Volume and Aspect Ratio on Splitting Tensile Strength

This is due to the tensile resistance of steel fiber incorporated in concrete where fibers in the plane of fracture resist the propagation of cracks by progressive pull-out, building up stresses, and therefore increasing f_{st}. It was also observed that in concrete with fiber addition, the specimen remained intact unlike the reference specimen that split into two. Failure in this type of concrete is not by splitting, rather by the appearance of cracks, and upon observation of the cracked surfaces, it was observed (Figure 5.15) that the crack passes through the coarse aggregates due to the improvement in matrix quality.

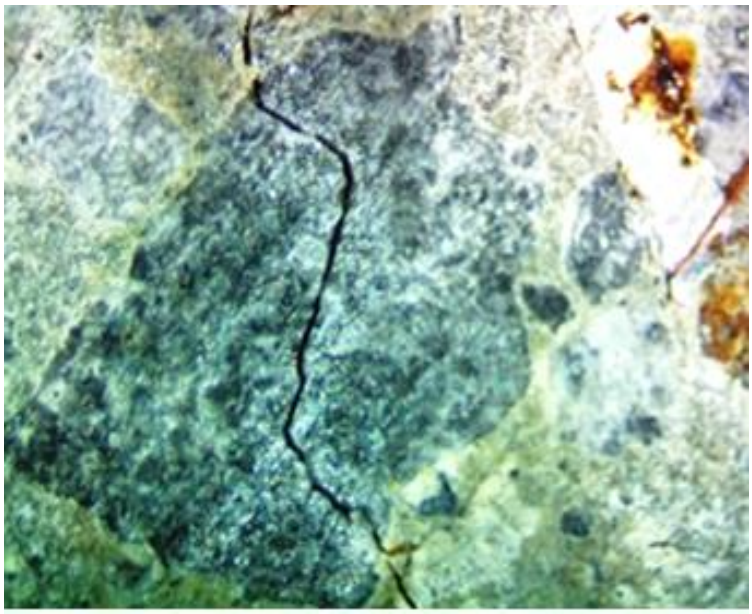

Figure 5.15: Transgranular Crack through the Surface of the Aggregate using a Stereo Microscope

5.3.3 Flexural Strength, f_r

This test is of special interest in pavement design. Results of f_r determined from Eqn. 4.1 is depicted in Figure 5.17. In aspect ratio 60, there was increase in flexural strength with respect to V_f at all levels, while aspect ratio 75, the increase was up to 1.75 % fiber addition. A close examination of Figure 5.27 shows that for aspect ratio 75, there was an improvement in the toughness based on the load – deflection curve without a corresponding increase in the P_{max}. It has been argued by Neville (1995) that during flexure test, it is expected that the maximum fiber stress could be higher if a comparison is made with a direct tension result due to blocking of the crack propagation path by a lesser-stressed material closer to the position of the neutral axis. In flexural strength test, the response could either be deflection softening or deflection hardening, and from all indications there was an increasing deflection hardening in all the specimens with fiber addition especially at higher volume fraction. These properties mentioned depends on the toughness characterization of the material and geometry of the specimen. Concrete with fiber addition results in a

significant amount of toughness, peak load and stiffness. However, regarding the stiffness the beams did not break by multiple microcracking as assumed, but a single crack resulted which was also not a flexural crack. In a nutshell, it is a borderline between flexural failure and very stiff kind of concrete. Flexural failure of the specimen was only observed at 0 % and 0.5 % steel fiber addition, subsequent specimens remained intact. Aspect ratio 60 specimens with fiber length of 30 mm exhibited pull-out while aspect ratio 75 with fiber length 60 exhibited fiber rupture at the stated fiber percentage.

Figure 5.16: Failure Mode of Notched Flexural Specimens

A comparison made between f_r and f_{st} tensile strengths in terms of f_c presented in Figure 5.18 shows that a linear relationship exists between the two, and that for both f_r and f_{st}, aspect ratio 75 performs better. As the f_c increases, the tensile strengths also increase with f_{st} the lowest. The same trend can be observed when the tensile strength is compared with V_f. There was a gradual increase at the beginning followed by a

substantial increase especially in the f_r when compared to the f_{st}. This can be attributed to the ductility of the composite in the tensile zone.

Table 5.10: Flexural Strength Results

Aspect Ratio 60 f_r (MPa)						
Fiber Volume (%)	Sample 1	Sample 2	Sample 3	Average	Standard Deviation	Variance
0.00	10.67	10.21	10.71	10.53	0.28	0.08
0.50	9.87	10.92	9.60	10.13	0.70	0.49
0.75	11.94	12.93	13.65	12.84	0.86	0.74
1.00	16.76	17.01	15.37	16.38	0.88	0.78
1.25	16.52	16.75	16.05	16.44	0.36	0.13
1.50	18.30	17.89	20.63	18.94	1.48	2.18
1.75	24.00	22.96	23.09	23.35	0.57	0.32
2.00	26.00	27.10	27.60	26.90	0.82	0.67
Aspect Ratio 75 f_r (MPa)						
Fiber Volume (%)	Sample 1	Sample 2	Sample 3	Average	Standard Deviation	Variance
0.50	10.86	11.53	11.06	11.15	0.34	0.12
0.75	14.17	14.89	15.07	14.71	0.48	0.23
1.00	20.02	21.37	20.38	20.59	0.70	0.49
1.25	20.13	21.68	20.23	20.68	0.87	0.75
1.50	20.62	22.18	21.07	21.29	0.80	0.64
1.75	33.05	32.60	27.71	31.12	2.96	8.77
2.00	28.63	26.10	27.23	27.32	1.27	1.61

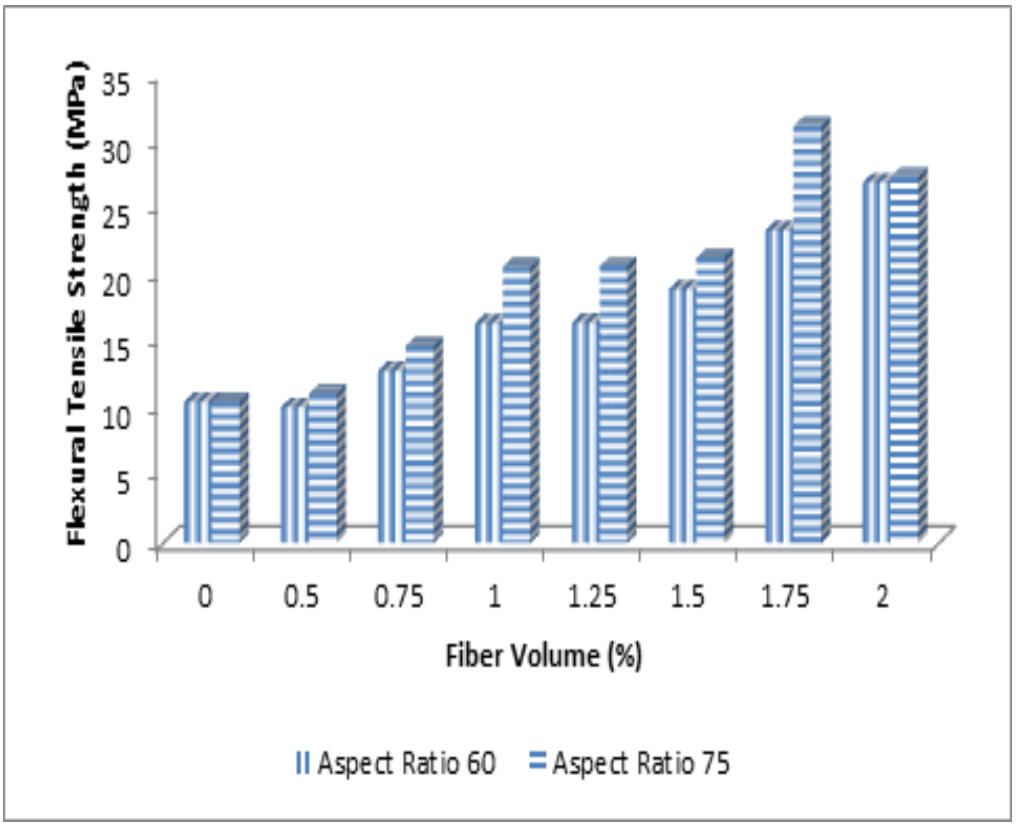

Figure 5.17: Effect of Fiber Volume and Aspect Ratio on Flexural Tensile Strength

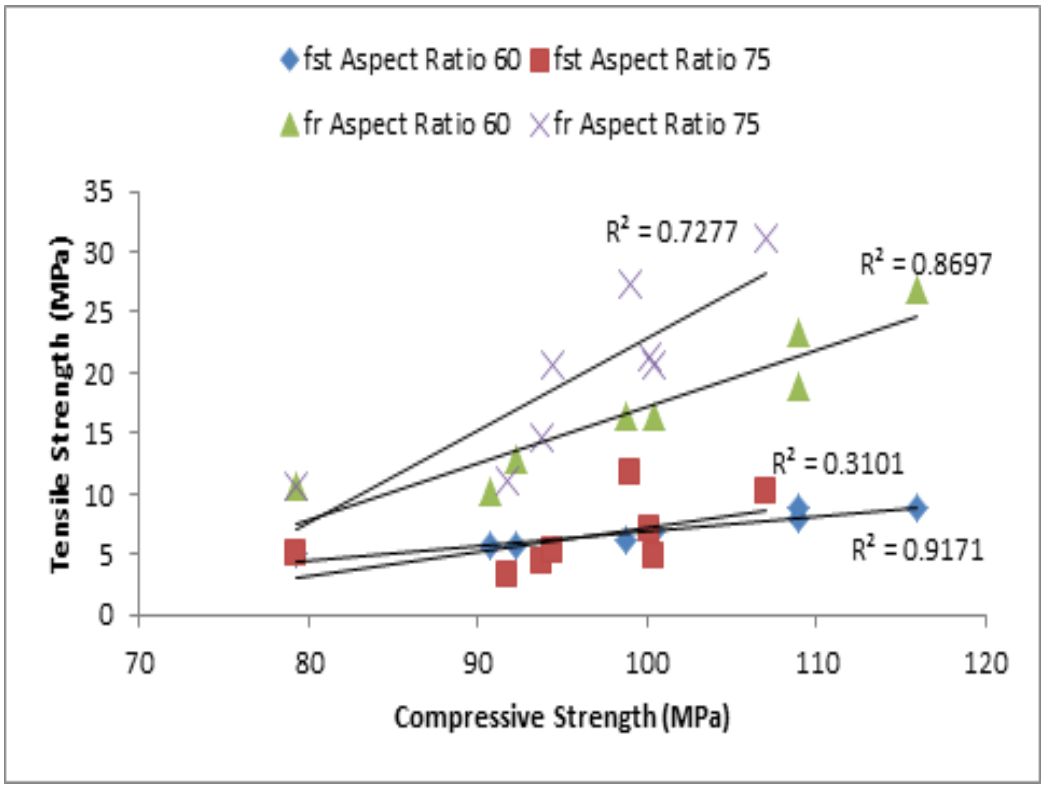

Figure 5.18: Relationships between Tensile Strength against Compressive Strength

5.3.4 Elastic Modulus (Chord Modulus)

The response to elastic modulus indicated that there was little or no effect by the fiber on the concrete. However, the range of values presented in Table 5.11 is from 44.95 – 50 GPa, but not in ascending order for both aspect ratios. Values obtained in aspect ratio 75 were comparatively marginally higher than their counterparts in aspect ratio 60 as can be seen in Figure 5.19. The inability of the fiber to have any effect on the results on the elastic modulus to the fact that at 40 % of the ultimate strength the specimen was loaded, the effect of the fiber has not manifested yet. In fact, in the concrete under consideration, the linear portion of the stress-strain diagram ended at 85% of the ultimate. It is known that the elastic modulus depends on the density and properties of the constituent materials as well, as the ITZ characteristics (Mehta and Monteiro, 2014).

There is conflicting results available in the literature regarding the effect of steel fiber in concrete. Rossi and Harrouche (1990) reported in a decrease in the elastic modulus with respect to fiber addition which increases with an increase in V_f compared with the reference specimen. Mansur *et al.,* (1999) working on the influence of fiber on the orientation of horizontal and vertical casting on prisms and cylinders reported that fibers have practically no significant influence of elastic modulus. In fact, for cylinders, fiber inclusion yielded a comparatively smaller value for compared with their prismatic opponents. Marar (2000) reported an increase with respect to fiber addition for aspect ratio 60, 75, and 83; Neves and Fernandes de Almeida (2005), reported that young modulus of steel fiber concrete with fiber addition up to 1.5 % decrease slightly with an increase in fiber. It was attributed to fibers parallel to the load acting as voids and additionally due to voids in the

concrete. In general, it is known that the elastic modulus is dependent on the type of aggregate, loading rate, proportion of the mix constituents among other things.

Table 5.11: Chord Modulus of Elasticity Results

Aspect Ratio 60 E_c (MPa)						
Fiber Volume (%)	Sample 1	Sample 2	Sample 3	Average	Standard Deviation	Variance
0.00	43.96	45.69	45.20	44.95	0.89	0.80
0.50	46.06	46.82	47.19	46.69	0.58	0.33
0.75	47.74	47.03	47.79	47.52	0.43	0.18
1.00	47.34	47.51	48.19	47.68	0.45	0.20
1.25	47.45	47.63	47.72	47.60	0.14	0.02
1.50	48.06	50.50	48.95	49.17	1.23	1.52
1.75	48.93	50.08	48.23	49.08	0.93	0.87
2.00	49.12	50.97	49.82	49.97	0.93	0.87
Aspect Ratio 75 E_c (MPa)						
Fiber Volume (%)	Sample 1	Sample 2	Sample 3	Average	Standard Deviation	Variance
0.50	46.88	46.15	48.12	47.05	1.00	0.99
0.75	46.91	47.63	49.10	47.88	1.12	1.25
1.00	47.30	48.00	47.38	47.56	0.38	0.15
1.25	47.23	47.00	49.74	47.99	1.52	2.31
1.50	48.96	49.87	50.69	49.84	0.87	0.75
1.75	49.18	49.70	50.16	49.68	0.49	0.24
2.00	49.86	50.40	49.74	50.00	0.35	0.12

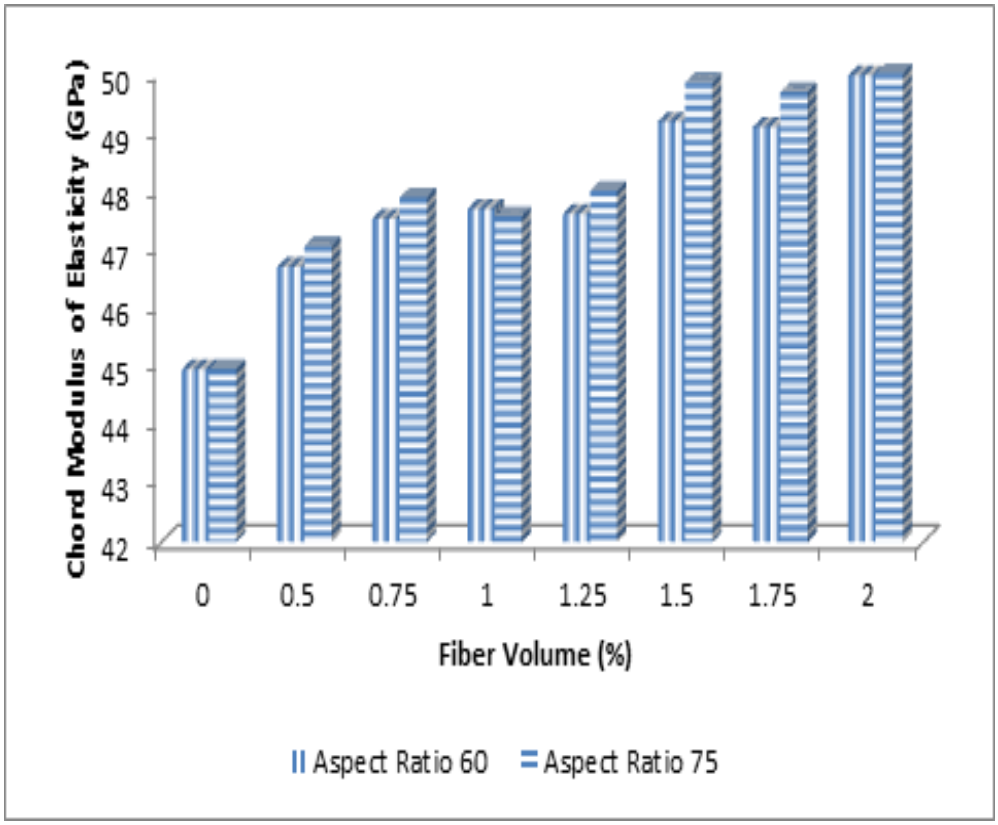

Figure 5.19: Effect of Fiber Volume and Aspect Ratio on Chord Modulus of Elasticity

5.3.5 Load – Deflection Relationship

In Figure 5.20 – 5.27 where load-deflection diagrams are depicted, two points are of significance. First one can be defined as the linear branch where there is absence of cracks with the exception of the shrinkage cracks and flaws inherent in the specimen, and second is the ultimate load (P_{max}) characterized by multiple microcrackings in the hardening branch due to the fiber bridging capacity of the composite. The point where linearity ends up can be defined as the limit of proportionality (LOP) which corresponds to the first crack. LOP in this case due to the addition of fibers is beyond 80 % of the ultimate load.

In Figure 5.20 – 5.21, it can be seen that the LOP extended up to the P_{max} which is similar to what is obtained in HPC without fiber addition where the ascending

portion of the load-deflection curve keeps rising steadily at the beginning and rapidly towards the peak load due to the brittleness of the concrete, and then a sudden failure occurs. This failure is represented by an unannounced or sudden drop in the graph.

From Figure 5.21, limit of proportionality equals the modulus of rupture (MOR) at fiber addition of 0.5 % (39.25 kg/m^3), and from 0.75 % (58.9 kg/m^3) and above, the linear portion of the graph extended up to LOP, before first crack occurred. Subsequently, hardening branch was observed in these specimens. An earlier study by Barros and Cruz (2001) reported a hardening branch after the first crack with a fiber dosage of 90 kg/m^3. Specimens with 0.5 % fiber addition were the ones that failed in flexure (with flexural crack) while the rest exhibited multiple microcrackings up to the final deflection point of the test.

An improvement in the matrix strength due to the 10 mm maximum size of the aggregate, addition of 10 % silica fume utilized, and the fact that the fibers are aligned perpendicular to the direction of the loading can be said to be responsible for the strain hardening effect observed in the specimens. Examination conducted on split specimens with 0 % fiber addition during indirect tensile strength showed that the propagation of the crack was transgranular, an indication of the matrix strength. Another contributing factor is the condition of the specimens at the time of the test, where the flexure specimens were only removed from the curing tank 20 minutes before each test, meaning the specimens were moist.

A sudden drop is observed in Figure 5.20 which is the control specimen after cracking, and it can be seen that there is no much difference between first crack load and the ultimate load since unstable crack propagation leads to the drop. However,

this effect was not observed in concrete with fiber addition. It should be noted that fiber addition has little or no effect prior to cracking. With increase in fiber content, the P-d curve becomes larger with higher peak load as a result of high fiber content to carry the load during cracking. After cracking stage, only the fibers carry the load through stress transfer at fiber-matrix interface.

In general, it can be seen that as the aspect ratio increases, the effect of reinforcement becomes more pronounced, however at 2 % V_f the toughness effect is displayed more compared to peak load.

Ductility index, μ which is the ratio of ultimate curvature to yield curvature was measured and is presented in Table 5.12. It can be seen that μ depends on the post-peak deformation of the concrete. From Figure 5.22 – 5.27, it is evidently clear that aspect ratio 75 is more ductile and has more toughness characterization than aspect ratio 60. The higher the index, the higher the energy consumption; It was also noticed that there is a significant improvement in the P_{max} in control specimens with respect to the concrete with fiber addition. This is because the first crack stress is a function of the matrix strength rather than the fiber.

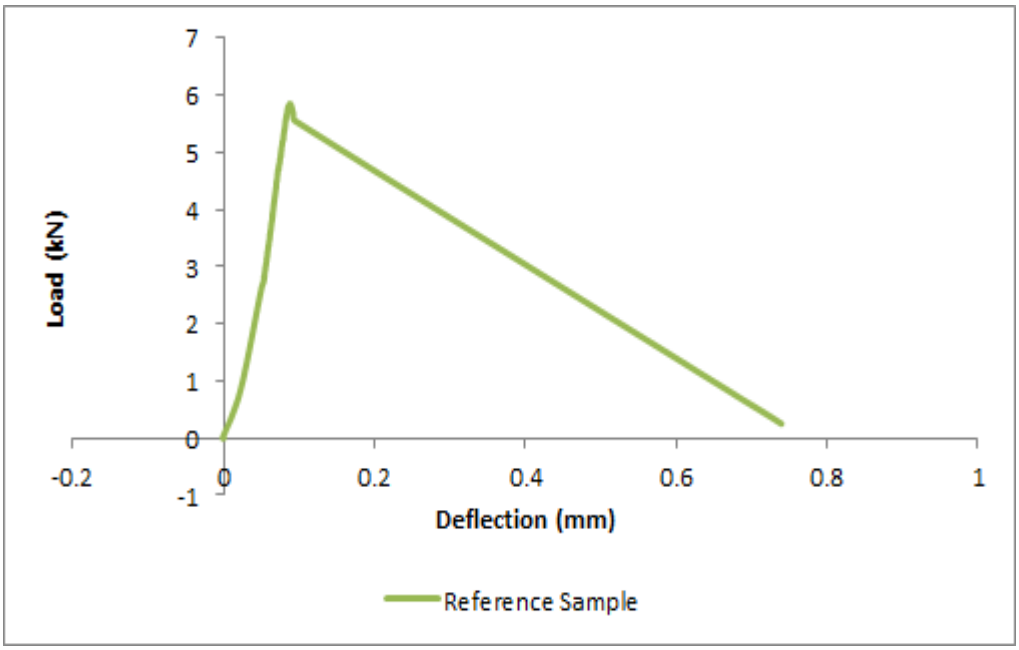

Figure 5.20: Load – Deflection Relationship of the Control Specimen

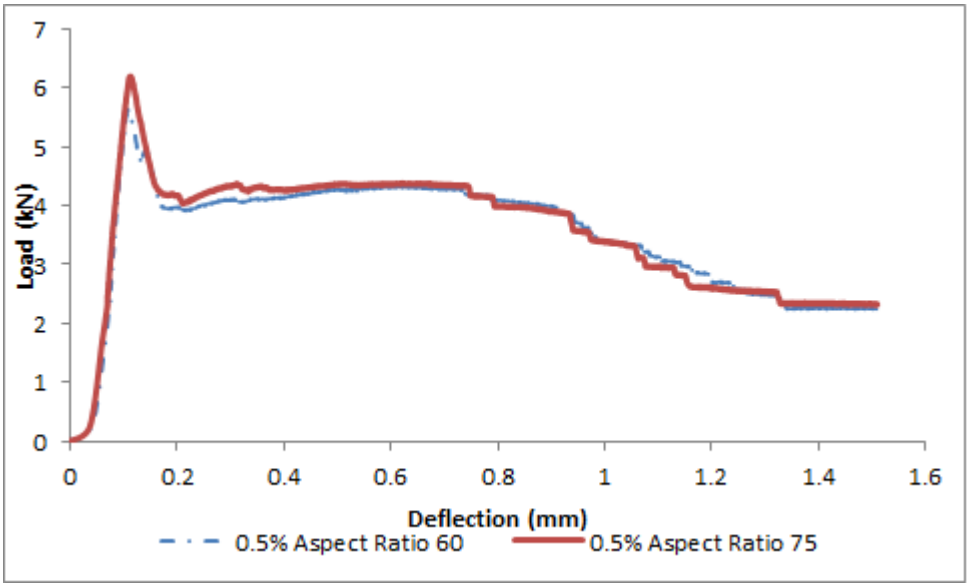

Figure 5.21: Load – Deflection Relationship for Aspect Ratio 60 & 75 at 0.5 % Fiber Addition

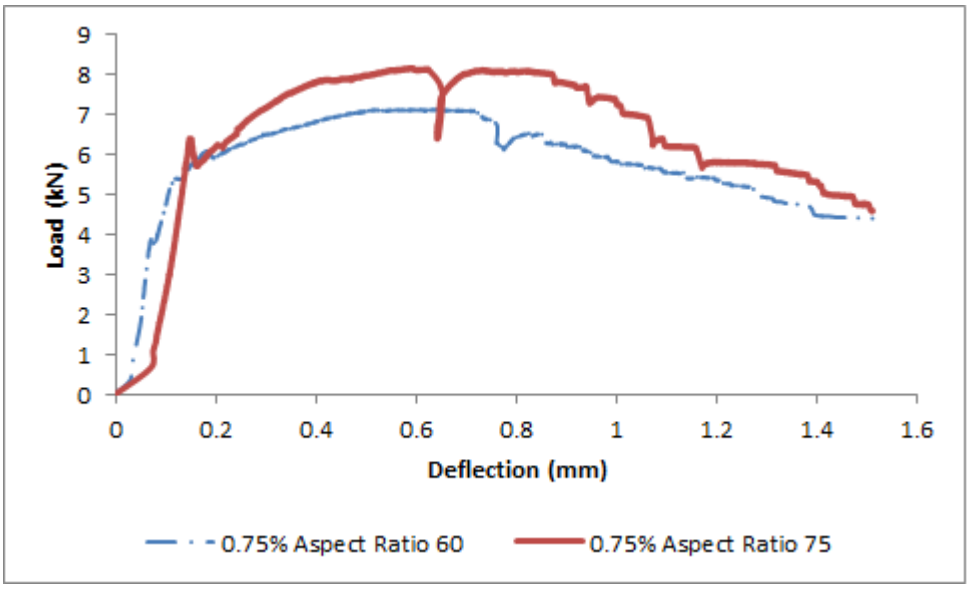

Figure 5.22: Load – Deflection Relationship for Aspect Ratio 60 & 75 at 0.75 % Fiber Addition

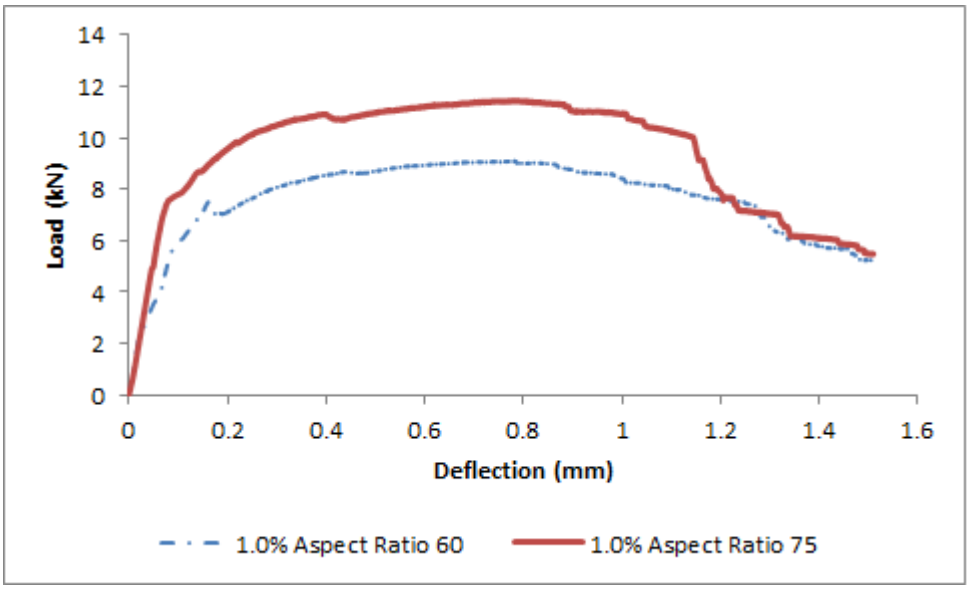

Figure 5.23: Load – Deflection Relationship for Aspect Ratio 60 & 75 at 1.0 % Fiber Addition

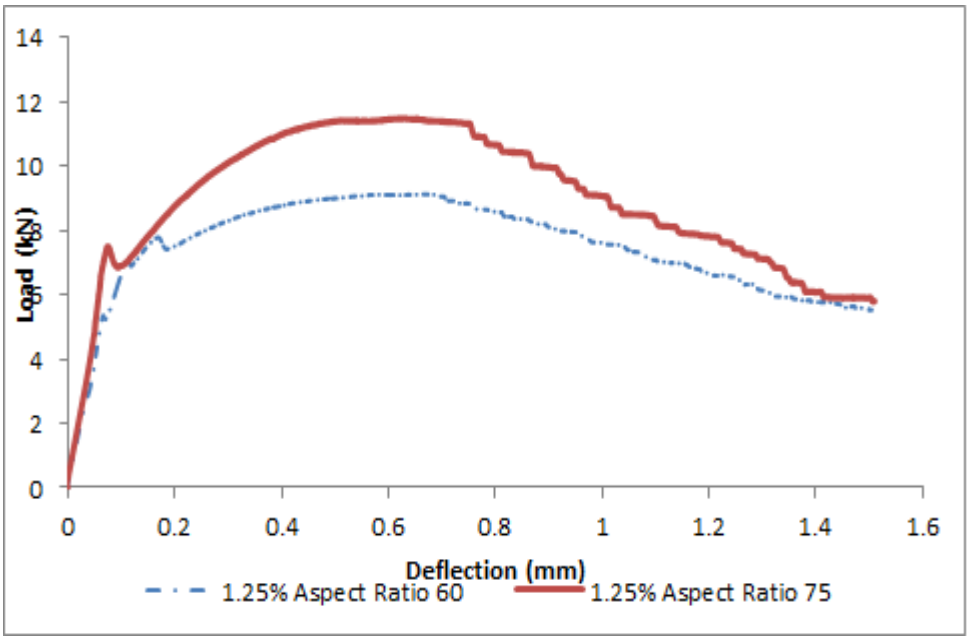

Figure 5.24: Load – Deflection Relationship for Aspect Ratio 60 & 75 at 1.25 % Fiber Addition

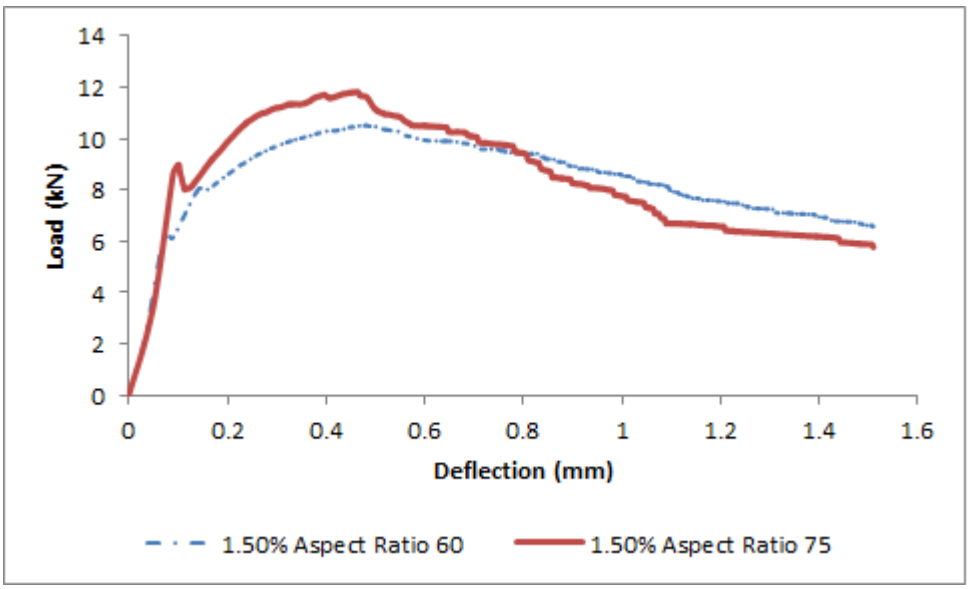

Figure 5.25: Load – Deflection Relationship for Aspect Ratio 60 & 75 at 1.5 % Fiber Addition

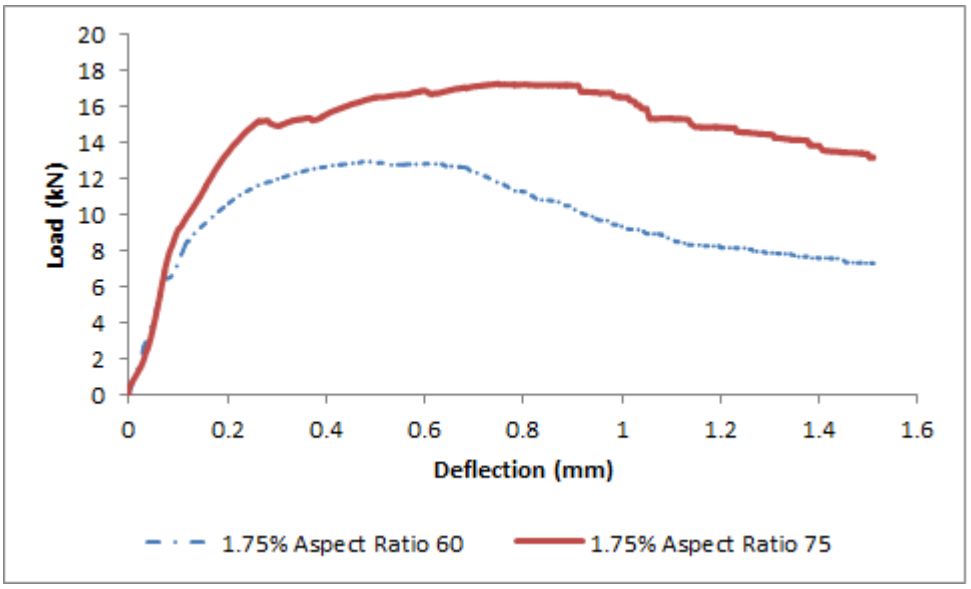

Figure 5.26: Load – Deflection Relationship for Aspect Ratio 60 & 75 at 1.75 % Fiber Addition

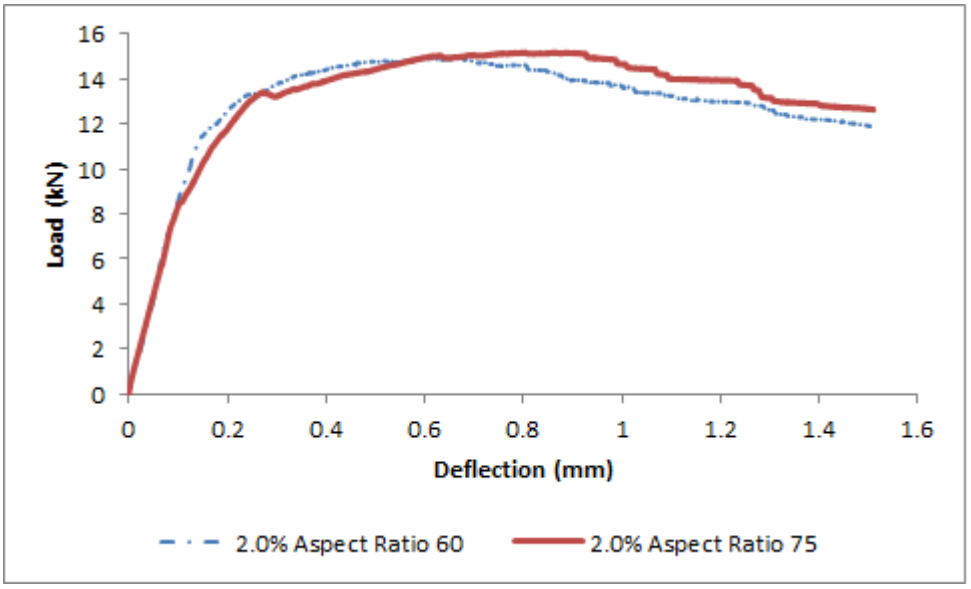

Figure 5.27: Load – Deflection Relationship for Aspect Ratio 60 & 75 at 2.0 % Fiber Addition

Table 5.12: Relationship for Deformation at Maximum Load

Aspect Ratio	Fiber Volume (%)	P_{max} (kN)	Deflection at Linearity End (mm) 'b'	Deflection at P_{max} (mm) 'a'	Ductility Index, μ (a/b)
	0.00	5.85	0.09	0.09	1.00
60	0.50	5.63	0.10	0.11	1.10
	0.75	7.14	0.07	0.65	9.40
	1.00	9.10	0.05	0.78	15.10
	1.25	9.13	0.07	0.68	10.20
	1.50	10.52	0.09	0.48	5.40
	1.75	12.97	0.07	0.49	7.60
	2.00	14.95	0.09	0.61	6.40
75	0.50	6.19	0.11	0.11	1.10
	0.75	8.17	0.14	0.59	4.10
	1.00	11.44	0.07	0.77	10.70
	1.25	11.49	0.07	0.62	9.00
	1.50	11.83	0.09	0.46	5.20
	1.75	17.29	0.08	0.75	9.40
	2.00	15.18	0.10	0.80	8.30

5.4 Effect of Proportion and Aspect Ratio of Fibers on Fracture Parameters of Concrete

High strength concrete have low porosity that results in improved bond strength at fiber – matrix interface, resulting in an increase in the density of ITZ from adequate compaction. This strengthening effect eventually has a significant effect on the fracture energy. In concrete with fiber addition, at higher volume fraction, the number of fibers crossing the crack area is increased requiring a greater amount of energy for crack propagation. Results presented in Table 5.13 indicate an increase in fracture energy, G_F with increase in compressive strength and fiber volume at the two aspect ratios under consideration depicted in Figure 5.28 – 5.29 respectively. The addition of the fiber increases the heterogeneity of the concrete, and during cracking,

the cracks is intercepted by the fibers aligned horizontally resulting from horizontal casting with cubic specimens. There is substantial energy dissipation during fiber pull-out and debonding mechanisms of the fiber.

A critical examination of G_F values for aspect ratio 60 and 75 indicate that the latter was higher than the former; however, the highest G_F value for aspect ratio 60 was 3,921.274 N/m while that of aspect ratio 75 was 4,455.617 N/m. This small difference regarding the two aspect ratios could be attributed to the tensile strength of the steel fibers where the former had 1,250 MPa and the latter 1,100 MPa, which might be the reason why they were closer despite aspect ratio 75 having a length twice that of aspect ratio 60 and a much larger diameter. The steel fibers allow for high energy absorption, fracture energy values, and high ductility. It has been reported in the previous section on the type of failure resulting from three-point bend test where only 0.5 % fiber addition failed by flexure. The difference in the fracture energy value is due to the pull-out and ruptures process in aspect ratio 60 and 75 respectively.

With respect to the l_{ch}, it is seen to increase with fiber addition and decreases with increase in tensile strength. This was significant in aspect ratio 75 where the maximum value stood at 5.9 m while that of aspect ratio 60 a mere 2.9 m. In both cases, they are significantly higher than the reference specimen which had l_{ch} of 0.89 m. This increase in ductility of the concrete could be attributed to the heterogeneity of the composite. Higher values are responsible for a more stable fracture process, in here aspect ratio 75 has a higher possibility. This means that the crack path of aspect ratio 75 is rougher than aspect ratio 60.

The fracture toughness also increases with increase in compressive strength and maximum size of aggregate as it has been reported in the literature. This results in a decrease in the brittleness associated with HSC from the heterogeneity. In Table 5.13, this increase is seen to increase with fiber addition and aspect ratio.

Table 5.13: Calculated Values of Concrete Fracture Parameters

Fiber (%)	AUC (kN/mm)	g (m/s^2)	d_o (1.5mm)	A_{lig} (m^2)	G_F (N/m)	Ec (GPa)	f_{st} (MPa)	l_{ch} (mm)	f_c (MPa)	P_{max} (kN)	α=(a/d)	F(α)	K_{ic} (MPa m^0.5)
0	2.08	9.8	0.0015	0.005	451.96	44.95	4.98	819.12	79.30	5.85	0.5	1.42	0.11
0.50-60	5.26	9.8	0.0015	0.005	1088.19	46.69	5.74	1542.20	90.70	5.63	0.5	1.42	0.10
0.75-60	8.69	9.8	0.0015	0.005	1775.10	47.52	5.82	2490.26	92.20	7.14	0.5	1.42	0.20
1.00-60	11.49	9.8	0.0015	0.005	2335.42	47.68	6.19	2906.22	98.70	9.10	0.5	1.42	0.42
1.25-60	11.26	9.8	0.0015	0.005	2288.47	47.59	6.78	2369.50	100.40	9.13	0.5	1.42	0.43
1.50-60	12.68	9.8	0.0015	0.005	2573.18	49.17	7.94	2007.08	108.90	10.53	0.5	1.42	0.66
1.75-60	14.92	9.8	0.0015	0.005	3022.01	49.08	8.77	1928.58	109.00	12.97	0.5	1.42	1.23
2.00-60	19.42	9.8	0.0015	0.005	3921.27	49.97	8.93	2456.97	116.00	14.95	0.5	1.42	1.88
0.50-75	5.35	9.8	0.0015	0.005	1105.21	47.05	3.30	4774.84	91.70	6.19	0.5	1.42	0.13
0.75-75	9.72	9.8	0.0015	0.005	1980.51	47.88	4.30	5128.11	93.80	8.17	0.5	1.42	0.31
1.00-75	14.13	9.8	0.0015	0.005	2862.26	47.56	4.80	5907.76	100.40	11.44	0.5	1.42	0.84
1.25-75	13.46	9.8	0.0015	0.005	2729.62	47.99	5.30	4663.68	94.40	11.49	0.5	1.42	0.86
1.50-75	12.76	9.8	0.0015	0.005	2589.23	49.84	7.00	2633.51	100.10	11.83	0.5	1.42	0.93
1.75-75	22.09	9.8	0.0015	0.005	4455.62	49.68	10.10	2169.76	107.00	17.29	0.5	1.42	2.92
2.00-75	19.91	9.8	0.0015	0.005	4019.95	50.00	11.80	1443.53	99.00	15.18	0.5	1.42	1.97

AUC: Area under the curve; g: Acceleration due to gravity; A_{lig}: Ligament length; d_o: Final deflection; α: notch-to-depth ratio; $1MN/\sqrt{m} = 3.23$

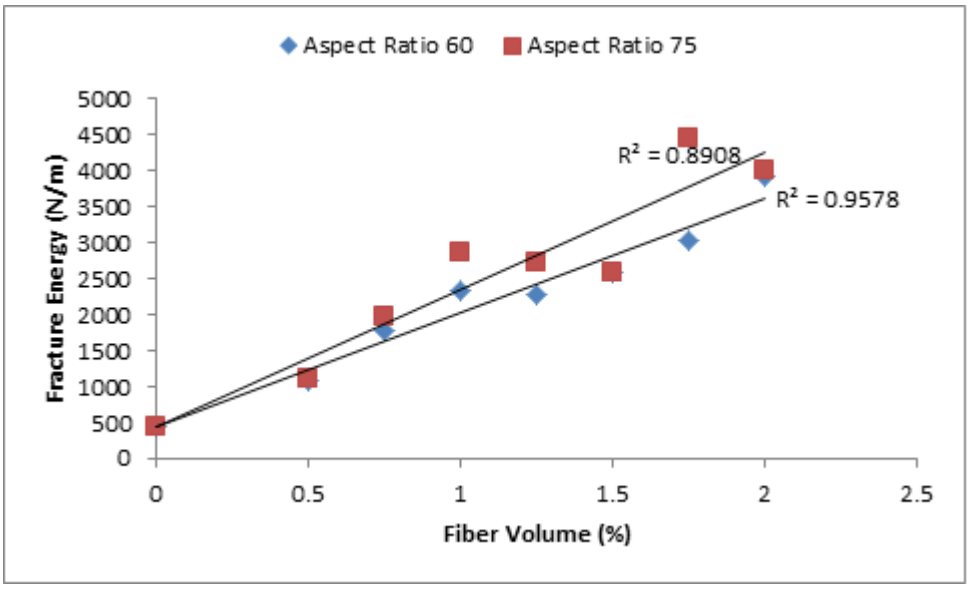

Figure 5.28: Relationship between Fracture Energy and Fiber Volume

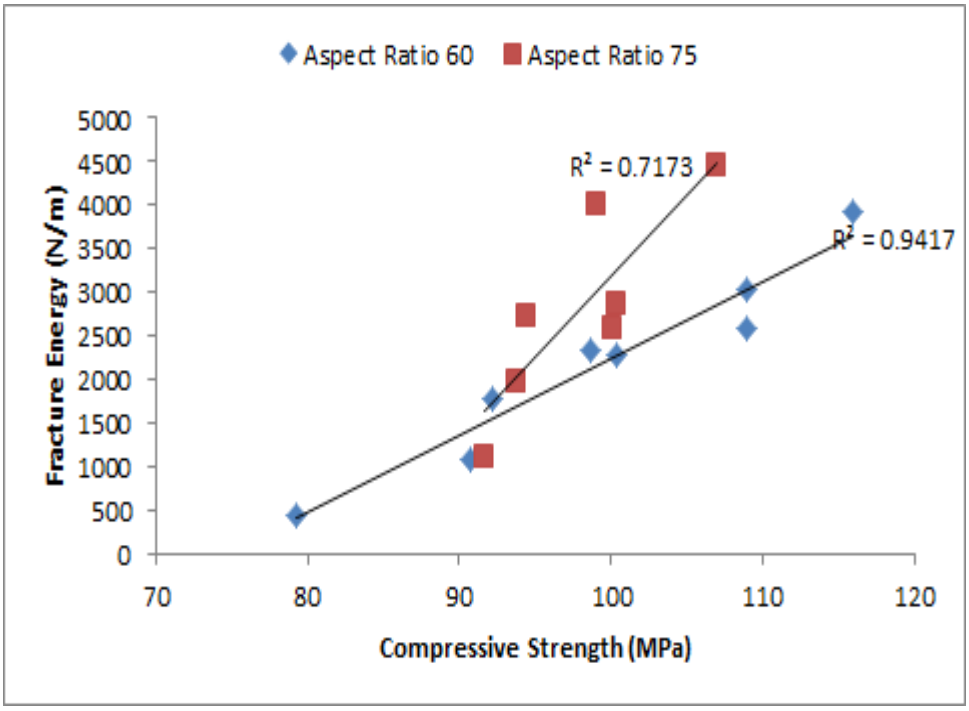

Figure 5.29: Relationship between Fracture Energy and Compressive Strength

5.5 Influence of Different Compressive Loading Levels on Residual Tensile Strength

In this section, the effect of different loading levels with respect to f_c value on tensile strength loss were studied by applying the specified compressive stresses given in

Table 4.6, perpendicular to the casting direction and then subjecting the specimen to f_{st} test. In brief, splitting tensile loading was applied in the same direction as the compressive loading to obtain residual tensile strength values presented in Table 5.15 for the different stress levels mentioned earlier for the two aspect ratios (60 and 75). Earlier on, f_{st} test was conducted on specimens without compressive loading to serve as the "virgin" tensile strength on reference samples, and values were obtained and are presented in Table 4.15. The first two stress levels selected represents compressive loading levels before linearity, while the third stress level is the point at which deviation from linearity is observed in the load – time diagram, which is the critical stress point. From this point onward, continuos crack propagation takes place even if the load is removed and is represented on a load – time diagram with a sharp bend in the diagram. The last stress level is a point selected after the end of linearity before failure of the specimen.

It could be seen from the results, that the linearity (third stress level) is within the range of 85 – 91 % of f_c. Tensile strength values obtained were mostly higher in the third and fouth stress level especially at higher percentage of steel fiber addition, this is more pronounced at 1.50 % fiber addition level and above.

In Figure 5.30, a depiction is provided on how the load – time diagram was used to follow the turning points of the curve for determining values presented in Table 5.14 for all the samples with fiber addition. Each diagram represent three samples that the average was taken to arrive at a single value for f_c after compressive loading.

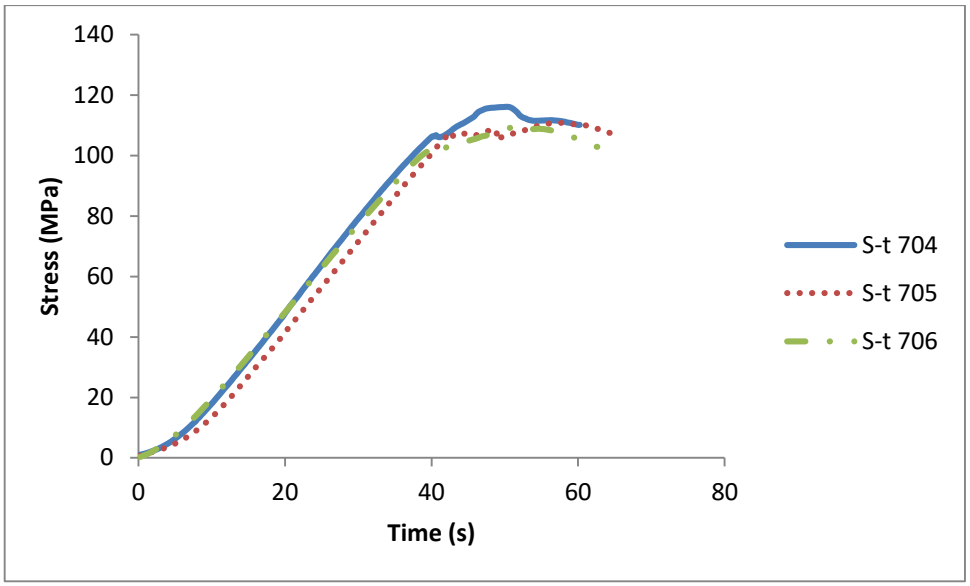

Figure 5.30: Representative Sample of Stress-Time Diagram from Load-Time for 1.75 % V_f Aspect Ratio 60

Table 5.14: Chosen Stress Levels as Percentage of Compressive Strength for TSL Determination

For Aspect Ratio 60					
Fiber Volume (%)	Compressive Strength, f_c (MPa)	f_{c1} (% of f_c)	f_{c2} (% of f_c)	f_{c3} (% of f_c)	f_{c4} (% of f_c)
0	79.30	40	60	70	75
0.50	90.70	75	85	89	95
0.75	92.20	70	80	86	95
1.00	98.70	70	80	90	96
1.25	100.40	70	80	89	95
1.50	108.90	70	80	87	95
1.75	109.00	70	80	91	95
2.00	116.00	70	75	85	95
For Aspect Ratio 75					
Fiber Volume (%)	Compressive Strength, f_c (MPa)	f_{c1}(% of f_c)	f_{c2} (% of f_c)	f_{c3} (% of f_c)	f_{c4} (% of f_c)
0	79.30	40	60	70	75
0.50	91.70	70	80	88	95
0.75	93.80	70	80	85	93
1.00	100.40	70	80	88	95
1.25	94.40	70	80	90	95
1.50	100.10	70	80	85	93
1.75	107.00	70	80	90	95
2.00	99.00	70	80	87	95

f_{ci} = percentage of f_c loading where i = 1, 2, 3, and 4

Table 5.15: Residual Tensile Strength (f_{tr}) after each Chosen Compressive Stress Level f_{ci}

Aspect Ratio 60					
Fiber Volume (%)	Tensile Strength, f_{st} (MPa)	f_{tr1} after f_{c1} loading (MPa)	f_{tr2} after f_{c2} loading (MPa)	f_{tr3} after f_{c3} loading (MPa)	f_{tr4} after f_{c4} loading (MPa)
0	4.98	4.79	4.43	3.45	3.43
0.50	5.74	3.87	2.44	4.01	4.58
0.75	5.82	3.53	3.31	1.91	5.14
1.00	6.19	5.37	3.48	3.88	1.32
1.25	6.78	3.27	5.60	4.74	5.22
1.50	7.94	5.38	8.56	5.92	6.80
1.75	8.77	7.84	8.71	8.00	8.14
2.00	8.93	4.85	3.62	8.46	10.26
Aspect Ratio 75					
Fiber Volume (%)	Tensile Strength, f_{st} (MPa)	f_{tr1} after f_{cl} loading (MPa)	f_{tr2} after f_{c2} loading (MPa)	f_{tr3} after f_{c3} loading (MPa)	f_{tr4} after f_{c4} loading (MPa)
0	4.98	4.79	4.43	3.45	3.43
0.50	3.30	4.55	3.52	3.40	4.53
0.75	4.30	4.40	4.15	2.79	5.27
1.00	4.80	2.18	7.12	4.10	4.32
1.25	5.30	2.57	4.48	3.56	3.52
1.50	7.00	2.12	7.71	7.20	6.58
1.75	10.10	4.56	10.21	7.64	10.63
2.00	11.80	5.48	7.69	8.00	10.33

f_{tri} = residual tensile strength after percentage of f_c loading where i = 1, 2, 3, and 4

Tensile strength loss (TSL) values calculated from Eqn. 4.9 shows a percentage change (decreament or increament) in f_{st} in the specimen subjected to different f_c loading levels, and results are compared with the reference specimen depicted in Figures 5.31 – 5.32 for the two aspect ratios under consideration. Specimens with aspect ratio 60 shows no definite trend, however, in aspect ratio 75, there was a lot of f_{st} gain which is represented with the bars in the negative direction (below zero

point – Figure 5.32). This could be attributed to the effect of the fiber addition, and it's resistance to crack propagation. Resulting from improvement in bridging capacity of the concrete, greater pull-out behavior with teething process in high aspect ratio, and fiber addition level. This sum up the advantage of using the fiber in HPC. Resistance offered by the fibers depends on the interface bond between fiber and matrix, at the same time a weak zone in the matrix. Correlating the results with that of the three-point bend test, it is evident that because of the pull-out in lower aspect ratio and rupture in higher aspect ratio at 0.5 % volume fraction, the resistance is very high in aspect ratio 75. This brings to fore the advantage of fiber length where a critical length is required which is restricted by fiber-matrix bond. It is seen that the higher aspect ratio results in higher tensile strength especially at higher volume fraction, increasing the ductility.

The aim of the fiber addition is to limit the crack propagation by stress transfer especially after the first crack by enabling the concrete to sustain very high strain compared with the reference concrete without fiber addition. It could be seen in Figure 5.31 – 5.32 that the TSL for the reference specimens increased with an increase in f_c loading at 40, 60, 70 and 75 % of f_c, however, the same cannot be said of concretes with fiber addition due to what has been highlighted. Looking at these same figures under consideration, we could also attribute the lack of trend in the results especially at aspect ratio 75 to pseudo-strain hardening effect where the material is characterized by multiple microcracking and high stiffness. Though, multiple microcracking was not observed in the flexural specimens, failure was by a single crack as seen in Figure 5.16. It has been mentioned earlier that the flexural specimens failed not by flexural failure apart from 0 – 0.5 % fiber addition, subsequent specimens failed by a single small cracks which indicates an

improvement in stiffness of the concrete. Though, there was improvement in ductility and strength, aspect ratio 75 exhibited the possibility of more strain hardening effect from Figure 5.32 compared with aspect ratio 60 due to longer fiber length.

Correlating the results with the literature in Section 3.9 where we learned that TSL is highest in NSC and lowest in HSC due to improvement in the matrix and limited amount of flaws in the concrete. This study showed a continuing trend and more significant in aspect ratio 75 due fiber addition.

The improvement in the aggregate – matrix interface due to the utilization of small D_{max} aggregates could also makes the likelihood of bond stress failure much less likely, which improves the aggregate – matrix – fiber interaction resulting in higher toughness and ductility of the composite. As can be seen the larger the aspect ratio, the more the effect of tensile strength gain is observed than in lower aspect ratio.

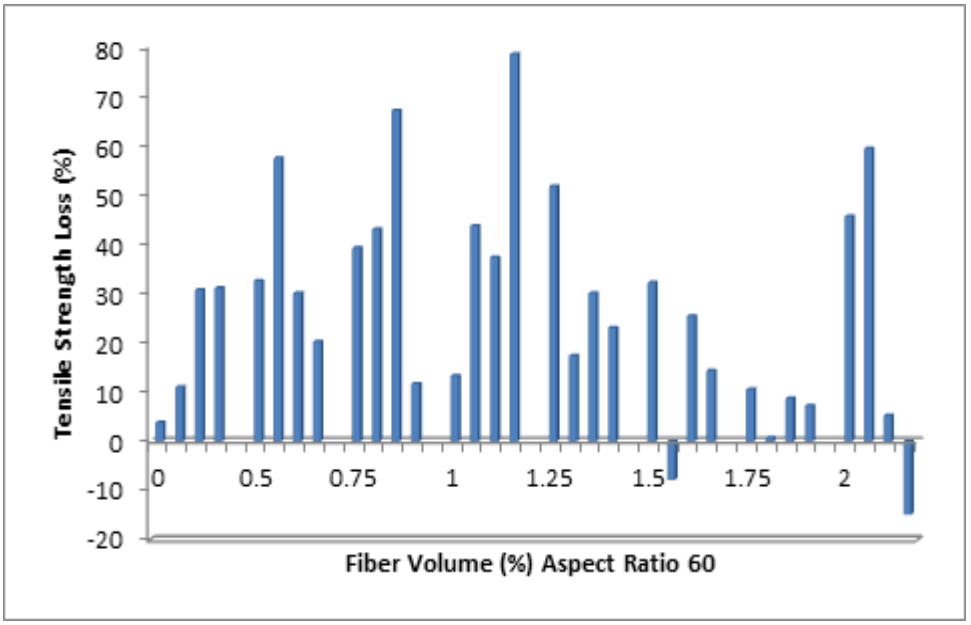

Figure 5.31: Effect of Fiber Volume of 60 Aspect Ratio Fibers on TSL for each Specified f_c Loading.

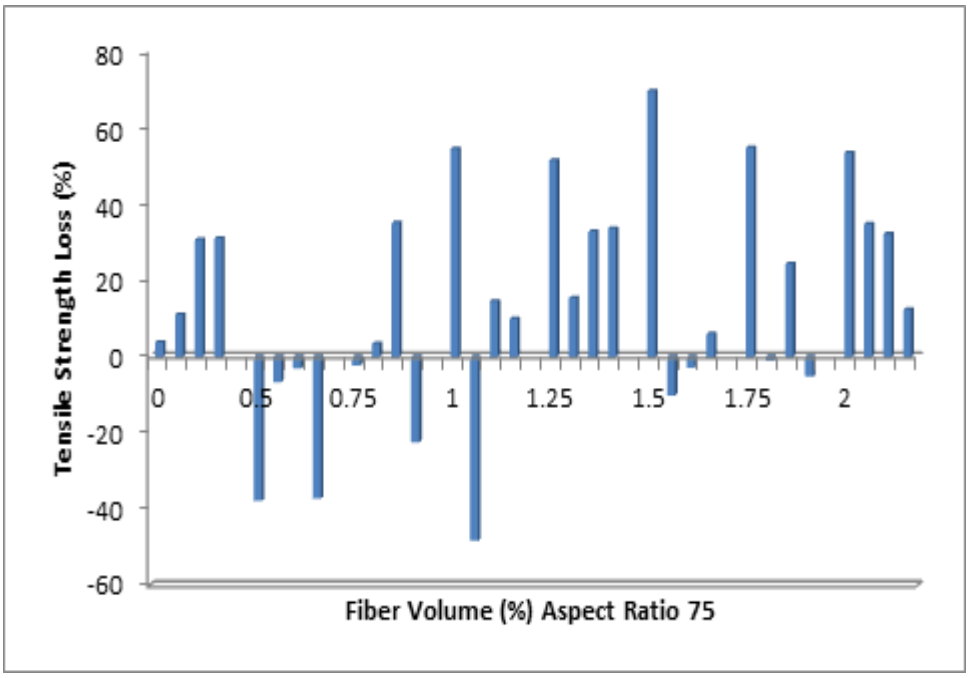

Figure 5.32: Effect of Fiber Volume of 75 Aspect Ratio Fibers on TSL for each Specified f_c Loading Levels.

5.6 Effect of Proportion and Aspect Ratio of Fibers on Failure Mechanism

In this section, crack formation and propagation of the split surfaces of the specimens loaded up to certain stress level (Table 5.14) and subjected to splitting tensile strength were examined. In each of the fibered concrete test series, there are five observation levels with at least three test specimens. This consist of 0 % level compressive loading where the specimen was only subjected to splitting tensile test, two points before the linearity, the linear point itself, and one more point post-linearity. However, the control or reference specimens were loaded at 0, 40, 60, 70, and 75 % of f_c.

5.6.1 Microcracking Behavior of Control Specimens

It was observed that the matrix was dark grey in color which is typical of HSC with silica fume addition, and the aggregate was light grey with some colored aggregates

in between, features of crushed limestone aggregates, and distinguishable. From 0 – 60 % of f_c loading levels, the matrix and aggregates were relatively stable with no noticeable cracks in the former or latter with exception of a few microcracks on the surface of the aggregates. However, upon close examination, some of the aggregates especially the colored ones had deficiencies inherent in them, such as holes, crevices, as well as spalling on their edges.

As can be seen in Figure 5.27, at 70 - 75 % of f_c which was the highest level of loading the control specimens were subjected to, it was observed that there were no failure patterns or cracks in the matrix. However, it was seen that there was distinct line of separation round the aggregate particles from the matrix that delineates the two components. Unfortunately, we could not load the specimen any further; as such we can only speculate that the end of the linear portion of the graph was not closer because the matrix and the aggregates were still a monolithic component. At 75 % of f_c about 60 MPa, and the test was discontinued, but the matrix was still intact, and the reason why the linear portion of the load – time diagram was still linear up to this level is due to the existence of small amount of microcracks in the specimen that have not reached critical width to cause a deviation in the curve.

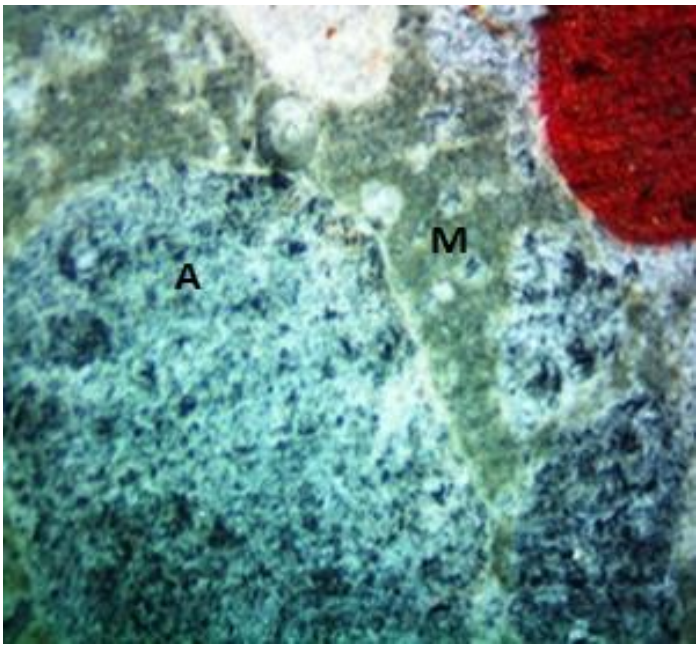

(a) 70%

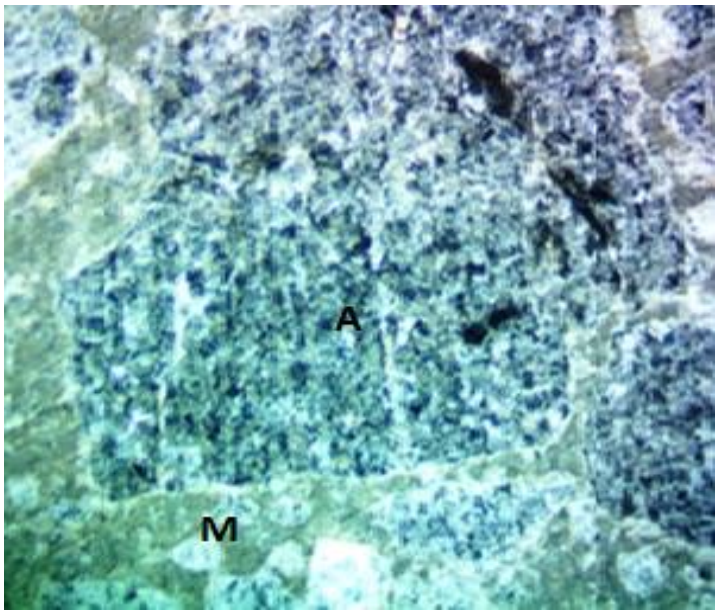

(b) 75%

Figure 5.33: Control Specimens under the Microscope at Different Percentages of f_c Loading (A=Aggregate; M= Matrix)

5.6.2 Microcracking Behavior of Concretes with Fiber Addition

With the knowledge acquired from the reference specimens without fiber addition loaded up to 75 % of f_c, we therefore decided to do the same for the fibred concrete loading compressively to 70 %, 80 %, the linearity end point, and the post-linear

portion. In light of this, discussion has been subdivided into 0 – 70 %, 70 – 80 %, the linearity end point, and the post-linearity.

5.6.2.1 First Linear Portion (0 – 70 %)

In this segment, observation regarding the stability of the matrix is still valid. The matrix and aggregate were still bonded monolithically up to this point with no separation, delamination or cracking resulting in the matrix. This is an indication of the quality of the matrix; however, delamination was noticed at the interface between the matrix and the steel fiber as well as matrix spalling at the mouth of the fiber. This could be attributed to the mismatch between the tensile strength of the fiber given in Section 4.1.4, and that of the matrix. Close examination shows the existence of gaps between the matrix and the smooth surface of the fibers. Also, crevices appear at the mouth of the fiber with spalling which was responsible for the gap noticed. There was also matrix debonding and sliding in the presence of the fiber, where at lower percentages this was minimal but at high fiber addition level, this became pronounced. Matrix cracking was also present at the tip of the hooked-end of the fiber creating a hole or depression that concentrate spalling zone.

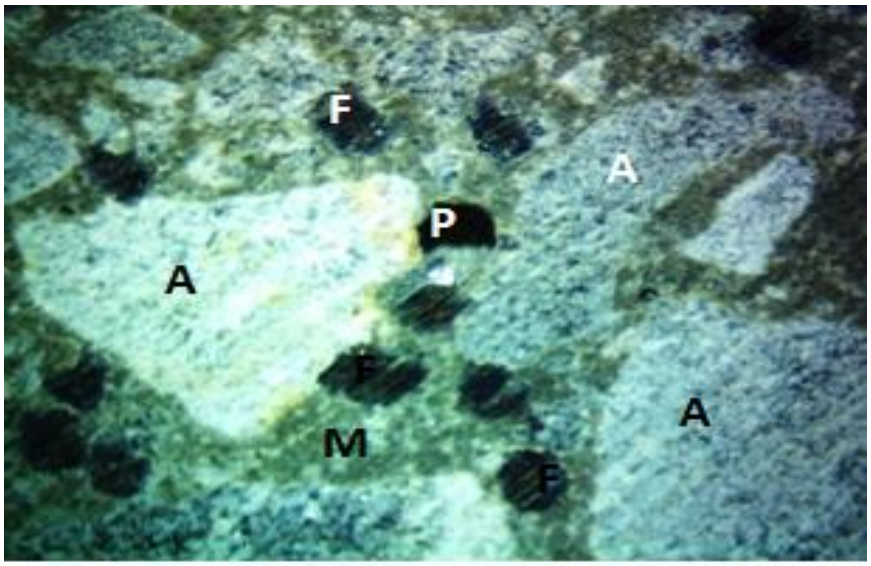

Aspect Ratio 60

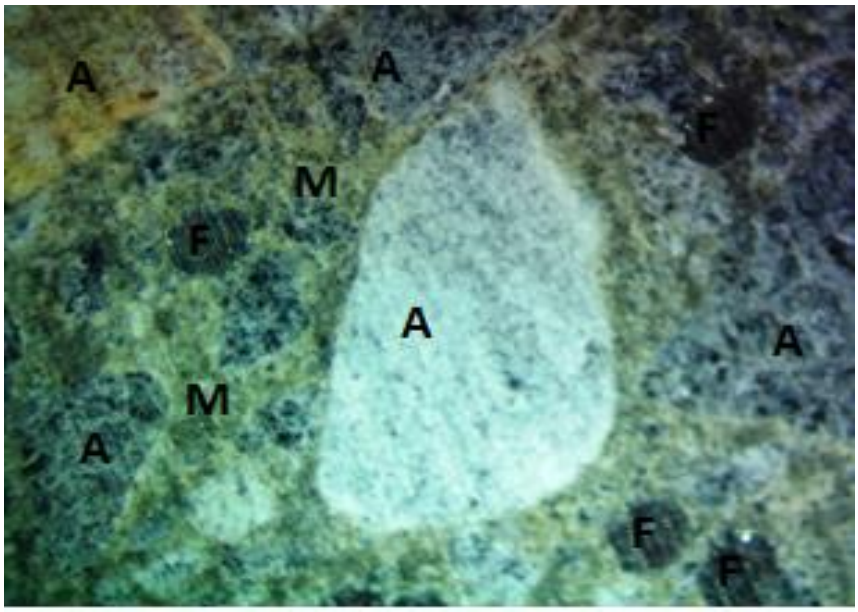

Aspect Ratio 75

Figure 5.34: Compressive Loading at 0 % Compressive Loading and 0.5 % Fiber Addition

Where: A: Aggregate; F: Fiber; M: Matrix; P: Porosity.

In general, with respect to this particular loading level, apart from what was highlighted, matrix was relatively stable. However, that does not eliminate the existence of microcracks that develop as a result of the accumulation of loading accompanied by mechanisms that dissipate energy, even though they are small, but the mismatch between the fiber and matrix is the prominent feature that causes some of the damages at this stage.

5.6.2.2 Second Linear Portion (70 – 80 %)

This is the portion that is just around the peak region where in normal concrete is characterized by propagation of bond cracks in multiple directions from aggregate shape. However, there was limited or no propagation of matrix cracks in most of the specimens. On the other hand, what was observed was the continuation of the matrix spalling seen earlier at around 0 – 70 % accompanied by debonding from the matrix, and at the fiber hooked - end. At this stage, these processes became extensive.

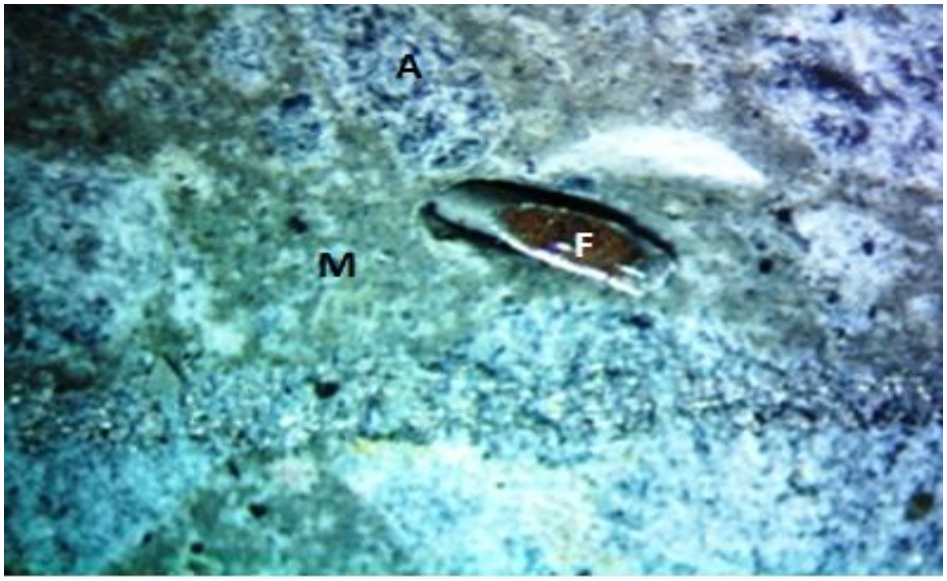

(a) Matrix Spalling at Fiber Mouth under Compressive Loading of 75 % Aspect Ratio 60

(b) Compressive Loading at 70 % Aspect Ratio 75

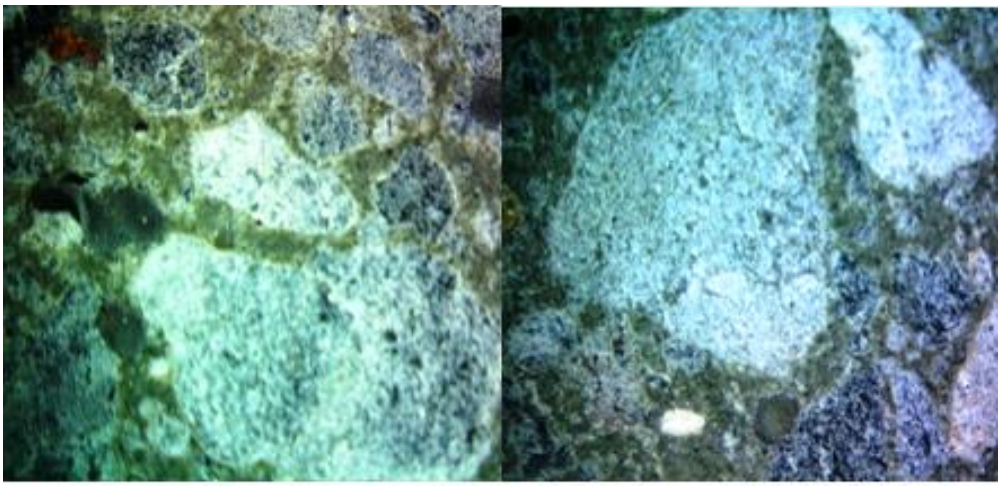

(c) Matrix Stability at 80 % Compressive Loading Aspect Ratio 60

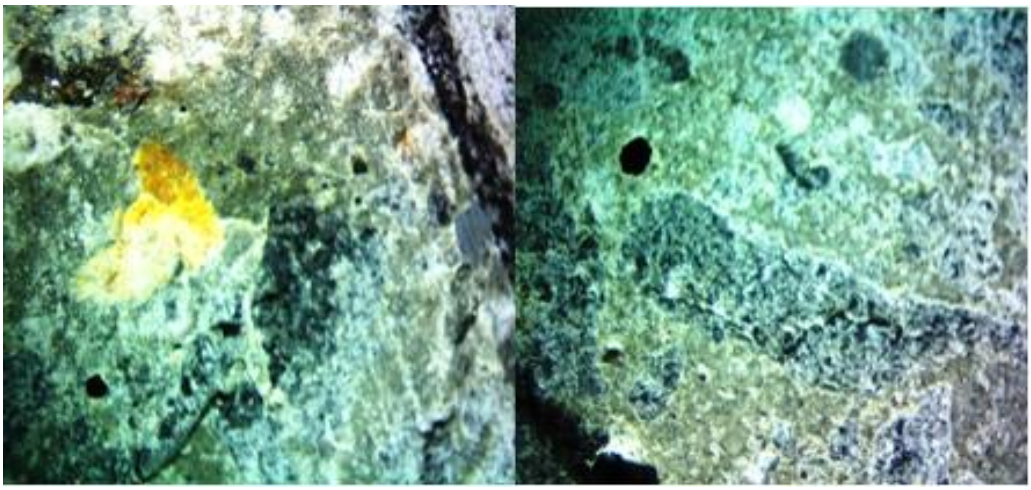

(d) Compressive Loading at 80 % Aspect Ratio 60

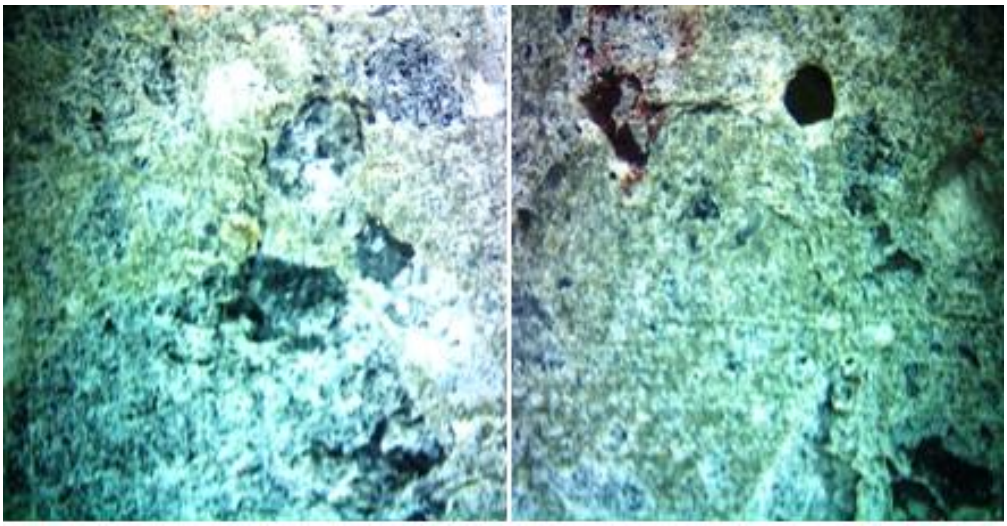

(e) Compressive Loading at 80 % Aspect Ratio 75

Figure 5.35: Bond and Matrix Cracking Prior to Peak (70 – 80 %)

It was also observed from Figure 5.35c that the shape of the aggregate becomes distinct and distinguishable from the matrix. Defects presents in the aggregates begin to manifest, and cuts from production process became pronounced. Sparsely distributed matrix cracks appear and coalesces, and sometimes proceed until they are blunted or intercepted by pores present in the specimens where they terminate. These cracks were more prominent in concrete with aspect ratio of 60 than aspect ratio of 75, and this could only be attributed to the crack arresting mechanism of the fibers. The frequency of this cracks diminished with increase in V_f.

5.6.2.3 Linearity End Point (80 - 91 %)

This region is characterized by strain localization where the bond cracks coalesce into the matrix as a single crack or multiple cracks as the case may be. This is why in Figures 5.31 – 5.32 tensile strength gain was observed in some cases which became significant in aspect ratio 75 specimens. However, the most significant observation in this region is the propagation of extensive networks of multiple branched microcrackings that extends to other quadrants (Figure 4.5). There was severe spalling and cracking of the matrix as seen in Figure 5.36; transgranular fracture of the aggregate particles was also observed. Spalling was seen to occur at the edges of the specimen, with perpendicular cracks appearing to the direction of the casting. The intensity of these cracks decreases with fiber addition and aspect ratio, where it is more extensive in aspect ratio 60. Aggregate – matrix interface had severe bond cracks that at times cause separation between the two components. These cracks extend into voids where they are intercepted, and continue at times. However, the severity of the cracks was extensive at the edges of the specimen and begins to decline as it moves towards the center of the specimen. These distributed networks of

cracks weaken the concrete, and this shows that the specimen is weaker at the extreme end compared to the center.

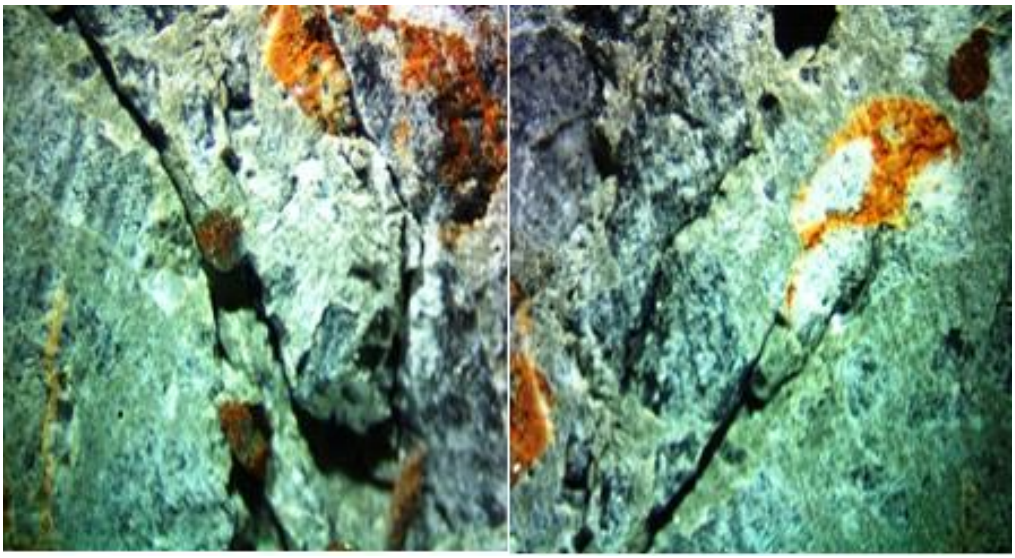

(a) Compressive Loading at 86 % Aspect Ratio 60

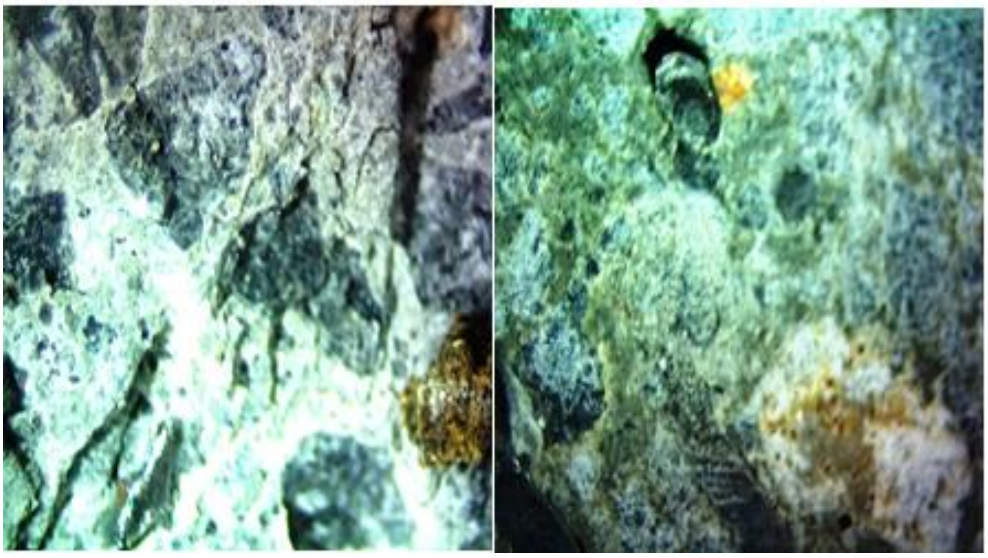

(b) Compressive Loading at 87 % Aspect Ratio 75

Figure 5.36: Severe Damage Occurring at Linearity (80 – 91%)

5.6.2.4 Post - linearity End Point (91 % and above)

In normal concretes, multiple cracks highlighted in the previous section reach critical width and length, and results in accelerated propagation and failure. Observations presented in Figure 5.37 – 5.38 for aspect ratio 60 and 75 showed upon surpassing

the linear portion of the curve, the damage zone begins to expand from the initial localized position. Bond cracks multiply and rapidly begins to coalesce with one another leading to matrix debonding from the aggregate. Severe spalling was noticeable on the surface of the specimen and it was extensive at the matrix - fiber interface especially at the mouth of the contact point between the two. Cracks extend into pores and voids, and propagate further, where the voids did not serve as a crack blunting measure. Severe cracking was observed at the edge of the specimen perpendicular to the casting direction, and depending on the aspect ratio. The severity decreases with increase in V_f levels, due to the amount of fiber per unit area, an indication that the fiber addition suppresses the severe damage in the weak zone of the specimen, and it was more effective at higher volume and at larger aspect ratio. Aggregate – matrix interface and transgranular damage was clearly observed with severe spalling round the aggregate particle.

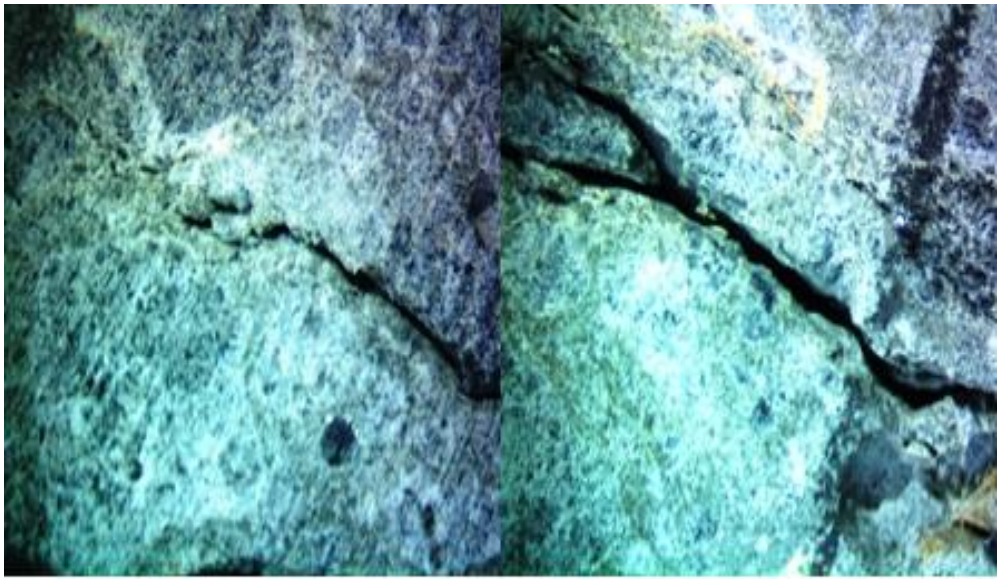

(a) (b)

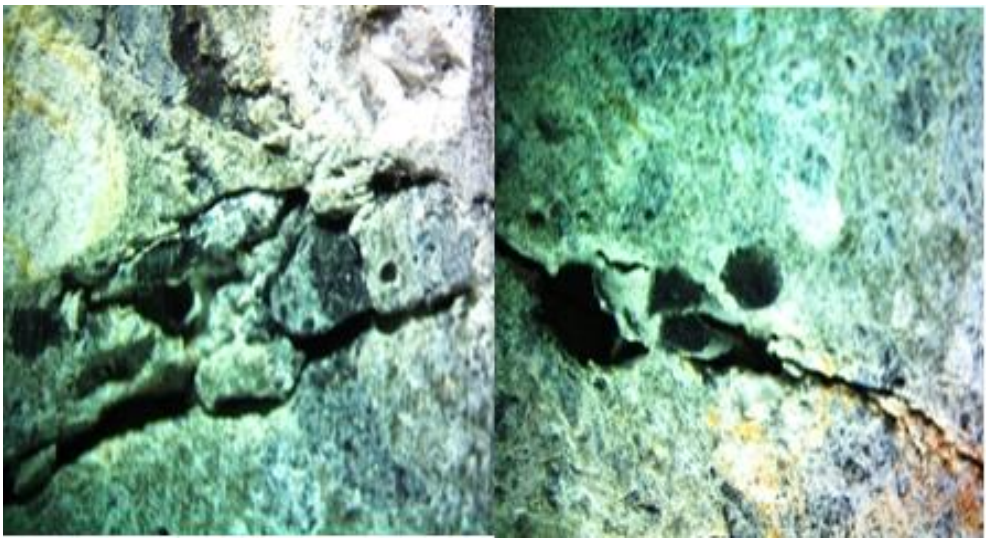

(c) (d)

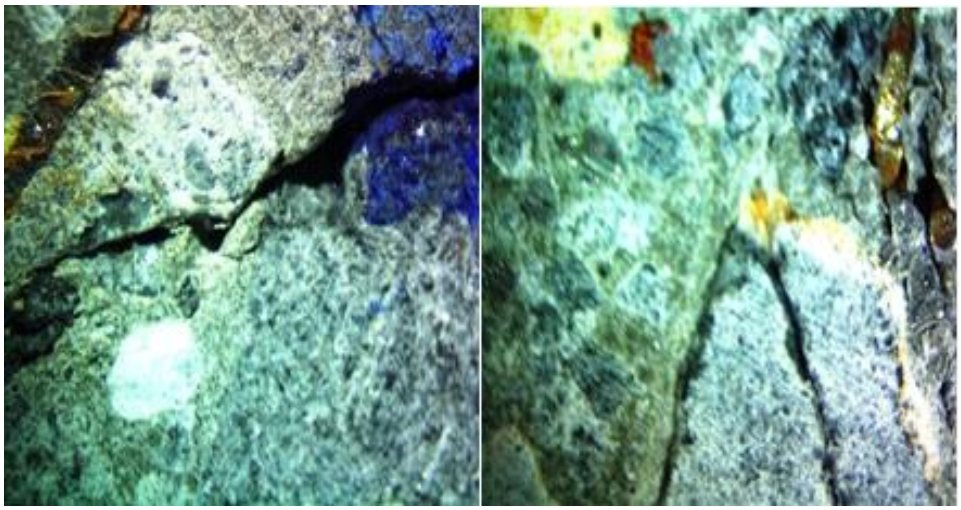

(c) (f)

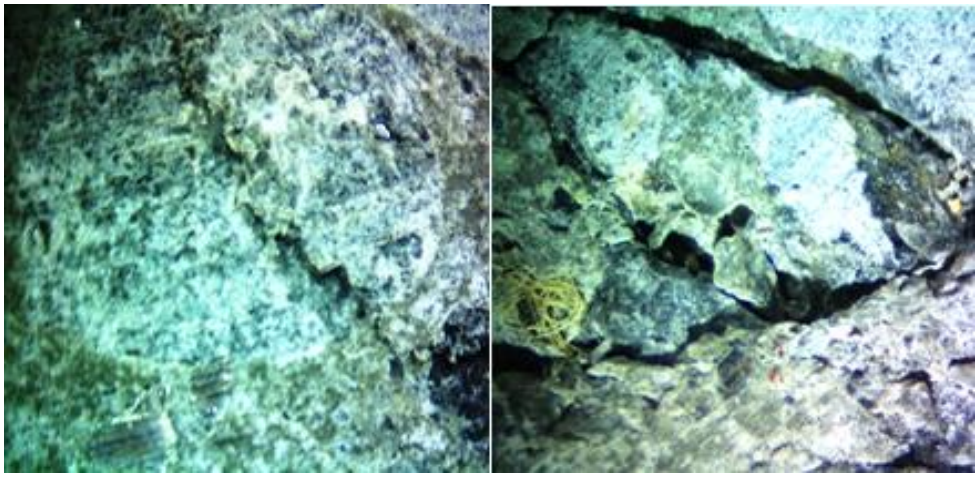

(g) (h)

Figure 5.37: Compressive Loading of 95 % Post-linearity at Aspect Ratio 60

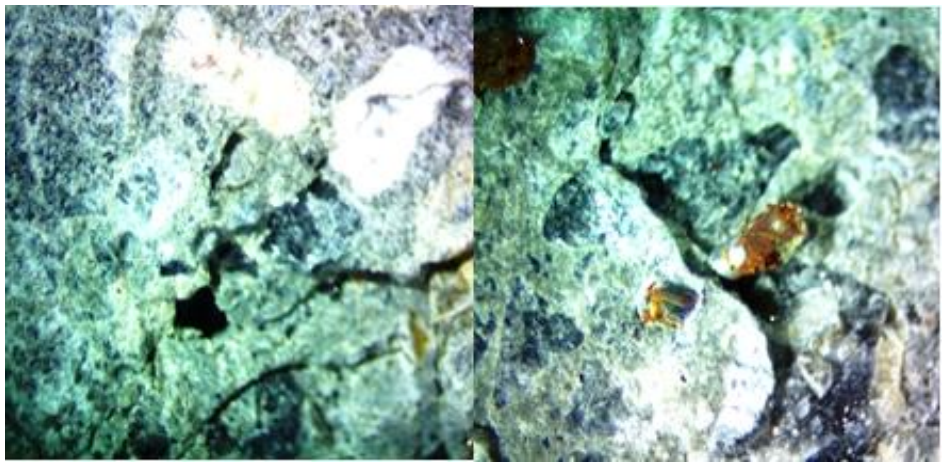

(a) (b)

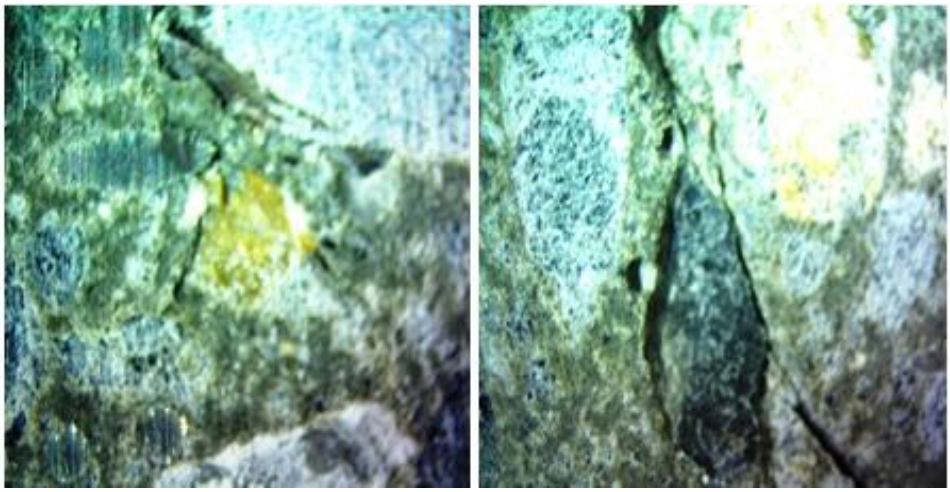

(c) (d)

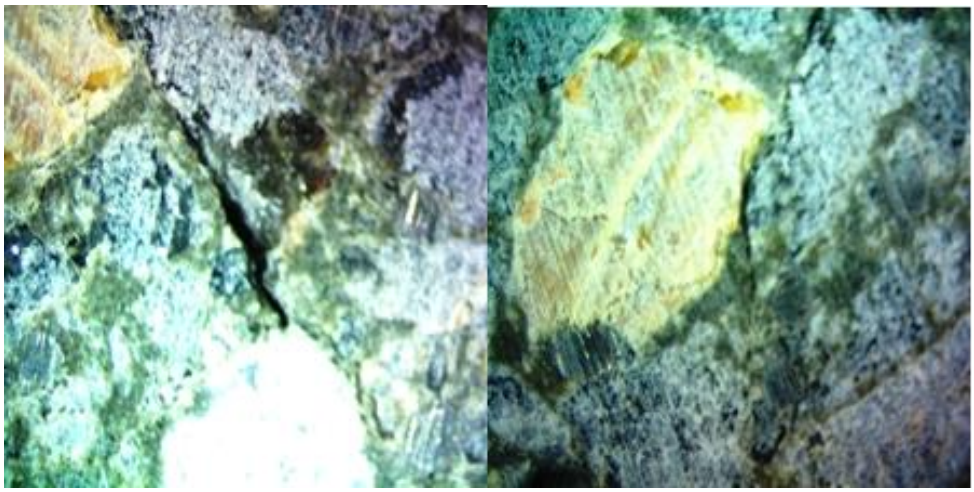

(e) (f)

Figure 5.38: Compressive Loading of 95 % Post-linearity Damage Cracks at Aspect Ratio 75

5.6.3 Effect of Proportion and Aspect Ratio of Fibers on Microcracking Definition

In Figure 5.39, the processes described in Section 5.6.2.1 – 5.6.2.4 are depicted in graphical manner itemizing them under the influence of compressive loading prior to the ultimate stress. It is seen that the pre-existing microcracks in the concrete are the ones that under the influence of load propagate from the ITZ, initiating the failure process under uniaxial compression where the tensile directions are free of any influence. This reinforces the notion that tensile strength is a criterion for crack initiation when it is exceeded resulting from stress concentration in the vicinity of a pore or aggregate particles.

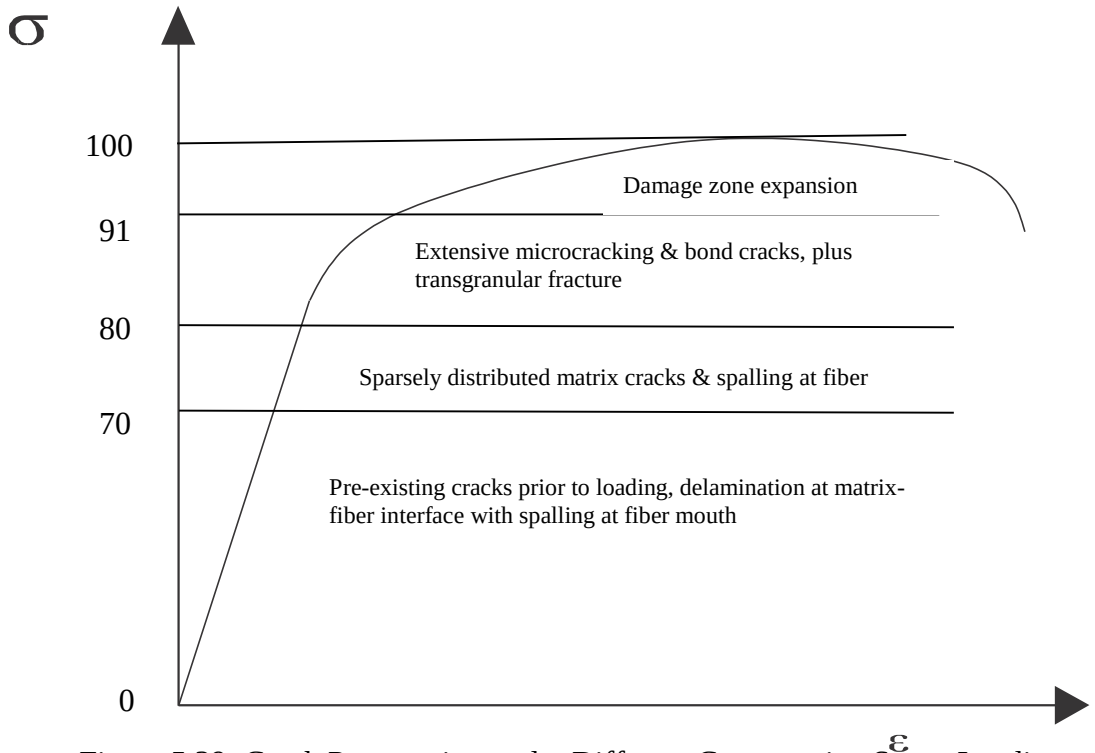

Figure 5.39: Crack Propagation under Different Compressive Stress Loading

These cracks highlighted have to attain “critical” length, width, depth, interconnectivity, and volume. When this occurs, matrix cracks begin to propagate couple with spalling at fiber – matrix interface noticed.

In the present study, the existence of sparsely distributed microcracks at 70 – 80 % of f_c at the interface could be attributed to the maximum size of the aggregate which was limited to 10 mm. whereas, if the size has been larger, the interface cracking would have dominated this region. Hence, the reason for the existence of limited bond cracks. Also, these bond cracks would have concentrated around the larger aggregates if they were present at increased stress loading.

In the third zone (80 – 91 % of f_c), the presence of the steel fiber aggravated the concentration of the extensive microcracks seen at the fiber – matrix interface especially at the fiber mouth which noticed extensive spalling. In normal concrete, this region harbor distributed cracks that manifest and metamorphosized into continuous cracks due to coalesce, but the presence of voids and entrapped air underneath the fibers and aggregates from horizontal casting increases the density of these cracks. Beyond this region (91 % and above), the localized damaged zone expands with rapid propagation of those cracks resulting in an explosive failure of the specimen under load control test despite the presence of the fibers.

5.6.4 Effect of Proportion and Aspect Ratio of Fibers on Critical Crack Widths (Linearity End Point)

It has been highlighted earlier that the linearity ended between 85 – 91 %, and this region was critically examined using the shaded quadrant (Figure 4.7) where extensive damage was observed at these loading levels. The total length of the crack

was constant covering the unit length of the quadrant (50 mm), however, the width of the crack varies based on the aspect ratio and V_f level. The most critically damaged quadrant was selected, and estimate of the critical width using the measurement application inbuilt in the microscope was made.

From Figure 5.34, wider crack sizes were observed at aspect ratio 60 and low V_f level due to the amount of fiber per unit area. Narrow crack widths were observed at aspect ratio 75 especially at higher V_f level. In some instances, measurement could not be obtained because the failure patterns were mostly branched network of microcracks beyond the capacity of the microscope; others were a combination of aggregate spalling, multiple microcracks, and degradation in the matrix. In general, it could be said that higher aspect ratio is more effective in mitigating the effect of major cracks. In light of the above, the measured crack widths were within the proposed crack width by Slate and Hoover (1984) of between 100 μm and 6 μm for upper and lower limits.

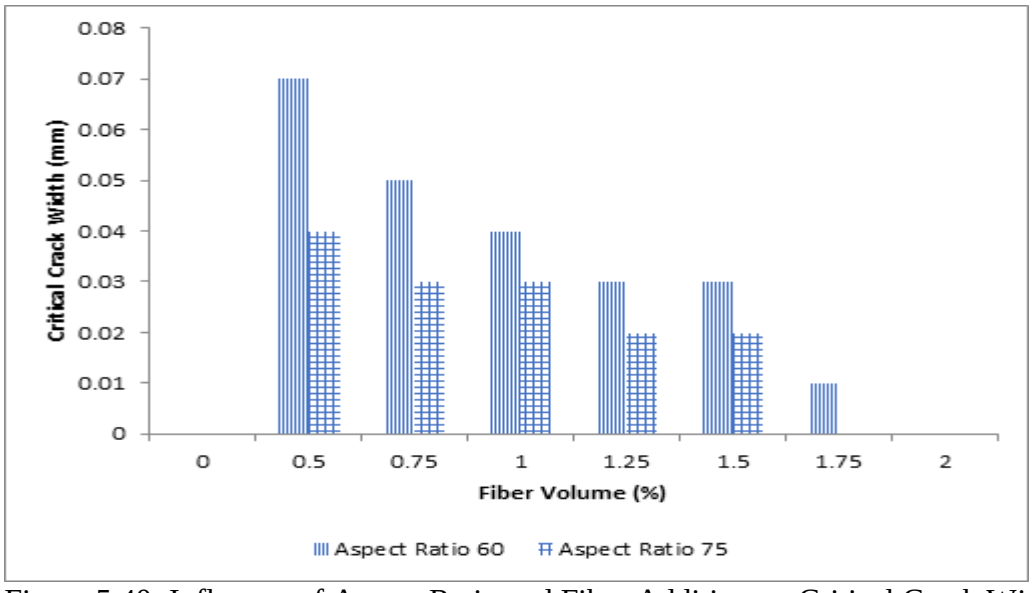

Figure 5.40: Influence of Aspect Ratio and Fiber Addition on Critical Crack Width

Chapter 6

CONCLUSIONS AND RECOMMENDATION

6.1 Conclusions

A wholistic investigation on HPC with steel fiber addition was conducted on fresh, hardened, and microcracking properties was conducted. The effect of uniaxial compressive loading on microcracking behavior was conducted, and the following conclusions have been drawn:

i. Steel fiber addition at higher V_f results in an increase in the viscosity of the mix, decreasing the flowability, and increasing the unit weight.

ii. An Increase in V_f values results in an increase in the VeBe time; decrease in the Compacting factor and Slump; and increasing the tendency for balling to occur, in essence the workability decreases significantly. Above compacting factor of 0.8 which approximately correspond to 1 % V_f (78.50 kg/m^3), this type of concrete will be difficult to implement in the field.

iii. There is a good correlation existing between fiber volume and the workability parameters for VeBe, compacting factor and slump respectively as seen from the coefficient of determination. Increasing the V_f results in low workability for compacting factor and density compared with VeBe time and slump.

iv. In general, a combination of two or more workability parameters should be used to evaluate the performance of a mixture.

v. For small proportions of V_f addition (up to 1 %), f_c of aspect ratio 75 specimens are higher than those of aspect ratio 60; but beyond 1 %, f_c of

aspect ratio 60 specimens increases significantly. At 2 % fiber addition, the strength effectiveness of aspect ratio 60 is greater than 75 (46.3 % and 34.9 % respectively). Higher V_f in lower aspect ratio results in significant increase in f_c compared with higher aspect ratio.

vi. In the same vain, for small proportions of V_f addition (up to 1.5 %), f_t of aspect ratio 60 specimens are higher than those of 75; but beyond 1.5 % (1.5 % - 2 %), f_t of aspect ratio 75 specimens becomes higher. At 2 % fiber addition, strength effectiveness of aspect ratio 75 is greater than 60 (136.0 % and 79.3 % respectively). The higher the V_f and aspect ratio, the more significant is the increase in f_t.

vii. Effect of steel fiber on f_t is about 2 – 3 times greater than on f_c depending on aspect ratio and proportions of fiber, it is also significant in f_t compared with f_c.

viii. TSL for the specimens with aspect ratio 60 shows no definite trend, however, in aspect ratio 75, f_t gain is observed. TSL for the reference specimen increased with f_c loading levels, but the same cannot be said of concretes with fiber addition. The larger the aspect ratio, the more the effect of tensile strength gain compared with the lower aspect ratio.

ix. Fiber volume addition especially at higher percentages results in a significant increase in flexural strength; linear portion of the ascending phase of load – deflection diagram is steeper, and strain hardening response is the dominant characteristics of the curve in the descending phase from 58.9 kg/m^3 V_f.

x. Fracture parameters increases with fiber volume addition and with compressive strength.

xi. In terms of failure mechanism, fewer bond cracks were observed prior to linearity, however, it cannot be said that they do not exists, probably the capability of the microscope did not capture them at that level.

xii. In control specimens (without fiber); at 70 – 75 % of f_c loading, no failure patterns or cracks formed in the matrix however, there were distinct lines of separation round the coarse aggregate particles from the matrix that delineates the two components.

xiii. At 70 – 80 % of f_c loading, processess observed in the previous stage at matrix – fiber interface became extensive. These cracks were more prominent in concrete with aspect ratio 60 than 75. The frequency of the cracks diminished with increase in V_f.

xiv. The end of linear portion of the graph varies from 85 - 91 % of f_c, an indication of the quality of the matrix, resulting from delay in the formation of the microcracks that causes a deviation in the linearity.

xv. At linearity end point (85 - 91 % of f_c), there was severe spalling of the matrix, and transgranular fracture of the aggregate particles. The intensity of these cracks decreases with V_f and aspect ratio, where it is more extensive in aspect ratio 60. The linearity end point increases with fiber addition.

xvi. At post – linearity point (91 % and above), at aggregate – matrix interface, transgranular damage was clearly dominant with severe spalling round the aggregate particle. Bond cracks is delayed, an indication of the quality of the matrix.

xvii. Failure pattern of the specimens after compressive loading were such that long concave cracks perpendicular to the direction of the casting were prominent. The intensity and concavity of the cracks diminishes with increase

in V_f and aspect ratio due to number of fibers per unit area, this reduces the damage cracks observed to branched networks of smaller cracks. Thereby suppressing the severity of the damage in the weak zone of the specimen.

xviii. Critical crack width sizes measured at critical compressive stress levels increases with increasing V_f and aspect ratio. Higher aspect ratio is more effective in mitigating the effect of major cracks.

6.2 Recommendation for Future Research

Future study should focus attention on the investigation of microcracking at the ITZ using scanning electron microscope as well as investigating the depth of microcracks and their effect on the durability of HPC with steel fiber addition.

REFERENCES

ACI 544.1R-96: (2001). *State-of-the-Art Report on Fiber Reinforced Concrete.* American Concrete Institute; Farmington Hills, MI, USA.

ACI 544.2R (1999). *Measurement of Properties of Fiber Reinforced Concrete*, American Concrete Institute; Farmington Hills, MI, USA.

Afroughsabet, V., Biolzi, L., & Ozbakkaloglu, T. (2016). High-Performance Fiber-Reinforced Concrete: A Review. *Journal of Material Science*, Vol. 51, pp. 6517-6551.

Aitcin, P.C., & Mehta, P.K. (1990). Effect of coarse aggregate characteristics on mechanical properties of high strength concrete. *ACI Materials Journal* 87(2): 103-107.

Aitcin, P.-C., (1998). *High-Performance Concrete*, E & FN SPON, New York, NY, USA.

Akcaoglu, T. (2003). Interfacial Transition Zone Behavior of Concrete by Means of a Single Coarse Aggregate Model, PhD Thesis, Eastern Mediterranean University, North Cyprus.

Akcaoglu, T., Tokyay, M., & Celik, T. (2004). Effect of coarse aggregate size and matrix quality on ITZ and failure behavior of concrete under uniaxial compression. *Cement and Concrete Composites,* 26(6), 633-638.

Akcaoglu, T., Tokyay, M., & Celik, T. (2005). Assessing the ITZ microcracking via scanning electron microscope and its effect on the failure behavior of concrete. *Cement and Concrete Research,* 35(2), 358-363.

Alexander, K.M., & Wardlaw, J. (1960). Dependence of cement-aggregates bond strength on size of aggregate. *Nature,* Vol. 187, pp. 230-231.

Anderson, T.L. (2005). *Fracture Mechanics: Fundamentals and Applications*. 3rd ed., Taylors & Francis.

Asmaro, W.P. (2013). Identification of Concrete Fracture Parameters using Digital Image Correlation and Inverse Analysis. PhD Dissertation, University of Windsor, Canada.

Atis, C. & Karahan, O. (2009). Properties of steel fiber reinforced fly ash concrete. *Construction and Building Materials*, 23, 392-399.

ASTM 820 (2016). Standard Specification for Steel Fibers for Fiber-Reinforced Concrete. ASTM International, West Conshohocken, PA, USA.

ASTM C33 (2016). Standard Specification for Concrete Aggregates. ASTM International, West Conshohocken, PA, USA.

ASTM C39 (2018). Standard Test Method for Compressive Strength of Cylindrical Concrete Specimens. ASTM International, West Conshohocken, PA, USA.

ASTM C29 (2017). Standard Test Method for Bulk Density ("Unit Weight") and Voids in Aggregate, ASTM International, West Conshohocken, PA, USA.

ASTM C117 (2013). Standard Test Method for Materials Finer than 75-µm (No . 200) Sieve in Mineral Aggregates by Washing. ASTM International, West Conshohocken, PA, USA.

ASTM C127 (2015). Standard Test Method for Relative Density (Specific Gravity) and Absorption of Coarse Aggregate. ASTM International, West Conshohocken, PA, USA.

ASTM C128 (2015). Standard Test Method for Relative Density (Specific Gravity) and Absorption of Fine Aggregate. ASTM International, West Conshohocken, PA, USA.

ASTM C136 (2014). Standard Test Method for Sieve Analysis of Fine and Coarse Aggregates, ASTM International, West Conshohocken, PA, USA.

ASTM C138 (2017). Standard Test Method for Density (Unit Weight), Yield, and Air Content (Gravimetric) of Concrete. ASTM International, West Conshohocken, PA, USA.

ASTM C143 (2015). Standard Test Method for Slump of Hydraulic-Cement Concrete. ASTM International, West Conshohocken, PA, USA.

ASTM C192 (2016). Standard Practice for Making and Curing Concrete Test Specimens in the Laboratory. ASTM International, West Conshohocken, PA, USA.

ASTM C469 (2014). Standard Test Method for Static Modulus of Elasticity and Poisson's Ratio of Concrete in Compression. ASTM International, West Conshohocken, PA, USA.

ASTM C494 (2017). Standard Specification for Chemical Admixtures for Concrete. ASTM International, West Conshohocken, PA, USA.

ASTM C496 (2017). Standard Test Method for Splitting Tensile Strength of Cylindrical Concrete Specimens. ASTM International, West Conshohocken, PA, USA.

ASTM C595 (2017). Standard Specification for Blended Hydraulic Cements. ASTM International, West Conshohocken, PA, USA.

Aydin, S. (2013). Effects of fiber strength on fracture characteristics of normal and high strength concrete. *Periodica Polytechnica,* 57/2 pp.191-200.

Babafemi, A.J. (2015). Tensile Creep of Cracked Macro Synthetic Fibre Reinforced Concrete. PhD Dissertation, University of Stellenbosch, South Africa.

Bahrner, V. (1940). The VeBe Consistency Testing Apparatus. Zement, 29 (9), 102-106.

Banthia, N. & Trottier, J. F. (1995). Concrete reinforced with deformed steel fibres. Part II: Toughness characterization. ACI Mater. J. 92(2), 146-54

Barros, J. A. O., & Cruz, J. S. (2001). Fracture Energy of Steel Fiber-Reinforced Concrete. *Mechanics of Composite Materials and Structures*, *8*, 29–45.

Bazant, Z.P., & Oh, B.H. (1983). Crack band theory for fracture of concrete. *Mater. Struct.* 16(93), 155-177.

Bayramov, F., Tasdemir, C., & Tasdemir, M.A. (2004). Optimisation of steel fibre reinforced concretes by means of statistical response surface method. *Cem. Concr. Comp.* 26, 665-675.

Bentur, A., & Mindess, S. (1986). The effect of concrete strength on crack patterns. *Cement and Concrete Research*, 16, 59-66.

Berra, M., & Ferrerra, G. (1990). Normal Weight and Total-Lightweight High-Strength Concretes: A Comparative Study. *ACI Special Publication,* Vol. 121, pp. 701-734.

Beygi, M.H.A., Kazemi, M.T., Amiri, J.V., Nikbin, I.M., Rabbanifar, S., & Rahmani, E. (2014). Evaluation of the effect of maximum aggregate size on fracture behavior of self-compacting concrete. *Construction and Building Materials*, 55, 202-211.

Broek, D. (1986). *Elementary Engineering fracture Mechanics*. The Hague, Netherlands; Hingham, Mass Martinus Nijhoff; Kluwer Academic Publishers, Boston.

Buyukozturk, O., Nilson, A.H. & Slate, F.O., (1971). Stress-Strain Response and Fracture of a Model of Concrete in Biaxial Loading. *Journal of the American Concrete Institute, Proc.*, Vol. 68, No. 8, pp. 590-599.

BS EN 1008 (2002). Mixing water for concrete. Specification for sampling, testing and assessing the suitability of water, including water recovered from processes in the concrete industry, as mixing water for concrete. British Standard Institution, BSI London.

BS EN 1097 – 2: (2010). Tests for mechanical and physical properties of aggregates. Methods for the determination of resistance to fragmentation. British Standard Institution, BSI, London.

BS EN 12350 - 2: (2009) Testing Fresh Concrete, *Slump Test*, British Standard Institution, BSI, London.

BS EN 12350: 3 (2009). Testing Fresh Concrete: VeBe Test. British Standard Institution, BSI, London.

BS EN 12350: 4 (2009). Testing Fresh Concrete: Degree of Compactability. British Standard Institution, BSI, London.

BS EN 12390-3 (2009). Testing hardened concrete. Compressive strength of test specimens. British Standard Institution, BSI, London.

BS EN 12390-6 (2009). Testing hardened concrete. Tensile splitting strength of test specimens. British Standard Institution, BSI, London.

BS 5168 (2016). Glossary of Rheological Terms. British Standard Institution, BSI, London.

Carino, N.J., & Slate, F.O. (1976). Limiting Tensile Strain Criterion for Failure of Concrete. *Journal of American Concrete Institute, Proc.,* Vol. 73, No. 3, pp. 160-165.

Carrasquillo, R.L., Slate, F.O., & Nilson, A.H. (1981). Microcracking and behavior of high strength concrete subjected to short-term loading. *ACI Journal,* 78 (3), 179-186.

Carrasquillo, R., & Slate, F. (1983). Microcracking and Definition of Failure of High- and Normal-Strength Concretes. *Cement, Concrete and Aggregates*, Vol. 5, No. 1, pp. 54-61.

Castro-Montero, A., Shah, S.P., & Miller, R.A. (1990). Strain field measurement in fracture process zone. *J. Eng. Mech.* 116 (11), 2463-84.

CEB-FIP (1990). High Strength Concrete. State of the Art Report Bulletin d'Information London, FIR SR 90/1 No. 197.

Crumbie, A.K. (1994). Characterisation of the microstructure of concrete. PhD Thesis, Imperial College of Science, Technology and Medicine, London.

Delibes Liniers, A. (1987). Microcracking of concrete under compression and its influence on tensile strength. *Materials & Structures*, Vol. 20 pp. 111-116.

de Larrard, F., & Belloc, A. (1997). The Influence of Aggregate on the Compressive Strength of Normal and High-Strength Concrete. *ACI Materials Journal,* 94(5)**,** 417-426.

Diamond, S., & Bentur, A. (1985). On the Cracking in Concrete and Fiber Reinforced Cements, *In Application of Fracture Mechanics to Cementitious Composites,* Shah, S.P. (ed.) NATO Workshop, Evanston, USA. 1984, Martinus Nijhoff, Dordrecht, Netherland, 87-140.

Diamond, S. (2004). The Microstucture of Cement Paste and Concrete – A Visual Primer. *Cement & Concrete Composites,* 26, 919-933.

Dowling, N.E. (2013). *Mechanical Behavior of Materials: Engineering Methods for Deformation,* Fracture and Fatigue. 4th Ed. Pearson.

Emery, J.M., Hochhalther, J.D., & Ingraffea, A., (2007). Computational Fracture Mechanics of Concrete Structures: A Retrospective through Multiple Lenses. *In Proceedings of FraMCos-6*, Catania, Italy.

Erdogan, F. (2000). Fracture Mechanics. *International Journal of Solids and Structures*, 37, 171 – 183.

Eren, O., Marar, K. & Celik, T. (1999). Effects of Steel Fibers on Some Mechanical Properties of High-Strength Fiber-Reinforced Concrete. *Journal of Testing and Evaluation,* Vol. 27 pp. 380-387.

Faber, K.T., & Evans, A.G. (1983). Crack deflection process – I: Theory. *Acta Metall.,* 31 (4), 565-76.

Feldman, R.F., & P.J. Sereda, (1970). A New Model for Hydrated Portland Cement and its Practical Implications. *Eng. J.* (*Canada*), Vol. 53, No. 8/9, pp. 53–59.

Gettu, R., Bazant, Z.P., & Karr, N.E. (1990). Fracture Properties and Brittleness of High-Strength Concrete. *ACI Materials Journal,* Vol. 87 No. 6, pp. 608-618.

Gettu, R., & Shah, S.P. (1994). *Fracture Mechanics In High Performance Concretes and Applications.* Edited by Shah, S.P. and Ahmad, S.H., Edward-Arnold pp. 161-212. United Kingdom.

Giaccio, G., Rocco, C., & Zerbino, R. (1993). The fracture energy of high-strength concretes. *Materials and Structures,* 26, 381-386.

Griffith, A.A. (1920). The Phenomena of Rupture and Flow in Solids. *Philosophical Transactions of the Royal Society of London. Series A, Containing Papers of a Mathematical or Physical Character*, Vol. 221 pp. 163 – 198.

Goldman, A., & Bentur, A. (1992). Effects of Pozzolanic and Non-reactive Microfillers on the Transition Zone in High Strength Concrete. In *Interfaces in Cementitious Composites. RILEM 8th International Conference Toulouse,* Maso J.C., Ed.; 53-61.

Gromicko, N., & Shepard, K. (2006). The History of Concrete. Available at http://www.nachi.org/history-of-concrete.htm

Hanna B. (1987). Contribution á l' étude de la structuration des mortiers de ciment portland contenant des particules ultra-fines. Thèse, Toulouse (In French).

Hashino, M. (1988). Difference of the w/c ratio, porosity and microscopical aspect between the upper boundary paste and the lower boundary paste of the aggregate in concrete. *Materials and Structures*, 21, 336-340

Hillerborg, A. (1983). Analysis of one single crack. In Wittman, F.H. (ed.) *Fracture Mechanics of Concrete,* Elsevier Science, Amsterdam, pp. 223-249.

Hsu, T.T.C. (1963). Mathematical analysis of shrinkage stresses in a model of hardened concrete. *Journal of American Concrete Institute, Proc.* Vol. 60 pp. 371-390.

Hsu, T.T.C, Slate, F.O., Sturman, G.M., & Winter, G. (1963). Microcracking of Plain Concrete and the Shape of the Stress-Strain Curve. *Journal of the American Concrete Institute, Proc.*, Vol. 60, No. 2, pp. 209-224.

Hsu, T.T.C. (1984). Fatigue and Microcracking of Concrete. *Materials and Structures*, Vol. 17 No. 97, pp. 51-54.

Hu, C., de Larrard, F., Sedran, T., Bonlag, C., Bose, F., & Deflorenne, F. (1996). Validation of BTRHEOM, the new rheometer for soft-to-fluid concrete. *Materials and Structures*, 29(194), 620-631.

Imam, M., Vandewalle, L. & Mortelmans, F., (1995). Are current concrete strength tests suitable for high strength concrete? *Materials & Structures*, Vol. 28 pp. 384-391.

Inglis, C.E. (1913). Stresses in a Plate Due to the Presence of Cracks and Sharp Corners. *Transaction of the Institute of Naval Architects*, Vol. 55, pp. 219-241.

Jones, R. (1952). A Method of Studying the Formation of Cracks in a Material Subjected to Stresses. *British Journal of Applied Physics* (London), Vol. 3, No. 7, pp. 229-232.

Jones, R., & Kaplan, M.F. (1957). The effect of coarse aggregate on the mode of failure of concrete in compression and flexure. *Magazine of Concrete Research*, 9 (26), 89 – 94.

Jornet, A., Guidali, E., & Muhlethaler, U. (1993). Microcracking in high performance concrete. Eds. J.E. Lindqvist and B. Nitz, Sp. Report 15: pp.6 (Swedish National Testing and Research Institute: Building Technology).

Kazemi, M.T., Golsorkhtabar, H., Beygi, M.H.A., & Gholamitabar, M. (2017). Fracture properties of steel fiber reinforced high strength concrete using work of fracture and size effect methods. *Constr. Build. Mater*., 142, 482-489.

Karihaloo, B.L. (1995). *Fracture Mechanics and Structural Concrete.* Concrete Design and Construction Series. Longman Scientific and Technical, Essex, England.

Khaloo, A.R., & Kim, N. (1996). Mechanical Properties of Normal to High-Strength Steel Fiber-Reinforced Concrete. *Cement, Concrete and Aggregates, CCAGDP*, 18(2), 92–97.

Koehler, E.P., & Fowler, D.W. (2003). Summary of Concrete Workability Test Methods, ICAR 105-1; University of Texas at Austin, USA.

Koksal, F., Sahin, Y., Gencel, O., & Yigit, i. (2013). Fracture energy-based optimisation of steel fibre reinforced concretes. *Engineering Fracture Mechanics,* 107, 29-37.

Krstulovic-Opara, N. (1993). Fracture Process Zone Presence and Behavior in Mortar Specimens. *ACI Materials Journal,* Vol. 90, No. 6 pp. 618-626.

Kurihara, N., Kuneida, M., Kamada, T., Uchida, Y. and Rokugo, K. (2000). Tension softening diagrams and evaluation of properties of steel fibre reinforced concrete. *Eng. Fract. Mech,* Vol. 65, pp. 235-45.

Lea, F.M. (1960). Cement research: retrospect and prospect, *Proc. 4th Int. Symp. On the Chemistry of Cement*, pp. 5 – 8, Washington DC.

L'Hermite, R. (1954). Present Day Ideas on Concrete Technology. 3rd Part, The Failure of Concrete, Bulletin No. 18, Union of Testing and Research Laboratories for *Materials and Structures* (RILEM), pp. 27-39.

Liu, T.C., Nilson, A.H. & Slate, F.O. (1972). Stress-Strain Response and Fracture of Concrete in Uniaxial and Biaxial Compression. *Journal of the American Concrete Institute, Proc.*, Vol. 69, No. 5, pp. 291-295.

Li, V.C., Lim, Y.M., Chan, Y. (1998). Feasibility study of a passive smart self-healing cementitious composite. *Composite. Part B Eng. 29*, 819–827.

Löfgren, I. (2005). Fibre-reinforced Concrete for Industrial Construction – A Fracture Mechanics Approach to Material Testing and Structural Analysis. PhD Thesis, Chalmers University of Technology, Göteborg, Sweden.

Mansur, M.A., Chin, M.S., & Wee, T.H. (1999). Stress-strain relationship of high-strength fiber concrete in compression. *ASCE Journal of Materials in Civil Engineering*, 11(1), 21-29.

Marar, K. (2000). The effect of steel fibers on some properties of normal and high strength concrete. PhD Thesis, EMU, Gazimagusa, North Cyprus.

Maso, J.C. (1980). La liason entre les granulats et la pate de ciment hydrate, In *7th International Symposium on the Chemistry of Cement*; Paris, 3: 1-9 (in French).

McCreath, D. (1968). The fracture mechanics of concrete. PhD Thesis, Imperial Collage, London.

Mehta, P.K., & Monteiro, P.J.M. (1993). *Concrete: Structure, Properties and Materials.* 2nd Ed., Prentice Hall, Englewood Cliffs, New Jersey.

Mehta, P.K., & Monteiro, P.J.M. (2014). *Concrete: Microstructure, Properties, and Materials,* 4th Ed., Mc Graw-Hill, New York.

Meyers, B. L., Slate, F. O., & Winters, G. (1969). Relationship between Time-Dependent Deformation and Microcracking of Plain Concrete. *Journal of the American Concrete Institute*, Proc., Vol. 66, No. 1, pp. 60-68.

Miller, R.A., Shah, S.P., & Bjekhagenm, H.I. (1988). Crack profiles in mortar measured by holographic interferometry. *Experimental Mechanics*, 28 (4), 388-394.

Mindess, S., & Diamond, S. (1982). The Cracking and Fracture of Mortars. *Materials and Structures,* Vol. 15 No. 86 pp. 107-113.

Mindess, S. (1994). Materials Selection, Proportioning and Quality Control. In *High Performance Concretes and Applications*, Edited by Shah S.P. and Ahmad,

S.H. Edward Arnold.

Moavenzadeh, F., & Bremmer, T.W. (1969). Fracture of Portland Cement Concrete. *International Conference on Structure, Solid Mechanics and Engineering Design in Civil Engineering*, Southampton University.

Nemati, K.M., & Gardoni, P. (2005). Microstructural and Statistical Evaluation of Interfacial Zone Percolation in Concrete. *Strength, Fracture and Complexity*, 3, 191-197.

Neves, R.D., & Fernandes de Almeida, J.C.O. (2005). Compressive behavior of steel fibre reinforced concrete. *Structural Concrete*, Vol. 6 No. 1, pp. 1-8.

Newman, K. (1968). Criteria for the Behavior of Plain Concrete under Complex State of Stress. In *Proc. International Conference on the Structure of Concrete*, Brooks A.E. Newman K., Ed., Cement and Concrete Association, London. pp. 255-274.

Neville, A.M. (1995). *Properties of Concrete*, 5th ed. Pearson.

Neville, A.M. (2005). *Properties of Concrete*, 14th Ed. Wiley, New York.

Oliveira, M.O.F. (1992). Fatigue and microcracking in high strength concretes. Doctoral Thesis, School of Civil Engineering, Technical University of Catalunya, Barcelona, Spain.

Ollivier, J.P., Maso, J.C., & Bourdette, B. (1995). Interfacial Transition Zone in Concrete. *Advanced Cement Based Materials,* Vol. 2, pp. 30-38.

Ono, H., & Ohgishi, S. (1989). Fracture Toughness J_{IC} and Fracture Energy G_f in the New Material Fibres Reinforced Concrete. In *Fracture Toughness and Fracture Energy,* Mihashi, H., takahashi, H. and Wittmann, F.H., eds., Balkema, Rotterdam, 73.

Ozturan, T., & Cecen, C. (1997). Effect of coarse aggregate type on mechanical properties of concretes with different strengths. *Cement and Concrete Research*, 27(2), 165-170.

Panzera, T.H., Christoforo, A.L., & Ribeiro Borges, P.H. (2013). High performance fibre-reinforced concrete (FRC) for civil engineering applications. *Advanced Fibre-Reinforced Polymer (FRP) Composites for Structural Applications*. Woodhead Publishing.

Petersson, P.E. (1980). Fracture energy of concrete: Practical performance and experimental results. *Cem. Concr. Res.* 10(1), 91-101.

Powers, T.C. (1968). *The Properties of Fresh Concrete*. John Wiley and Sons, Inc., New York.

Rao, G.A. (2001). Nonliear fracture and size effect in high strength and high performance concrete – An experimental approach. PhD Thesis, Indian Institute of Science, Bangalore, India.

Rao, G.A., & Prasad, B.R.R. (2002). Fracture energy and softening behavior of high-strength concrete. *Cem. Concr. Res.,* 32, 247-252.

Richart, F.E., Brantzaeg, A., & Brown, R.L. (1928). A Study of the Failure of Concrete under Combined Compressive Stresses, Bulletin No. 185, Univ. of Illinois Engineering Experimental Station, Urbana, Illinois.

Richart, F.E., Brantzaeg, A., & Brown, R.L. (1929). The Failure of Plain and Spirally Reinforced Concrete in Compression, Bulletin No., 1980, Univ. of Illinois Engineering Experimental Station, Urbana, Illinois.

Ritchie, A.G.B. (1962). The Triaxial Testing of Fresh Concrete. *Magazine of Concrete Research*, 14(40), 37-42.

RILEM (1985). Committee on Fracture Mechanics of Concrete – Test Methods, Determination of the Fracture Energy of Mortar and Concrete by Means of Three-Point Bend Tests on Notched Beams. *Materials and Structures*, Vol. 18, No. 106 pp. 285 – 290.

Robinson, G.S. (1976). Behavior of Concrete in Biaxial Compression. *Journal of Structural Division, ASCE, Proc.*, Vol. 93 No. ST1, pp. 71-86.

Rossi, P., & Harrouche, N. (1990). Mix design and mechanical behavior of some steel-fibre-reinforced concretes used in reinforced concrete structures. *Materials and Structures*, 23, 256-266.

Roylance, D. (2001). Introduction to Fracture Mechanics. Available from web.mit.edu/course/3/3.11/www/modules/frac.pdf

Rusch, H. (1959). Physikalische Fragen der Betonprüfung, *Zement-Kalk-Gips,* Vol. 12, No. 1 pp.1-9.

Sabir, B.B., Wild, S., & Asili, M. (1997). On the tortuosity of the fracture surface in concrete. *Cement and Concrete Research,* 27 (5), 785-795.

Sahin, Y., & Koksal, F. (2011). The influences of matrix and steel fibre tensile strengths on the fracture energy of high-strength concrete. *Constr. Build. Mater.,* Vol. 25, pp. 1801-1806.

Sell, R (1959). Investigation into the Strength of Concrete under Sustained Loads, Bulletin No. 5, Union of Testing and Research Laboratories for *Materials and Structures (RILEM),* pp. 5-13.

Scrivener, K.L., & Pratt, P.L. (1986). A preliminary study of the microstructure of the cement paste – aggregate bond in mortars. In: *Proceedings of the 8th International Congress of the Chemistry of Cement,* Rio de Janeiro III, pp. 466-471.

Scrivener, K.L. (1989). The Microstructure of Concrete. In: Skalny J, editor. *Materials Science of Concrete*, Vol. 1. Westerfield, OH. American Ceramic Society, 127-162.

Scrivener, K.L., Crumbie, A.K., & Laugesen, P. (2004). The Interfacial Transition Zone (ITZ) between Cement Paste and Aggregate in Concrete. *Interface Science,* 12, 411 – 421.

Shah, S.P., & Winter, G. (1966). Inelastic behavior and fracture of concrete. *ACI Journal*, 63(9), 925-930.

Shah, S.P., & Chandra, S. (1968). Critical Stress, Volume Change and Microcracking of Concrete. *Journal of the American Concrete Institute, Proc.,* Vol. 65, No. 9, pp. 770-781.

Shah, S.P., & Sankar, R. (1987). Internal Cracking and Strain-Softening Response of Concrete under Uniaxial Compression. *ACI Materials Journal,* Vol. 84, No. 3, pp. 200-212.

Shah, S.P. (1988). Fracture toughness of cement-based materials. *Materials and Structures*, 21, 145-150.

Shah, S.P., & Ahmad, S.H. (1994). *High Performance Concretes and Applications*. Edward Arnold, Great Britain.

Shah, S.P., Swartz, S.E., & Ouyang, C. (1995). *Fracture Mechanics of Concrete: Applications of Fracture Mechanics to Concrete, Rock, and Quasi-Brittle Materials.* John Wiley & Sons, New York.

Singh, S., Shukla, A., & Brown, R. (2004). Pullout Behavior of Polyropylene Fibers from Cementitious Matrix. *Cement and Concrete Research*, 34(10), 1919-1925.

Slate, F.O. & Meyers, B.L. (1969). Deformation of Concrete. In: *Proceedings of the Fifth International Symposium on the Chemistry of Cement,* Vol. III, Cement Association of Japan, Tokyo, pp. 142-151.

Slate, F.O. & Hoover, K.C. (1984). Microcracking in Concrete. In: *Fracture Mechanics of Concrete: Material Characterization and Testing,* Eds. A. Carpinteri and A.R. Ingraffea, pp. 137 – 58 (Martinus Nijhoff, The Hague).

Song, P.S. & Hwang, S. (2004). Mechanical properties of high-strength steel fiber-reinforced concrete. *Construction and Building Materials*, 18, 669 – 673.

Tasdemir, C., Tasdemir, M.A., Lydon, F.D., & Barr, B.I.G. (1996). Effect of silica fume and aggregate size on the brittleness of concrete. *Cem. Concr. Res.*, 26(1), 63-68.

Tasuji, M.E., Slate, F.O., & Nilson, A.H. (1978). Stress-Strain Response and Fracture of Concrete in Biaxial Loading. *Journal of the American Concrete Institute, Proc.*, Vol. 75, No. 7, pp. 306-312.

Tattersal, G.H. (1991). *Workability and Quality Control of Concrete*, E & FN SPON, New York.

Theocaris, P.S., & Koufopoulos, T. (1969). Photoelastic analysis of shrinkage microcracking in concrete. *Magazine of Concrete Research,* Vol. 21 pp. 15-22.

Tinic, C. & Bruhwiler, E. (1985). Effect of Compressive loads on the tensile strength of concrete at high strain rates. *International Journal of Composite Lightweight Concrete,* 7 pp. 103-108

Traina, L.A. & Mansour, S.A. (1991). Biaxial Strength and Deformational Behavior of Plain and Steel Fiber Concrete. *ACI Materials Journal*, Vol. 88 pp. 354-364.

Van Breugel, K. (2012). Self-healing Material Concepts as Solution for Aging Infrastructure. In *37th Conference on Our World in Concrete & Structures*, 29-31 August, Singapore.

Van Mier, J.G.M. (1985). Influence of damage orientation distribution on the multi-axial stress-strain behavior of concrete. *Cem. Concr. Res.*, Vol. 15 pp. 859-862

Van Mier, J.G.M. (1986). Fracture of Concrete under Complex Stress. *HERON*, 31(3)

Van Mier, J.G.M. (1990). Internal crack detection in single edge notched concrete plates subjected to uniform boundary displacement. In *Micromechanics of*

Failure of Quasi Brittle Materials, Shah, S.P., Swartz, S.E. and Wang, M.L., Eds., Elsevier Applied Science Publishers, London.

Van Mier, J.G.M. (1991). Crack Face Bridging in Normal, High Strength and Lytag Concrete. In van Mier, JGM., Rots, JG and Bakker, A. (eds.) *Fracture Processes in Concrete, Rock and Ceramics.* Spon, London.

Van Mier, J.G.M., Stang, H., & Ramakrishnan, V. (1996). Practical Structural applications of SFRC and HPFRCC. In *High Performance Fiber Reinforced Cement Composites 2.* Edited by A.E. Naaman and H.W.Reinhardt. E&FN Spon, London, UK.

Van Mier, J.G.M. (1997). *Fracture Processes of Concrete*, CRC Press.

Van Mier, J.G.M. (2010). A fundamental explanation of softening. *FraMCoS-7* Seoul.

Vile, G.W.D. (1968). The Strength of Concrete under Short-term Static Biaxial Stress. In *Proc., International Conference of the Structure of Concrete*, Cement and Concrete Association, London pp. 131-145.

Wu, K.R., Chen, B., Yao, W., & Zhang, D. (2001). Effect of coarse aggregate type on mechanical properties of high-performance concrete. *Cement and Concrete Research*, 31**,** 1421-1425.

Zhou, F.P., Barr, B.I.G., & Lydon, F.D. (1995). Fracture properties of high strength concrete with varying silica fume content and aggregates. *Cem. Concr. Res.* 25(3), 543-552.

APPENDICES

Appendix A: Concrete Mix Design

S/No	Item	Result
1	Target mean strength	70 MPa @ 28 days
2	Cement strength class	42.5 N (Slag)
3	Free water-cement ratio	0.31
4	Slump	80 mm (1 hour after batching)
5	Water content	145 kg/m^3
6	Cement content	467.74 kg/m^3
7	Relative Density of Coarse Aggregate (Dmax 10 mm)	2.68
8	Silica fume content	10 % of Cement (46.7 kg/m^3)
9	Water – cementitious ratio	145/(470 + 47) = 0.28
10	Superplasticizer	2 % of Cement (9.35 kg/m^3)
11	Volume of Coarse Aggregate	1050 kg/m^3
12	Fine Aggregate	2/3 * 1050 = 700 kg/m^3
13	Adjusted water content after trial mixes	145 + 20 = 165 kg/m^3
14	Adjusted superplasticizer content	10 + 3.55 = 13.55 kg/m^3
15	Superplasticizer (HRWR) content	13.55/470 = 0.0288 = 3%
16	Adjusted water – cementitious ratio	165/(470 + 47) = 0.319 =0.32
17	Steel Fiber addition	0.50 – 2.00 % @ 0.25 %

Cement (kg/m^3)	Water (kg/m^3)	Coarse Aggregate (kg/m^3)	Fine Aggregate (kg/m^3)	Silica Fume (kg/m^3)	HRWR (kg/m^3)
470	165	1050	700	47	14

Appendix B: Publications

Abubakar, A.U. & Akçaoğlu, T. (2016). Self-Healing in Cementitious Composites: A New Paradigm in Crack Repair. In *Materials Science and Technology Society of Nigeria Conference*, Zaria, Kaduna State, Nigeria.

Abubakar, A.U., Akçaoğlu, T., & Marar, K. (2018). P-value significance level test for high-performance steel fiber concrete (HPSFC). *Computers and Concrete*, Vol. 21 No. 5, pp. 485 – 493. (SCI EXPANDED)

Abubakar, A.U., Akçaoğlu, T., & Marar, K. (2018). Impact resistance of high-performance steel fiber concrete under long term exposure to environmental conditions. In *3rd International Conference on Civil Engineering and Materials Science (ICCEMS 2018)* Chengdu, China (SCOPUS CITED)

Abubakar, A.U., Akçaoğlu, T., & Marar, K. (2018). Flexural response in high-performance steel fiber concrete. *Advances in Concrete Construction* (under review) (SCI EXPANDED)

Abubakar, A.U., Akçaoğlu, T., & Marar, K. (2018). Evaluation of Workability Parameters for Hooked-End High-Performance Steel Fiber Concrete Mixes. *ASTM Journal of Testing & Evaluation* (under review) (SCI EXPANDED)

Abubakar, A.U. & Akçaoğlu, T. (2018). Microcracking in High-Performance Steel Fiber Concrete at Critical Stress Region under Uniaxial Compression. *International Journal of Fracture* (under review) (SCI INDEXED)